DEPARTMENT OF THE AIR FORCE

AIR UNIVERSITY (ATC)

AIR FORCE INSTITUTE OF TECHNOLOGY

Wright-Patterson Air Force Base, Ohio

ON THE GENERATION OF STRESS AND DEFORMATION IN ELASTIC SOLIDS BY HIGH POWERED LASERS

by

Peter J. Torvik
Professor of Mechanics

AFIT TR 80-6 September 1980

ON THE GENERATION OF STRESS AND DEFORMATION IN ELASTIC SOLIDS BY HIGH POWERED LASERS

by

Peter J. Torvik
Professor of Mechanics

AFIT TR 80-6
September 1980

UNCLASSIFIED

SECURITY CLASSIFICATION OF THIS PAGE (When Data Entered)

REPORT DOCUMENTATION PAGE

READ INSTRUCTIONS BEFORE COMPLETING FORM

1. REPORT NUMBER: AFIT-TR-80-6	2. GOVT ACCESSION NO.: AD-A096373
3. RECIPIENT'S CATALOG NUMBER:	
4. TITLE (and Subtitle): ON THE GENERATION OF STRESS AND DEFORMATION IN ELASTIC SOLIDS BY HIGH POWERED LASERS .	5. TYPE OF REPORT & PERIOD COVERED: Technical Report, 1 Apr 79-30 Aug 80
6. PERFORMING ORG. REPORT NUMBER:	
7. AUTHOR(s): Peter J. Torvik	8. CONTRACT OR GRANT NUMBER(s): AFWL PO 79-063 and 80-014
9. PERFORMING ORGANIZATION NAME AND ADDRESS: Air Force Institute of Technology, Wright-Patterson AFB OH 45433	10. PROGRAM ELEMENT, PROJECT, TASK AREA & WORK UNIT NUMBERS:
11. CONTROLLING OFFICE NAME AND ADDRESS: Air Force Institute of Technology, Wright-Patterson AFB OH 45433	12. REPORT DATE: Sep 80
	13. NUMBER OF PAGES: 126
14. MONITORING AGENCY NAME & ADDRESS (if different from Controlling Office): 130	15. SECURITY CLASS. (of this report): Unclassified
	15a. DECLASSIFICATION/DOWNGRADING SCHEDULE:

16. DISTRIBUTION STATEMENT (of this Report)

Approved for public release; distribution unlimited.

17. DISTRIBUTION STATEMENT (of the abstract entered in Block 20, if different from Report)

18. SUPPLEMENTARY NOTES

Approved for public release; IAW AFR 190-17

Fredric C. Lynch

FREDRIC C. LYNCH, Major, USAF
Director of Public Affairs

19. KEY WORDS (Continue on reverse side if necessary and identify by block number)

Laser Effects
Thermal Stress

20. ABSTRACT (Continue on reverse side if necessary and identify by block number)

The various mechanisms by which stresses may be generated in an elastic solid by the absorption of laser energy are reviewed. Through the use of simplification and idealizations, analyses of the stresses generated by each mechanism are developed and discussed. The role of the mechanical boundary conditions on the stresses generated is given particular attention. In each case, emphasis is given to the prediction of failure times.

DD FORM 1 JAN 73 1473 EDITION OF 1 NOV 65 IS OBSOLETE

UNCLASSIFIED

SECURITY CLASSIFICATION OF THIS PAGE (When Data Entered)

012200

Preface

This report describes work accomplished between 1 April 1979 and 30 August 1980 under the sponsorship of the LEAPS Division, Air Force Weapons Laboratory, through project orders 79-063 and 80-014. The author has attempted to set down some of the fundamental principles of thermoelasticity and apply them to the determination of stresses by the absorption of high intensity laser radiation, and to investigate the stresses in elastic plates generated by the thermal and mechanical response to the absorbed energy.

The author wishes to acknowledge the cooperation of the Department of Engineering Mechanics of the Ohio State University, where most of the work presented herein was performed while the author was a visiting Professor of Mechanics through the end of 1979.

The financial support of AFWL/PGV made the effort possible, and the support and encouragement of AFWAL personnel, especially Captain Peyerl, Dr. William Laughlin and Dr. Ralph Rudder, contributed significantly to such results as were obtained. Finally, the assistance of the secretarial team at the School of Engineering, Air Force Institute of Technology, and of the Instructional Media personnel in the preparation of graphics is greatly appreciated.

Peter J. Torvik

Table of Contents

List of Figures

On the Generation of Stress and Deformation in Elastic Solids by High Powered Lasers

Peter J. Torvik

I. INTRODUCTION

The absorption of some fraction of the energy in a high powered laser beam at the surface of a solid generates stress and deformation through several mechanisms. These may be broadly divided into two categories: (1) where the stress arises through the thermal expansion of the target material, and (2) where the stress in the target arises through a pressure loading resulting from the thermal expansion of the medium (typically air). The blow-off phenomenon, in which the stress is generated in the target by the rapid expansion of vaporized target material, may be regarded as a third category or may be arbitrarily assigned to either of the first two.

A second rationale for classifying the various regimes of stress generation is furnished by the time scales of the problem. First, the time scale introduced through mechanical inertia of the target must be considered. If the heating rates are sufficiently low, it is evident that acceleration terms in the target response can be neglected and a static stress analysis performed. Such problems may be termed thermal stress problems. On the other hand, under very short heating times, significant temperature changes may occur before significant deformation has occurred. In such cases, the influence of target material inertia is to serve as a constraint thereby raising the levels of thermal stress. These may be labeled as thermal shock problems.

The finite values of target conductivity introduce a second time scale into the target response. If heating rates are very low, a state of thermal equilibrium will result with input energy being balanced by "losses" to the surrounding media or through radial conductions away from the heated area.

These may be regarded as static thermal stress problems. For more rapid heating rates, changes in temperature must be taken into account, but the stress and deformation analysis may be performed by neglecting mechanical inertia and performing a static stress and deformation analysis with time regarded as a parameter. Such problems, where thermal inertia is considered but mechanical inertia is not, will be termed quasi-static thermal stress problems. In comparison, the thermal shock regime is seen to exist when both mechanical inertia and thermal inertia must be considered. The fourth possibility, that thermal inertia may be neglected but mechanical inertia must be considered, occurs in a partially transparent poor conductor where absorption of a pulse occurs in depth. The initial temperature profile and, hence, the gradients and resulting stresses will form and be propagated quite independently of the thermal diffusion process. For purposes of classification, these may be called isothermal shock problems and are of particular significance in the absorption of x rays. However, this class would appear to be of an academic interest only in targets essentially opaque to laser radiation, where absorption occurs at the surface and thermal stresses are generated after a temperature change arises through conduction.

A further classification of thermal stress problems may be made into problems of coupled and uncoupled thermoelasticity. In coupled thermoelasticity, the temperature change resulting from a mechanical strain induced adiabatically is taken into account. This effect is not to be expected to be of significance in the presence of the very large temperature changes arising from the absorption of intense laser radiation. A second deviation from classical thermoelasticity arises if non-Fourier solids are considered in which the heat conduction law is modified so as to provide finite, rather than infinite, velocities for the propagation of thermal disturbances. Solutions to

such nonclassical problems should be reviewed in order to determine if this effect is of importance in the generation of thermal stresses by laser heating.

Three of these four regimes of uncoupled thermoelasticity will be considered in the second section of this monograph with the goals being as follows: (1) to determine circumstances under which significant thermal stresses will be generated, and (2) to provide readily used formulae, charts and algorithms for estimating the magnitude of the thermal stress. Consideration of isothermal shock will be left for a later work.

In the third section, the generation of stress and deformation by mechanisms involving a pressure loading will be considered with the emphasis again being on determining circumstances under which the stresses and deformations are significant and on providing means of estimating the magnitude of the effect.

In the fourth section, damage mechanisms will be treated. Of particular interest is determining the likelihood that fluctuations in stress by whatever mechanism produced will be of such magnitude as to cause failure through catastrophic (unstable) crack growth or eventual fracture through crack propagation. In order to better assess the significance of stresses and deformations produced by laser heating, comparisons will be made with other damage mechanisms, notably melt through and thermal softening.

II. UNCOUPLED THERMOELASTICITY

The classification scheme introduced in the introduction was based on two time scales. The first was the thermal time scale, which arises from the diffusive nature of the heat conduction equation. As will be seen in more detail later, solutions to one-dimensional, linear heat conduction problems typically show a dependence on time and spatial coordinate in the combination $\kappa t/x^2$, where κ is the thermal diffusivity, t is time and x the characteristic coordinate. Thus, for times t long compared to a critical time

$$t_c = L^2/\kappa \tag{1}$$

where L is a characteristic dimension of the object, the temperature field may be regarded as static. Conversely, for $t < t_c$, significant changes in the temperature field will occur and must be accounted for through solving the diffusion equation for the temperature field subject to appropriate thermal boundary conditions.

The second time scale of interest is the propagation time for elastic disturbances

$$t_{c_E} = L/C_e$$

where L is again a critical dimension of the heated object and C_e is an elastic wave speed, of order 2-5 km/sec in an unbounded solid. Table I depicts the result of this classification and sets down the terminology to be used in this section.

TABLE I

Classification of Uncoupled Thermoelastic Problems

	Thermal Inertia		Mechanical Inertia	
	$t < L^2/\kappa$	$t > L^2/\kappa$	$t < L/C_e$	$t > L/C_e$
Static Thermal Stress		X		X
Quasi Static Thermal Stress	X			X
Isothermal Shock		X	X	
Thermal Shock	X		X	

For an isotropic Fourier solid, the components of the heat flux vector, q_i, are related to the spatial gradients of the temperature field through

$$q_i = -k \frac{\partial T}{\partial x_i} \tag{2}$$

and conservation of energy leads to

$$\rho \dot{\mathcal{E}} = \sigma_{ij} \dot{\epsilon}_{ij} - q_{i,i} \tag{3}$$

where k is the thermal conductivity, ρ is the density, $\mathcal{E}$ is the internal energy, σ_{ij} are the stresses, and ϵ_{ij} the strains. For an elastic solid

$$\rho T \dot{\eta} = -q_{i,i} \tag{4}$$

where the entropy η is given by

$$\eta = -\frac{\partial \phi}{\partial T} \tag{5}$$

and

$$\phi = \mathcal{E}(\epsilon_{ij}, T) - \eta(c_{ij}, T)T \tag{6}$$

is the free energy. From (3), (4) and (6), Equation (5) follows, and that

$$\sigma_{ij} = \rho \frac{\partial \phi}{\partial \epsilon_{ij}} \tag{7}$$

The specific heat at constant volume, C_v, is defined from Equation (3), with $\dot{\epsilon}_{ij} = 0$, or

$$\rho C_v \dot{T} = \rho \dot{\mathcal{E}} = -q_{i,i} \tag{8}$$

Equation (4) may be written as

$$-q_{i,i} = \rho T \left[\frac{\partial \eta}{\partial \epsilon_{ij}} \dot{\epsilon}_{ij} + \frac{\partial \eta}{\partial T} \dot{T} \right] \tag{9}$$

$$= \rho T \left[\frac{-\partial^2 \phi}{\partial \epsilon_{ij} \partial T} \dot{\epsilon}_{ij} - \frac{\partial^2 \phi}{\partial T^2} \dot{T} \right] \tag{10}$$

substituting Equation (7) and noting from (8) and (10) that

$$\rho C_v = -\rho T \frac{\partial^2 \phi}{\partial T^2} \tag{11}$$

we arrive at

$$-q_{i,i} = T\left(-\frac{\partial \sigma_{ij}}{\partial T}\right)\dot{\epsilon}_{ij} + \rho C_v \dot{T} \tag{12}$$

For an elastic material undergoing temperature change

$$\sigma_{ij} = \lambda\delta_{ij}\varepsilon_{kk} + 2\mu\varepsilon_{ij} - (3\lambda + 2\mu)\delta_{ij}\alpha_T(T - T_o) \tag{13}$$

where λ,μ are the Lame constants, α_T is the coefficient of thermal expansion, and T_o is the uniform temperature in the reference (unstrained) state. Substituting (13) and (2) into (12) leads to

$$k\frac{\partial^2 T}{\partial x_i \partial x_i} = \rho C_v \frac{\partial T}{\partial t} + T(3\lambda + 2\mu)\alpha_T \dot{\varepsilon}_{kk} \tag{14}$$

Linearization (by fixing T at a constant value) leads to the coupled theory of thermoelasticity. Neglecting the last term leads to the familiar governing differential equation of linear heat conduction

$$\kappa\nabla^2 T = \frac{\partial T}{\partial t} \tag{15}$$

where the thermal diffusivity, κ, is defined by

$$\kappa = \frac{k}{\rho C_v} \tag{16}$$

This development is a summary of the more comprehensive treatment given in standard sources, such as Boley and Weiner[1]. Numerous solutions to Equation (15) for various boundary conditions are given in the standard work on heat conduction in solids[2]. Solutions of particular interest to laser heating problems have also been identified[3].

---

[1]Boley, B. A. and Weiner, J. H., Theory of Thermal Stresses, John Wiley, New York, 1960.

[2]Carslaw, H. S. and Jaeger, J. C., Conduction of Heat in Solids, Oxford University Press, 1959.

[3]Torvik, P. J., Thermal Response Calculations and Their Role in the Design of Experiments, AFIT TR 73-6, 1973.

The strains ϵ_{ij} are related to displacements, U_i, through

$$\epsilon_{ij} = \frac{1}{2} \left(\frac{\partial U_i}{\partial x_j} + \frac{\partial U_j}{\partial x_i} \right) \tag{17}$$

in the infinitesimal theory. Conservation of linear momentum requires that

$$\frac{\partial \sigma_{ij}}{\partial x_j} = \rho \ddot{U}_i \tag{18}$$

where the stresses σ_{ij} are related to strains through Equation (13) and, hence, to displacements. Substitution of (13) and (17) into (18) produces

$$(\lambda + \mu) \frac{\partial}{\partial x_i} \left(\frac{\partial U_k}{\partial x_k} \right) + \mu \frac{\partial^2 U_i}{\partial x_j \partial x_j} - (3\lambda + 2\mu) \alpha_T \frac{\partial T}{\partial x_i} = \rho \frac{\partial^2 U_i}{\partial t^2} \tag{19}$$

The problem of uncoupled thermoelasticity is the solution of Equation (19) where the temperature gradients are determined from the solution of (15) subject to appropriate boundary conditions.

A. Static Thermal Stresses

Thermal stress arising from a static temperature field will not be encountered frequently with high levels of incident intensity, but one particular case is of such significance as to merit consideration.

Consider a flat sheet of thickness l and large lateral dimension. Energy is absorbed at rate I_a per unit area, per unit time, uniformly over a circle of radius a. We assume that the temperature under the beam, T_1, is essentially uniform and steady. An energy balance on the disk of thickness l and radius a immediately under the beam leads to

$$I_a \pi a^2 = 2(\pi a^2)[hT_1 + \epsilon\sigma\{(T_o + T_1)^4 - T_o^4\}] - 2\pi alk \left.\frac{\partial T}{\partial r}\right|_{r=a} \tag{1}$$

The first term on the right represents losses to the surroundings at temperature T_o, and the second, losses from the heated disk due to radial conduction. For simplicity, the loss term may be approximated by

$$h^*T_1 = (h + \epsilon\sigma\bar{T}^3)\, T_1 \tag{2}$$

where

$$\bar{T}^3 = [(T_o + T_1)^2 + T_o^2][2T_o + T_1] \tag{3}$$

T_1 being the maximum temperature reached relative to the surroundings, ϵ being the emissivity, σ being the Stefan-Boltzman constant, and T_1 being the final temperature of the heated disk measured with respect to the temperature of the surroundings.

The approximation of a uniform temperature under the heated spot is appropriate from two points of view. First, the precise details of the temper-

ature distribution are dependent on local properties of the beam, generally not well characterized. Secondly, local surface melting under the beam will serve to "smear" the temperature into a uniform value, namely, the melting temperature. It is presumed in Equation (1) that the thermal inertia is negligible, i.e.

$$\rho C_p \pi a^2 l \dot{T} \ll I_a \pi a^2 \tag{4}$$

Outside the heated region, $r \geq a$, we have

$$k\nabla^2 T - 2h^* T/l = \rho C_p \dot{T} \tag{5}$$

with boundary conditions $T(r) = T_l$, $T(\infty) = 0$, and the gradient at $r = a$ given by Equation (1). Again neglecting the thermal inertia and defining a Biot number

$$\beta = \frac{h^* l}{k} \tag{6}$$

we find

$$T = AK_o(\sqrt{2\beta}\, r/l) \tag{7}$$

where

$$A = T_l(K_o(\sqrt{2\beta}\, a/l))^{-1} \tag{8}$$

Here K_o is the modified Bessel function of the second kind and order zero. If $T_l \leq T_m$, the melting temperature, we see from Equation (1) that

$$I_a \leq 2h^* T_l + 2\frac{k}{a}\sqrt{2\beta}\,\frac{K_1(\sqrt{2\beta}\, a/l)}{K_o(\sqrt{2\beta}\, a/l)}\, T_l \tag{9}$$

We may expect losses from the heated area to the surroundings (the first term on the right hand side) to be negligible compared to losses due to radial conduction (the second term). For small arguments,

$$K_o(z) \sim -\ln z \tag{10a}$$

$$K_1(z) \sim 1/z \tag{10b}$$

Thus

$$T_1 \sim \frac{I_a a^2}{2k1} \ln \left(\frac{1}{a\sqrt{2\beta}}\right) \quad \text{when } \sqrt{2\beta}\,\frac{a}{1} << 1 \tag{11}$$

and the temperature for small r decays logarithmically.

From the temperature distribution

$$T = T_1 \qquad r \leq a \tag{12a}$$

$$T = T_1 \frac{K_o(\sqrt{2\beta}\ r/1)}{K_o(\sqrt{2\beta}\ a/1)}, \quad r \geq a \tag{12b}$$

with T_1 given by (9) or (11), as appropriate, we may compute thermal stresses using results given previously.[1]

For any axially symmetric temperature distribution T(r), the stresses and displacements are:

$$\sigma_{rr} = \frac{-\alpha E}{r^2} \int_c^r Tr\,dr + \frac{EC_1}{1-\nu} - \frac{EC_2}{(1+\nu)r^2} \tag{13}$$

$$\sigma_{\theta\theta} = \frac{\alpha E}{r^2} \int_c^r Tr\,dr - \alpha ET + \frac{EC_1}{1-\nu} + \frac{EC_2}{(1+\nu)r^2} \tag{14}$$

[1] Boley, B. A. and Weiner, J. H., Theory of Thermal Stresses, John Wiley, New York, 1960, pp 288-290.

$$U_r = \frac{(1+\nu)\alpha}{r} \int_c^r Trdr + C_1 r + \frac{C_2}{r} \tag{15}$$

for arbitrary C. Here we require:

in Region I: ($r < a$) that U_r remain bounded.

in Region II: $r > a$ that $\sigma_{rr} = 0$ as $r \to \infty$.

on $r = a$ that the normal traction and displacements of Region I match those of Region II. If we neglect the change in modulus resulting from the temperature increase, for $r \leq a$:

$$\sigma_{rr} = -E\alpha T_1/2 \tag{16}$$

$$\sigma_{\theta\theta} = -E\alpha T_1/2 \tag{17}$$

$$U_r = (1+\nu)\alpha T_1 r/2 \tag{18}$$

for $r \geq a$:

$$\sigma_{rr} = \frac{-\alpha E}{r^2} \int_a^r rTdr - \frac{ET_1\alpha a^2}{2r^2} \tag{19}$$

$$\sigma_{\theta\theta} = \frac{\alpha E}{r^2} \int_a^r rTdr + \frac{ET_1\alpha a^2}{2r^2} - E\alpha T \tag{20}$$

$$U_r = \frac{\alpha(1+\nu)}{r} \int_a^r rTdr + (1+\nu) \frac{\alpha T_1 a^2}{2r} \tag{21}$$

For the temperature field given by Equations (7) and (8), for $r > a$

$$\int_a^r rTdr = \frac{T_1}{K_o(pr)} \cdot \frac{1}{p^2} [paK_1(pa) - prK_1(pr)] \tag{22}$$

where

$$p \equiv \sqrt{2\beta}/l \tag{23}$$

and T_1 is determined from the incident flux through Equation (9). Hence

$$\sigma_{rr} = -\frac{\alpha E T_1}{(pr)^2}\left\{\frac{[paK_1(pa) - prK_1(pr)]}{K_o(pa)} + \frac{(pa)^2}{2}\right\} \tag{24}$$

$$\sigma_{\theta\theta} = \frac{\alpha E T_1}{(pr)^2}\left\{\frac{[paK_1(pa) - prK_1(pr)]}{K_o(pa)} + \frac{(pa)^2}{2} - (pr)^2\,\frac{K_o(pr)}{K_o(pa)}\right\} \tag{25}$$

We note σ_{rr} to be everywhere compressive but that $\sigma_{\theta\theta}$ becomes tensile for $r > r^*$ where

$$pa\left\{K_1(pa) + \frac{paK_o(pa)}{2}\right\} = pr^*\{K_1(pr^*) + pr^*K_o(pr^*)\} \tag{26}$$

For large values of pa, asymptotic expansions may be used to give:

$$\frac{1}{2}(pa)^{3/2}\,e^{-pa} = (pr^*)^{3/2}\,e^{-pr^*} \tag{27}$$

Approximate solutions then give the following results

pa	r*/a
5	1.2
10	1.08
20	1.04

From these few values, we see that the ratio r*/a does indeed approach unity for large pa, as expected. Thus, the region of large compressive circumferential stress becomes small, the radius at which tensile stresses develop is reduced, and the magnitude of those tensile stresses increases as pa is increased. Recalling that a large pa corresponds to a poor conductor, and that stresses decay as r increases, we see that large tensile circumferential stresses are a peculiar problem to poor thermal conductors.

One aspect of these results is somewhat astonishing. We note from Equations (16) and (17) that the stresses under the heated region are independent of the value of pa and hence of the quantity:

$$\frac{h^*}{k} \cdot \frac{a^2}{l} \tag{28}$$

i.e., the thermal conductivity outside the heated region does not affect stresses within. Thus, in good conductors, such as ductile metals, large maximum shear stresses will be found under the heated region, but tensile stresses outside will be small. Thus failure will be localized to the heated region. For poor conductors, however, large tensile stresses will also be found outside the heated region, thus introducing the possibility of cracking, or crack growth, in the portions of a target not heated directly.

For computational purposes, let us define

$$F_1(pa) = paK_1(pa) + \frac{(pa)^2}{2} K_o(pa) \tag{29}$$

$$F_2(pr) = prK_1(pr) + (pr)^2 K_o(pr) \tag{30}$$

Then Equation (26) may be rewritten

$$\frac{\sigma_{\theta\theta}}{E\alpha T_1} = \frac{\{F_1(pa) - F_2(pr)\}}{(pa)^2 K_o(pa)} \cdot \left(\frac{a}{r}\right)^2 \tag{31}$$

Figure 1 depicts graphically the functions F_1, F_2 for a range of arguments and shows that small pa does not give rise to small pr. Rather, we note that the radius, r*, at which the circumferential stress becomes tensile remains large. From Equation (31) tensile stresses develop for $F_1(pa) = F_2(pr^*)$. From the graph we may deduce the following

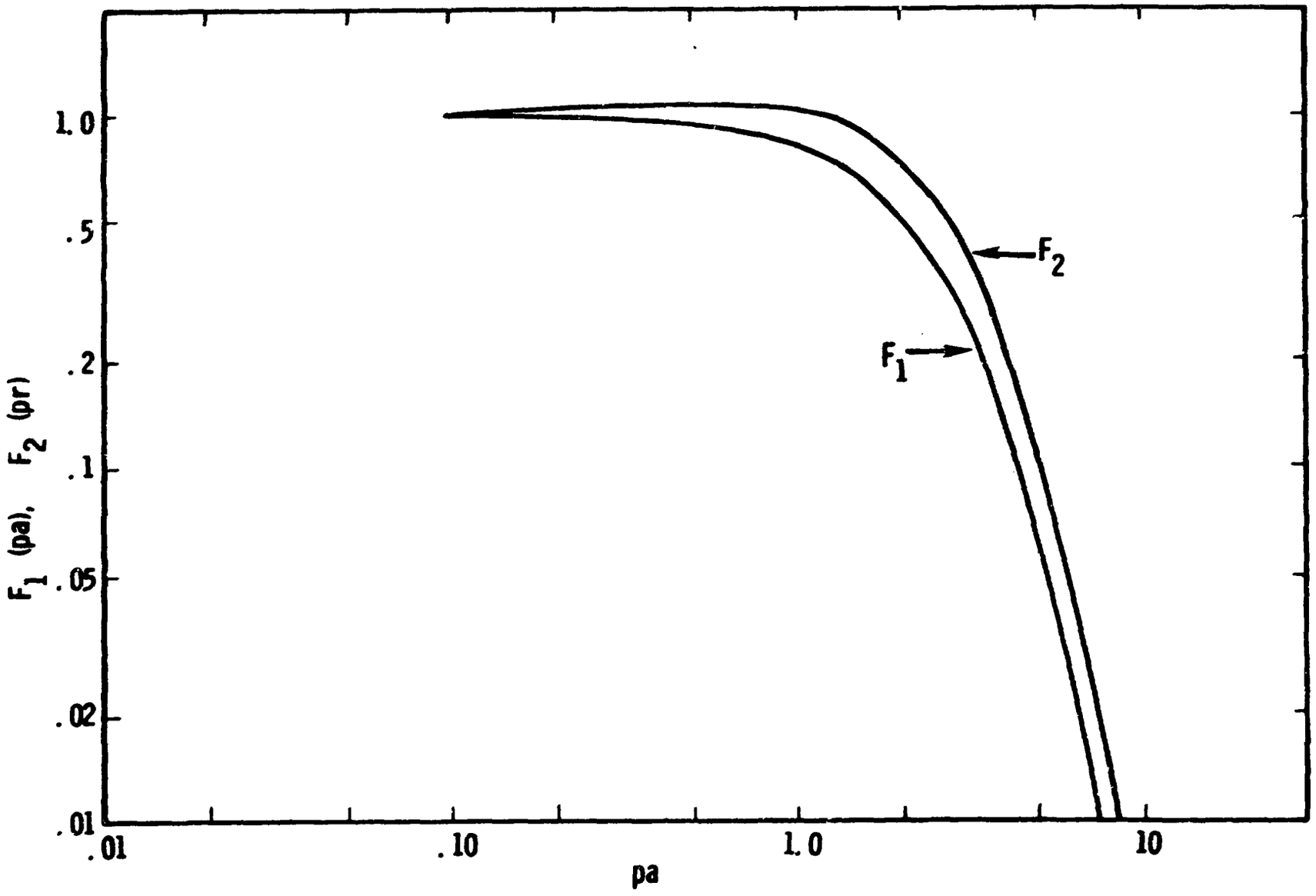

Figure 1. Solution Functions for Stresses at Long Time.

pa	pr*	r*/a
.01	1.2	120
.1	1.2	12
.5	1.4	7
1.0	1.75	1.75
2.0	2.7	1.35
5.0	5.7	~1.14

Because of the decay of stress with r^2 (Equation (31)), the tensile stress which eventually develops in a good conductor will be negligible. Thus tensile stresses of significance, i.e. near to the heated region, will develop only for poor conductors. (It also shows the asymptotic expansions used (Equation (27)) become applicable for pa greater than 5).

Hand computations for a few specific instances demonstrate this phenomenon.

Example 1. For a ceramic material 1/4 cm thick in turbulent flow, under a beam of 10 cm diameter, taking $h = 10^{-3}$ watt/cm^2°C and k = ~.01 Joule/sec cm °C, we find pa ≈ 6. In this case, r*/a ≈ 1.1 and stresses are found as follows from Figure 1 and Equation (31).

r/a	pr	$\sigma_{\theta\theta}/E\alpha T_1$
1.12	6.8	~0
1.16	7	.093
1.2	7.2	.145
1.4	8.4	.257
1.5	9	.256
1.6	9.6	.231
2.0	12	.169

Example 2. A disk of alumina (Al_2O_3) 1/2 cm thick in the same turbulent flow ($h = 10^{-3}$ watt/cm^2°C) with k ~ .2 Joule/sec cm °C and a 6 cm diameter beam leads to pa = .4. In this case, tensile stresses develop at pr* = 1.3. A few stresses are

r/a	pr	$\sigma_{\theta\theta}/E\alpha T_1$
~3	1.3	~0
3.5	1.4	.0161
5	2.0	.0507
6.25	2.5	.0547
7.5	3.0	.0519
9.0	3.6	.045

Example 3. A disk of aluminum (k = 2 Joule/sec cm ^{o}C), otherwise identical to the preceding example leads to pa ~ .1. In this case, tensile stresses develop for pr* = 1.2 or r/a = 12. Some stresses are

r/a	pr	$\sigma_{\theta\theta}/E\alpha T$
12	1.2	~0
14	1.4	.0135
20	2.0	.0267
22	2.2	.0276
25	2.5	.0275
30	3.0	.0257
50	5.0	.0144

For very good conductors k → ∞ and pa → 0. In this case pr* → 1.2 and r* → ∞ as k → ∞. Since $\text{Lim}_{pa\to 0} F_1(pa) \to 1$, we may develop a simple bound on the maximum tensile stress possible in a good conductor. Setting $K_o(pa) = -\ln(pa)$ and

$$F_1(pa) = 1$$

in Equation (31), and differentiating with respect to r, we find that the maximum tensile stress always occurs at pr = 2.32. Hence, a bound on the tensile stress, valid for pa < .3, is

$$\left.\frac{\sigma_{\theta\theta}}{E\alpha T_1}\right|_{max} = -\frac{0.0687}{\ln(pa)} \qquad (32)$$

Thus the tensile stress always develops but at increasingly large ($r/a = 2.32/pa$) distances from the heated area.

It is easy to show that for large pa (the perfect insulator) the maximum tensile stress occurs just outside the heated area and is of magnitude

$$\frac{\sigma_{\theta\theta}}{E\alpha T_1} = \frac{1}{2}$$

These computed values, together with the stress distribution for a perfect insulator ($k = 0$) are sketched in Figure 2. The decrease in the maximum tensile stress for decreasing pa (increasing conductivity) is evident. The bound (Equation (32)) is given as the dashed line and represents the envelope enclosing all peaks obtained for $pa < 0.3$.

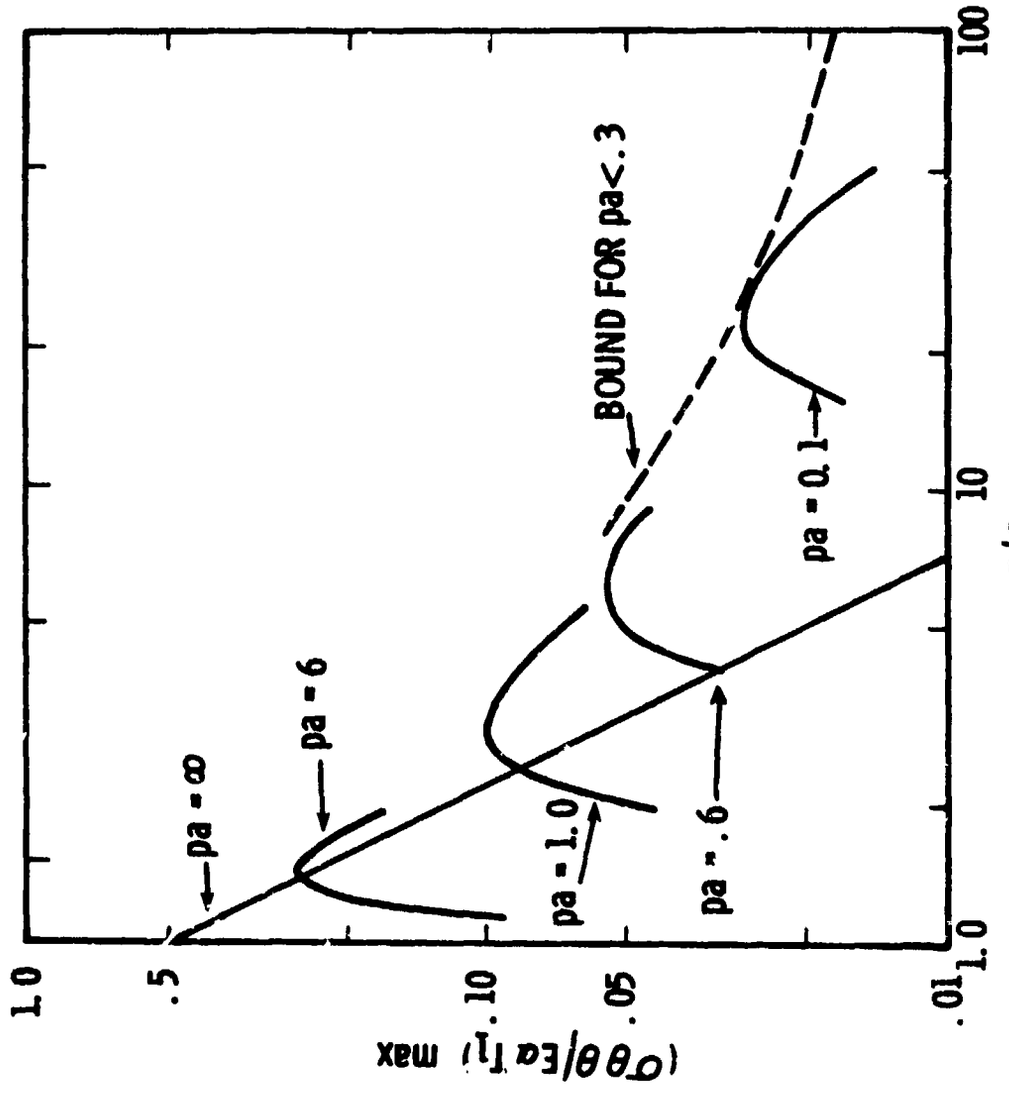

Figure 2. Stress Distribution ($\sigma_{\theta\theta}$) for Various Values of p_a.

B. Quasi-Static Thermal Stresses

1. Local Heating of Thin Sheets

As a first example of a quasi-static thermal stress distribution, let us consider the process whereby the long-time stress distribution given in the preceding section is developed. We first consider the special case of the poor conductor, for which the temperature outside of the heated area remains at the ambient temperature, but assume a uniform temperature $T_1(t)$ for $r \leq a$. These assumptions are appropriate for heating times short compared to radial diffusion times,

$$t_o << t_d = a^2/k \tag{1}$$

but long compared to the thermal diffusion time through a thin sheet

$$t_o << l^2/k \tag{2}$$

In this case

$$T_1 = T_1(t) = \frac{I_a}{\rho C_p l} t \tag{3}$$

for a beam of uniform absorbed intensity I_a.

In consequence of this temperature distribution, thermal expansion occurs over $o < r < a$ which is partially restrained by the surrounding material which is still (since we are ignoring thermal conduction) at $T = T_o$. Thus, the stress field which results is that resulting from forcing a disk of radius

$$a' = a(1 + \alpha T_1) \tag{4}$$

into a hole of radius a in a sheet of the same thickness. The displacements

in the inner and outer regions are the well known radial distributions of the Lame problem,

$$U_i = Ar + B/r \tag{5a}$$

$$U_o = Cr + D/r \tag{5b}$$

matching normal stress on r = a and requiring continuity

$$a' + U_i = a + U_o \tag{6}$$

leads to C = B = 0 and

$$D = a^2\alpha\left(\frac{1+\nu}{2}\right)T_1 \tag{7}$$

$$A = -\alpha\left(\frac{1-\nu}{2}\right)T_1 \tag{8}$$

From which we find

$$\sigma_{rr_i} = -\frac{E\alpha T_1}{2} \tag{9}$$

$$\sigma_{rr_o} = -\frac{E\alpha T_1}{2}\left(\frac{a^2}{r^2}\right) \tag{10}$$

In addition to these radial stresses, circumferential stresses also develop and are of magnitude

$$\sigma_{\theta\theta_i} = -\frac{E\alpha T_1}{2} \tag{11}$$

$$\sigma_{\theta\theta_o} = \frac{E\alpha T_1}{2}\left(\frac{a^2}{r^2}\right) \tag{12}$$

for the assumed state of plane stress. It is these tensile stresses outside of the heated region which we may expect to have an effect on crack propagation. The maximum value is

$$\sigma_{\theta\theta_{max}} = \frac{E\alpha T_1}{2} \tag{13}$$

In a ductile material, some yielding is to be expected when the maximum shear stress exceeds a critical value. In the heated region,

$$\tau_{max_i} = \frac{E\alpha T_1}{4} \tag{14}$$

everywhere, and outside the heated region

$$\tau_{max_o} = \frac{E\alpha T_1}{2} \tag{15}$$

at the edge of the heated zone.

We may note a fracture criterion for a brittle material which is a poor thermal conductor. Under these conditions, a uniform deposition of energy Q over a circle of radius a will lead to fracture if

$$Q_{crit} = 2\sigma_{crit} a^2 \left(\frac{\rho C_p}{E\alpha}\right) \tag{16}$$

and σ_{crit} is the tensile stress producing fracture.

We may take thermal softening into account. If the modulus of the heated material is

$$E(T_1) = E_1 \tag{17}$$

then the matching of stresses and displacements at r = a leads to

$$D = T_1 a^2 \alpha \div \left[1 + \frac{1 - \nu}{1 + \nu} \frac{E_o}{E_1}\right] \tag{18a}$$

$$A = - T_1 \alpha \div \left[1 + \frac{E_1}{E_o} \left(\frac{1 + \nu}{1 - \nu}\right)\right] \tag{18b}$$

and stresses

$$\sigma_{rr_i} = - T_1 \alpha \div \left[\frac{1 - \nu}{E_1} + \frac{1 + \nu}{E_o}\right] \tag{19}$$

$$\sigma_{\theta\theta_i} = - T_1 \alpha \div \left[\frac{1 - \nu}{E_1} + \frac{1 + \nu}{E_o}\right] \tag{20}$$

$$\sigma_{rr_o} = - T_1 \alpha \left(\frac{a^2}{r^2}\right) \div \left[\frac{1 - \nu}{E_1} + \frac{1 + \nu}{E_o}\right] \tag{21}$$

$$\sigma_{\theta\theta_o} = T_1 \alpha \left(\frac{a^2}{r^2}\right) \div \left[\frac{1 - \nu}{E_1} + \frac{1 + \nu}{E_o}\right] \tag{22}$$

The maximum tensile stress again occurs just outside the heated region and is

$$\sigma_{\theta\theta_{max}} = \frac{E_o \alpha T_1}{\left[(1 + \nu) + \frac{E_o}{E_1} (1 - \nu)\right]} \tag{23}$$

If the temperature is such that the modulus is reduced by 50%, and $\nu = 1/3$, then the maximum tensile stress can be seen to be 75% of the value observed without the thermal softening effect. The maximum shear stresses are also readily seen to be reduced by the thermal softening effect in the same ratio

$$\frac{\tau_{\text{max softened}}}{\tau_{\text{max nominal}}} = \frac{2}{\left[(1 + \nu) + \frac{E_o}{E_1} (1 - \nu)\right]} \tag{24}$$

Thus, while thermal softening relieves some of the stresses, it does not eliminate them completely.

As a demonstration of the manner in which thermal softening within the heated region curtails the development of tensile stresses outside, let us consider a hypothetical material, for which

$$E(T) = E_o \cos\left(\frac{\pi}{2} \frac{T}{T_m}\right) \tag{25}$$

Heating is presumed to occur in accord with Equation (3), and tensile stresses as given by Equation (22) to develop.

We find

$$\frac{\sigma_{\theta\theta_{max}}}{E\alpha T_m} = \frac{t}{t_m} \left[(1 + \nu) + (1 - \nu) \sec\left(\frac{\pi}{2} \frac{t}{t_m}\right)\right]^{-1} \tag{26}$$

where

$$t_m = \rho C_p l T_m / I_a \tag{27}$$

is the time required to produce meeting. This result is depicted graphically as Figure 3.

Let us now consider the occurrence of yielding in the heated region of an elastic, perfectly plastic material of negligible thermal conductivity, recognizing that these two assumptions are in large part mutually exclusive, for those materials which yield plastically, e.g. metals, tend to be good thermal conductors. As is well known, ductile metals have yield points which are strongly temperature dependent. Thus, if the process described in the preceding progresses to some temperature such that

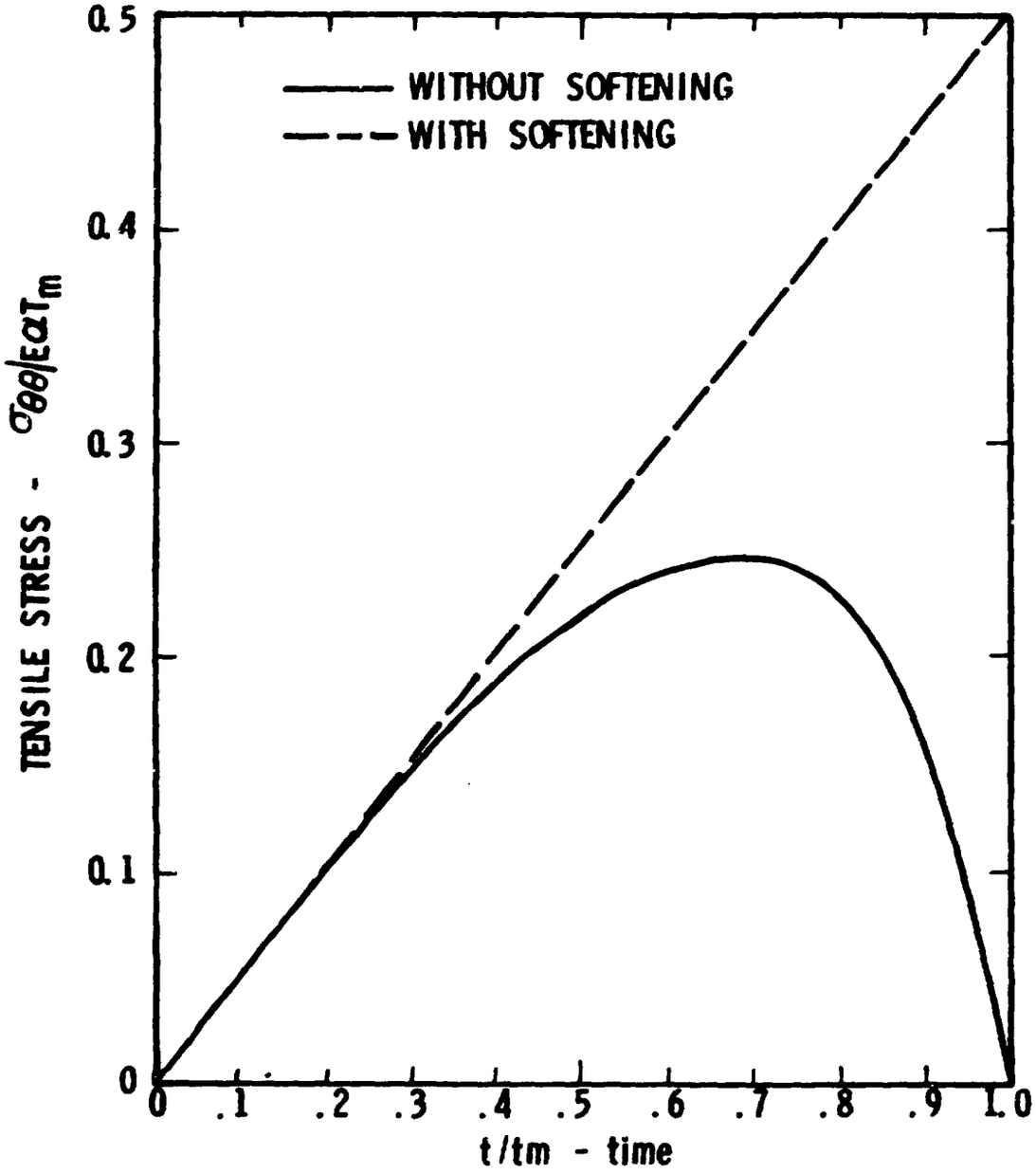

Figure 3. Thermal Stress (Tensile) in Hypothetical Material.

$$\sigma_{rr_i} = \sigma_{\theta\theta_i} = \frac{E\alpha T_1}{2} = \sigma_y(T_1) \tag{28}$$

further heating will not increase the stresses for either $r < a$ or $r > a$. Rather, further heating will reduce the yield points and hence the stresses. If heating is stopped at some temperature T_f ($T_1 < T_f < T_m$), the stress distribution at that time will be

$$\sigma_{rr_i} = \sigma_{\theta\theta_i} = \sigma_{rr_o} = -\sigma_{\theta\theta_o} = -\sigma_y(T_f) \tag{29}$$

if thermal softening and heat conduction for $r > a$ is neglected. We now suppose that the entire plate returns to the ambient temperature, and a process of elastic recovery occurs. The stresses which develop during this process are readily seen to be

$$\tilde{\sigma}_{rr_i} = \tilde{\sigma}_{\theta\theta_i} = E\alpha(T_f)/2 \tag{30}$$

$$\tilde{\sigma}_{rr_o} = -\tilde{\sigma}_{\theta\theta_o} = \left\{E\alpha(+T_f)/2\right\}(a^2/r^2) \tag{31}$$

superposing these onto the stresses at the end of the heating period gives the final state of stress inside $r = a$ as

$$\sigma_{rr_i} = \sigma_{\theta\theta_i} = E\alpha\,\frac{T_f}{2} - \sigma_y(T_f) \tag{32}$$

and for $r = a$ in the exterior

$$\sigma_{rr_o} = -\sigma_{\theta\theta_o} = E\alpha\,\frac{T_f}{2} - \sigma_y(T_f) \tag{33}$$

Thus, it is seen that large residual tensile stresses can develop. If

the elastic perfectly plastic material is heated to the melting point, and the melt remains in place, these final stresses can be as large as

$$\sigma_{max} = E\alpha T_m/2 \tag{34}$$

which may be of the order of the yield stress at room temperature. Moreover, these large tensile residual stresses may produce fracture. Thus, a single large pulse, not quite capable of producing melt through, may give rise to mechanical failure. The time history of the process is depicted graphically in Figure 4. The process occurs as follows. During $0 < t < t_1$, heating occurs, (OA) and elastic stresses equal to $\sigma_y(T_1)$ develop. From $t_1 < t < t_f$, heating continues, but the heated disk deforms plastically (AB) and the stresses fall to $\sigma_y(T_2)$. For $t > t_f$, cooling takes place, and the material loads elastically (BC) to the final stress, given by Equation (33). In a work hardening material, the stress at t_f will be greater and the final value, σ_f, reduced.

This damage mechanism appears to be of such significance as to merit further study. In particular, the degree to which radial conduction away from the heated region and strain hardening alleviates the stresses should be examined.

Proceeding in the same manner as in Section A, it can be shown that conduction for $r > a$ during heating does not affect the state of residual stress after cesssation of heating and the establishment of thermal equilibrium. The influence of strain hardening may be developed as follows. We assume the stress strain curve for the material is

$$\sigma = E\varepsilon \text{ for } \sigma < \sigma_y \tag{35a}$$

$$\sigma = \sigma_y + \beta E(\varepsilon - \sigma_y/E) \text{ for } \sigma > \sigma_y \tag{35b}$$

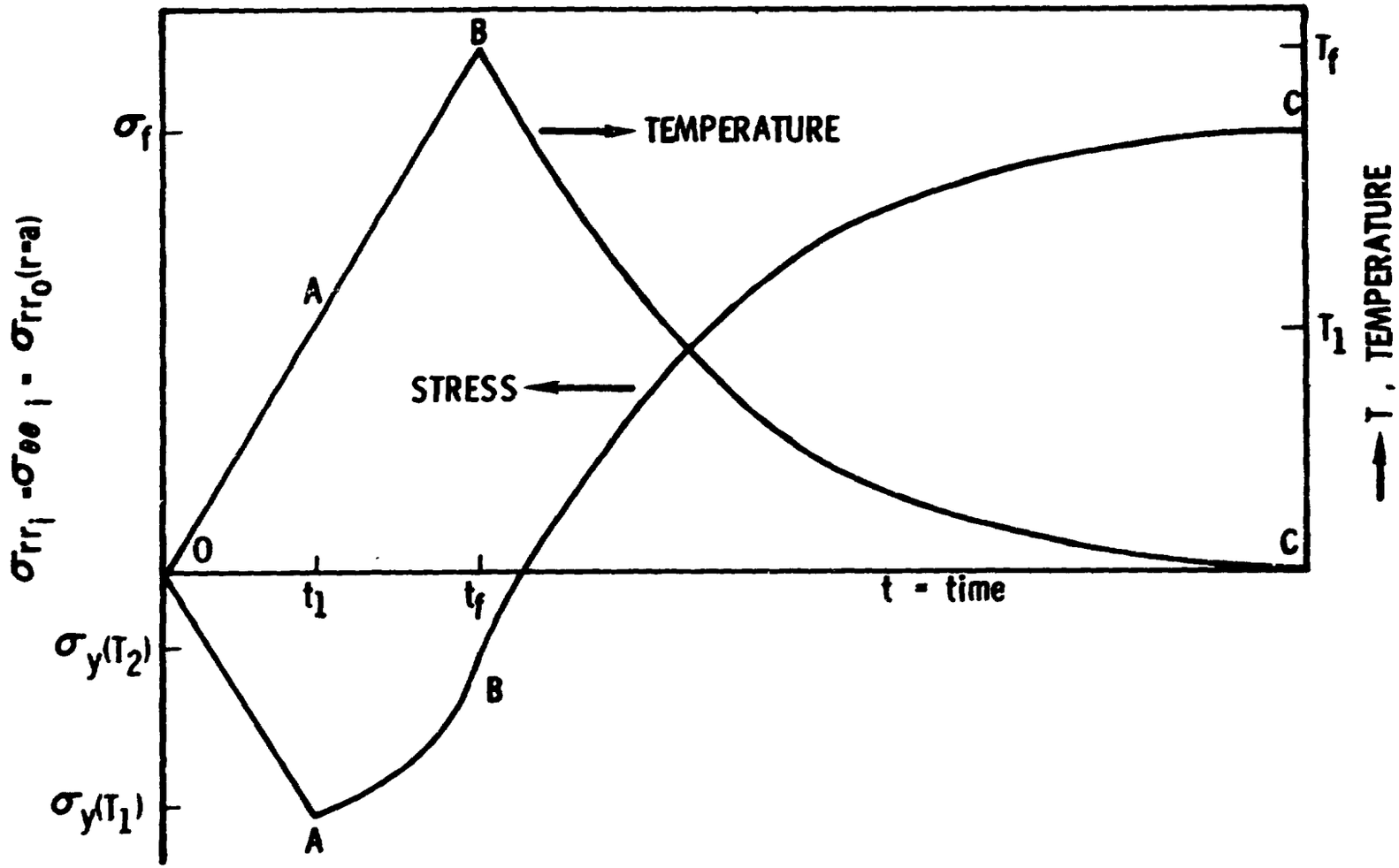

Figure 4. Generation of Residual Stress.

where σ_y is taken to be a function of temperature but E and β are not. This stress-strain curve is depicted graphically as Figure 5.

Let us again suppose the region $r < a$ is again raised to a temperature T_1 and that yield initiates uniformly on $r < a$ according to a maximum shear criterion. We then assume that heating continues to a temperature $T_2 > T_1$ with the final strains being

$$E_{rr} = E_{\theta\theta} = \frac{U(a)}{a} \tag{36}$$

Hence

$$\sigma_{\theta\theta_i} = \sigma_{rr_i} = \sigma_y(T_2)(1 - \beta) + \beta E \frac{U(a)}{a} \tag{37}$$

These radial stresses and displacements must match (at $r = a$) those of the exterior region, $\sigma_{rr} = -C_4E/[(1+\nu)r^2]$ and $U_r = C_4/r$ at $r = a$. Hence

$$C_4 = \frac{+\sigma_y(T_2)(1 - \beta)a^2}{E\{-\beta + \frac{1}{1+\nu}\}} \tag{38}$$

and the stresses in $r < a$ become

$$\sigma_{rr_i} = \sigma_{\theta\theta_i} = \frac{-\sigma_y(T_2)(1 - \beta)}{[1 - (i + \nu)\beta]} \tag{39}$$

while for $r > a$

$$\sigma_{rr_o} = \frac{-\sigma_y(T_2)(1 - \beta)}{[1 - \beta(1 + \nu)]} \frac{a^2}{r^2} \tag{40a}$$

$$\sigma_{\theta\theta_o} = \frac{\sigma_y(T_2)(1 - \beta)}{[1 - \beta(1 + \nu)]} \frac{a^2}{r^2} \tag{40b}$$

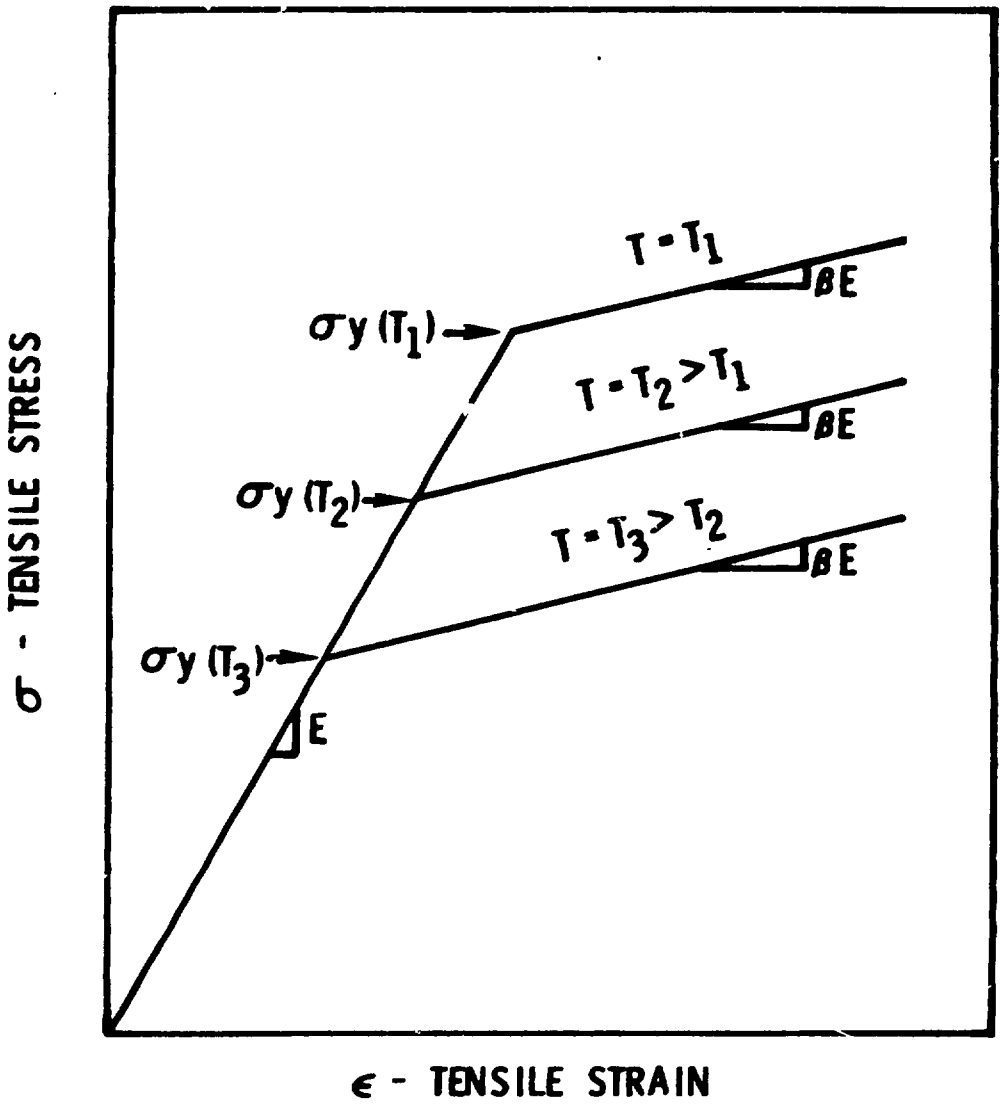

Figure 5. Stress-Strain Relationship for Hypothetical Strain-Hardening Material.

Cooling to the ambient temperature again leads to the superposition of Lame stresses, and the final residual stress state is:

$$\sigma_{rr_i} = \sigma_{\theta\theta_i} = \frac{E\alpha(T_2)}{2} - \frac{\sigma_y(T_2)(1 - \beta)}{[1 - (1 + \nu)\beta]} \tag{41a}$$

$$\sigma_{rr_o} = -\sigma_{\theta\theta_o} = \{\frac{E\alpha T_2}{2} - \frac{\sigma_y(T_2)(1 - \beta)}{[1 - (1 + \nu)\beta]}\} \frac{a^2}{r^2} \tag{41b}$$

We conclude that strain hardening will reduce the magnitude of the residual stresses appreciably only if the final temperature, T_2, is only slightly above the value at which yielding occurred. For example, if the relationship between yield stress is taken to be

$$\sigma_y = \sigma_{y_o}(1 - \frac{T}{1200^\circ C}) \tag{42}$$

which, at least qualitatively, describes data available[1] for several materials,

$$\nu = \frac{1}{3} \tag{43}$$

$$\beta = \frac{1}{3} \tag{44}$$

the residual stress without strain hardening is

$$\sigma_R = \frac{E\alpha T_2}{2} - \sigma_{y_o}(1 - \frac{T_2}{1200^\circ C}) \tag{45}$$

[1] Holmes, B. S., and Desmond, T. P., Thermal Mechanical Damage Study, Monthly Status Report #8, Contract # F29601-78-C-0041, SRI International, May, 1979.

and

$$\sigma_R = \frac{E\alpha T_2}{2} - \frac{6}{5}\sigma_{y_o}\left(1 - \frac{T_2}{1200^\circ C}\right) \qquad (46)$$

if strain hardening is included.

2. Uniform Heating of Plates

In the preceeding section, thermal stresses resulting from radial variations in temperature were considered, while a uniform temperature was assumed through the thickness. We turn now to the other limiting case - that of variations in temperatures through the thickness of a plate, with no temperature variations in the transverse direction, as would be encountered if energy is absorbed at a uniform rate, I_a, over a sufficiently large area.

a. The Free Plate.

We first assume the plate to be free, that is, that there are no boundary constraints. For convenience, we take the plate to be rectangular of thickness h, bounded by planes Z=0 and Z=h.

Ignoring mechanical inertia, we see that a state of plane stress will result, i.e, $\sigma_{ZZ} = 0$. Through considerations of symmetry, we see also that $\sigma_{xy} = 0$ and that $\sigma_{xx} = \sigma_{yy} = \sigma(Z)$. The stress strain relationships then give

$$E\varepsilon_{xx} = (1-\nu)\,\sigma(Z) + E\alpha\,T = EF(Z) \tag{1}$$

$$E\varepsilon_{yy} = (1-\nu)\,\sigma(Z) + E\alpha\,T = EF(Z) \tag{2}$$

and inplane displacements may be obtained through integration of the strains. The result is of the form:

$$U_x = x\,F(Z) + h(Z, y) \tag{3}$$

$$U_y = y\,F(Z) + g(Z, x) \tag{4}$$

The thickness strain, and displacement are (respectively)

$$\varepsilon_{ZZ} = -\frac{2\nu}{E}\,\sigma(Z) + \alpha\,T = G(Z) \tag{5}$$

$$U_Z = \int G(Z)dZ + k(x, y) \tag{6}$$

Shear stresses are then seen to be

$$\sigma_{xZ} = \mu\left\{x\,F'(Z) + \frac{\partial h}{\partial Z} + \frac{\partial k}{\partial x}\right\} \tag{7}$$

$$\sigma_{yZ} = \mu\left\{y\,F'(Z) + \frac{\partial g}{\partial Z} + \frac{\partial k}{\partial y}\right\} \tag{8}$$

Since $\sigma_{xx} = \sigma_{yy} = \sigma(Z)$ and $\sigma_{xy} = 0$, the equilibrium equations require that

$$\frac{\partial \sigma_{xZ}}{\partial Z} = 0 \quad \text{or} \quad XF''(Z) + \frac{\partial^2 h}{\partial Z^2} = 0 \tag{9}$$

$$\frac{\partial \sigma_{yZ}}{\partial Z} = 0 \quad \text{or} \quad yF''(Z) + \frac{\partial^2 g}{\partial x^2} = 0 \tag{10}$$

Since h is independent of x, and g of y, we see that $F' = \text{const} = C_1$. Hence

$$F(Z) = C_1 Z + C_2 \tag{11}$$

and we arrive at a stress disbribution

$$\sigma(Z) = \sigma_{xx} = \sigma_{yy} = \frac{E}{1-\nu} \{C_1 Z + C_2 - \alpha T\} \tag{12}$$

where temperature, T, is measured with respect to an ambient, unstressed, state.

If we require the plate edges to be free, the moment per unit length must vanish, i.e.,

$$M_T = 0 = \int_o^h \sigma(Z - h/2)\, dZ = 0 \tag{13}$$

and the in-plane force per unit length must also vanish, i.e.,

$$F_T = \int_o^h \sigma dZ = 0 \tag{14}$$

These give

$$C_2 = \frac{2\alpha}{h^2} \int_o^h (2h - 3Z)\, T dZ \tag{15a}$$

$$C_1 = \frac{6\alpha}{h^3} \int_o^h (2Z - h)\, T dZ \tag{15b}$$

From which we may deduce the final expression for the thermal stress in a free plate, uniformly heated over one entire face, to be

$$\sigma_{xx} = \sigma_{yy} = \frac{E\alpha}{1-\nu} \left[\frac{6Z}{h^3} \int_o^h (2Z-h)\, T dZ + \frac{2}{h^2} \int_o^h (2h - 3Z)\, T dZ - T \right] \tag{16}$$

It is readily shown that a uniform or linear temperature produces no stress, even if the coefficients are time dependent, as in

$$T = A(t)Z + B(t) \tag{17}$$

For a plate absorbing energy at a rate I_a per unit area, per unit time, on the plane Z = h, with no losses on the face Z = 0, the temperature may be shown to be

$$T(Z,t) = \frac{I_a t}{\rho C_p h} + \frac{I_a h}{2k}\left(Z^2/h^2 - 1/3\right) - \sum_{n=1}^{\infty} \frac{2I_a h}{kn^2\pi^2}(-1)^n e^{-\kappa n^2\pi^2 t/h^2} \cos\left(\frac{n\pi Z}{h}\right) \quad (18)$$

For large values of time, the series makes negligible contributions, and the temperature may be satisfactorily approximated[1] by the first two terms. Of these, the first is recognized as leading to no stress. Thus, for long times, the stresses are generated by the quadratic term in the temperature, and are

$$\sigma_{xx} = \sigma_{yy} = \frac{E\alpha\, I_a h}{2(1-\nu)k}\left[\frac{Z}{h} - \frac{Z^2}{h^2} - \frac{1}{6}\right] \quad (19)$$

The maximum value occurs at the front and rear faces, and is a compressive stress of magnitude

$$\sigma = -\frac{E\alpha\, I_a h}{12(1-\nu)k} \quad (20)$$

The maximum tensile stress occurs at the mid-plane, and is of magnitude

$$\sigma = \frac{E\alpha\, I_a h}{24(1-\nu)k} \quad (21)$$

These, we note, are static stresses even though the generating temperature (Equation 18) increases linearly, with time, at long times.

---

[1] Torvik, P.J., Thermal Response Calculations and Their Role in the Design of Experiments, AFIT-TR-73-6. Also in Proceedings of 1973 DOD Laser Effects and Hardening Conference, Monterey CA, Oct 1973.

At short times, stresses generated by the series terms must also be included

$$\sigma_{trans} = \frac{E\alpha\, I_a\, h}{k(1-\nu)}\left[\frac{2}{\pi^2}\sum\frac{(-1)^n}{n^2} e^{-\kappa n^2\pi^2 t/h^2} \cos\frac{n\pi}{h} Z - \left(\frac{2Z}{h} - 1\right)\frac{24}{\pi^4}\sum_{odd}\frac{1}{n^4} e^{-\kappa n^2\pi^2 t/h^2}\right] \qquad 22$$

This result, with some notational changes, is to be found in Boley[1] and has been shown to be negligible for slowly varying heat inputs. In heat additions which are as step functions in time, as are of interest here, these terms are of significance for short times.

Some numerical results, obtained by Garrison[2], are presented in Figures 6 and 7. In figure 6 the distribution of stress through the thickness is shown for several instants of time. The general increase with time of the peak tensile stress and the movement of the place of occurence to the center of the plate can be seen. At $\kappa t/h^2 > 1$, the stresses are indistinguishable from the static value. The compressive stress at the heated surface first increased and then decreased. These temporal changes are more clearly seen in Figure 7. The peak compressive stress is seen to reach a value in a finite plate some 30% greater than the asymptotic value for long times, as given by Equation 19.

b. The Influence of Constraints.

This simple example of one dimensional temperature variation in a plate presents an opportunity to investigate the influence of mechanical constants at the boundary on the stress distribution. Computing the solutions for the displacement (using the symmetry of x and y axes), we find

$$U_x = C_1\, x\, Z + C_2 x + D \qquad (23a)$$

$$U_y = C_1\, y\, Z + C_2 y + D \qquad (23b)$$

$$U_Z = \int_o^Z \left\{\frac{(1+\nu)}{1-\nu}\alpha T - \frac{2\nu}{1-\nu}(C_1 Z + C_2)\right\} dZ - \frac{C_1}{2}(x^2 + y^2) + E \qquad (23c)$$

---

[1]Boley and Wiener, p 285.

[2]Garrison, Jan N., Thermal Stresses as a Laser Heating Damage Mechanism, AFIT Thesis, GAE/MC/75-4, November 1976.

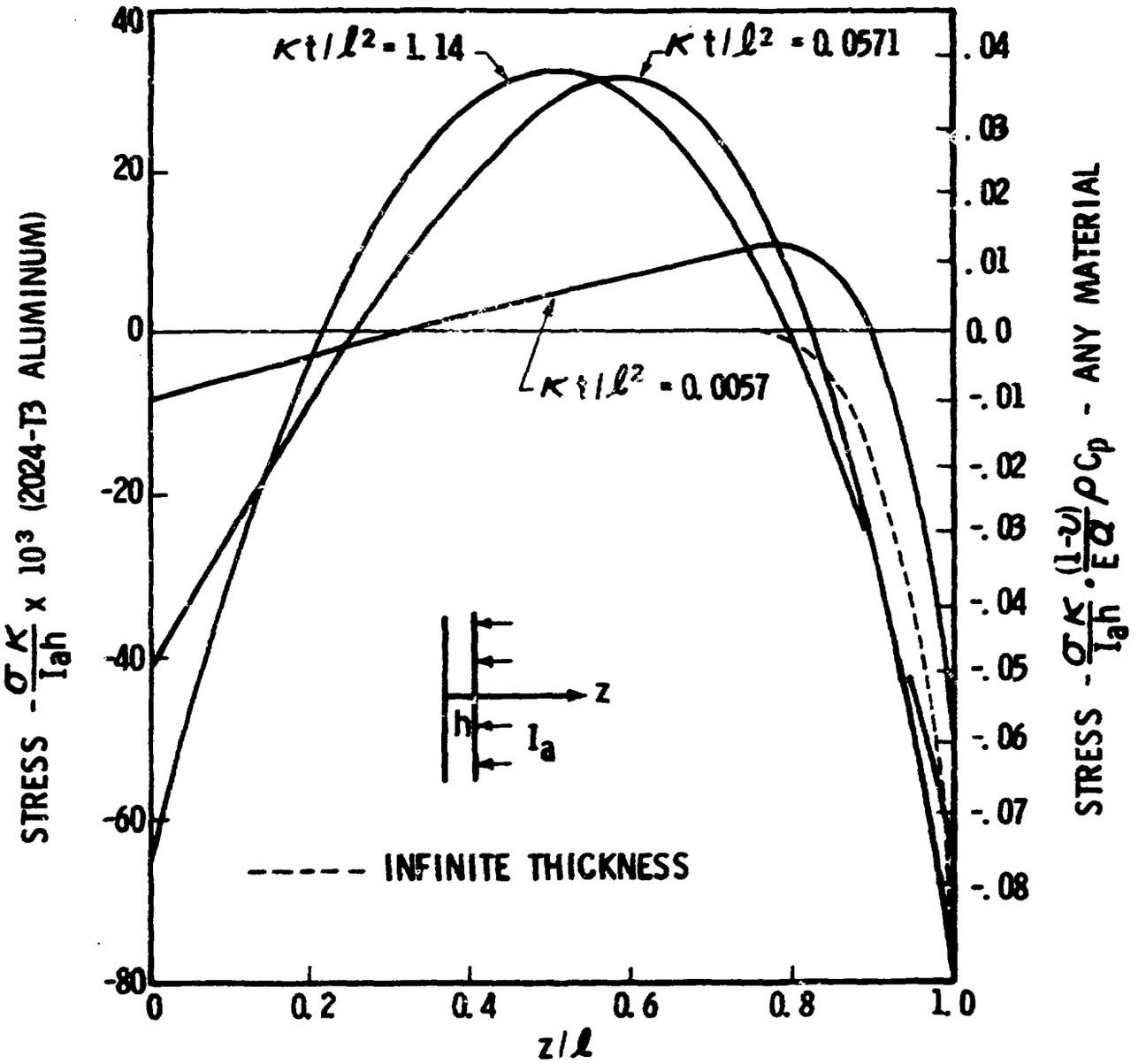

Figure 6. Transient Thermal Stress Distribution for One-Dimensional Axial Heat Flux (Dimensionless).

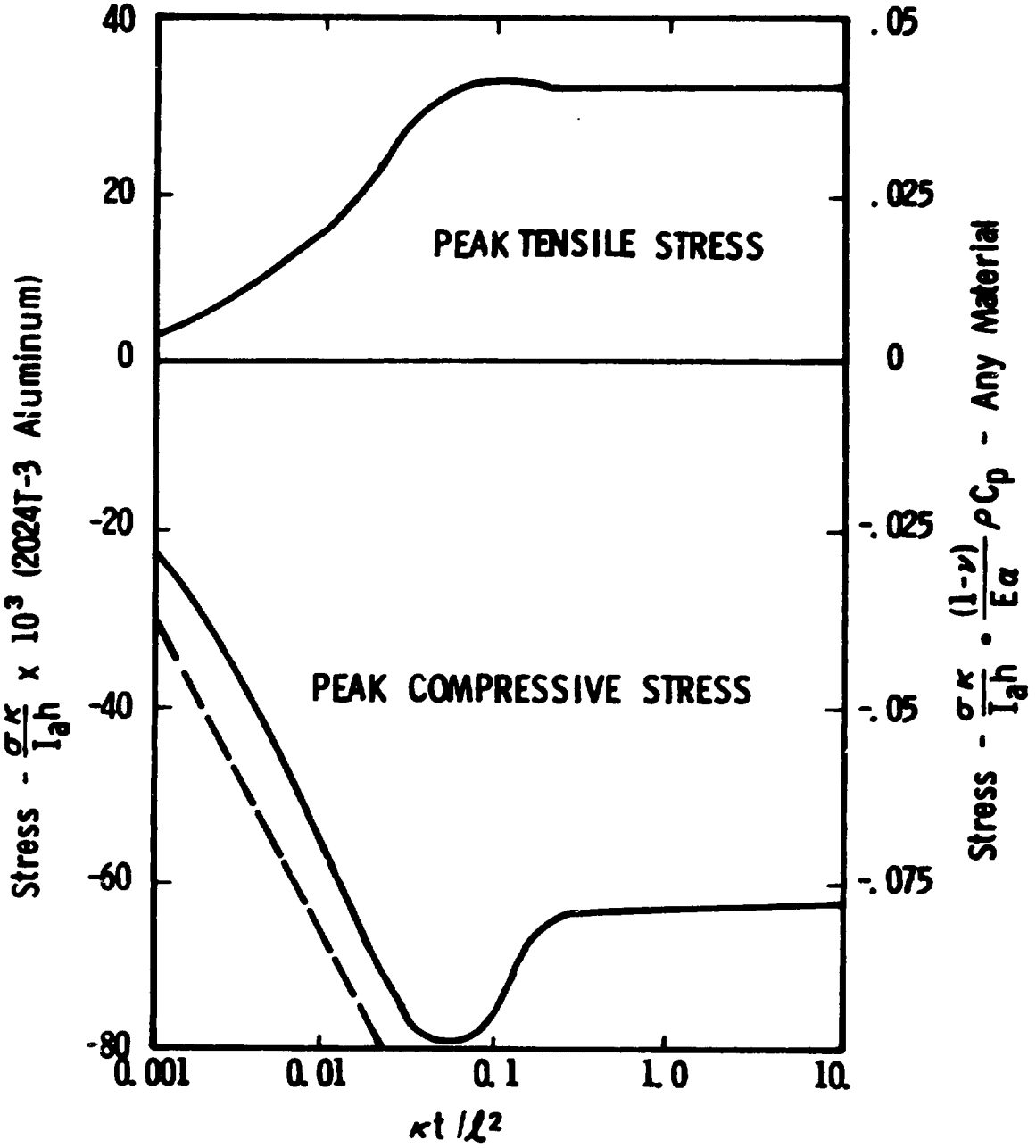

Figure 7. Peak Thermal Stress Versus Dimensionless Heating Time for One-Dimensional Axial Heat Flux (Dimensionless).

As our example, we consider a square plate with side length a, bounded by x = 0, y = 0, x = a, y = a. Four possible boundary conditions are possible:

I The edges free.

II The edges constrained to prevent rotation, but in-plane expansions freely allowed.

III The edges constrained against in-plane displacement at the mid-plane, but rotations allowed.

IV The edges constrained against both displacement and rotations.

The stresses for case I are those of Equation 16.

If no rotations are allowed, inspection of the displacements reveal that $C_1 = 0$. Ensuring the absence of in-plane forces requires

$$\int_o^h \sigma dZ = 0 \tag{24}$$

or

$$C_2 = \frac{\alpha}{h} \int T dZ \tag{24}$$

hence the stresses are, for case II,

$$\sigma_{xx} = \sigma_{yy} = \frac{E\alpha}{1-\nu} \{\frac{1}{h} \int_o^h T dZ - T\} \tag{25}$$

If now we require that in-plane displacements vanish, for Z = h/2, on the boundary, we see from equation 23 that

$$C_2 = \cdots h/2 \tag{26}$$

Vanishing of edge moment requires that

$$\int_o^h (Z - h/2)\, \sigma\, (Z)\, dZ = 0 \tag{13}$$

or

$$C_1 = -\frac{12\alpha}{h^3} \left(\frac{h}{2} \int_o^h T dZ - \int_o^h ZT dZ\right) \tag{27a}$$

$$C_2 = \frac{6\alpha}{h^2} \left(\frac{h}{2} \int_o^h T dZ - \int_o^h ZT dZ\right) \tag{27b}$$

Finally, for case III.

$$\sigma_{xx} = \sigma_{yy} = \frac{E\alpha}{1-\nu}\left\{\frac{6}{h^2}\left(\frac{h}{2}\int_o^h T\,dZ - \int_o^h ZT\,dZ\right) - \frac{12Z}{h^3}\left(\frac{h}{2}\int_o^h T\,dZ - \int_o^h ZT\,dZ\right) - T\right\} \quad (28)$$

The fourth case arises for $U_x = U_y = 0$ for all x, y, t, or $C_1 = 0 = C_2 = 0$. Then

$$\sigma_{xx} = \sigma_{yy} = \frac{E\alpha}{1-\nu}(-T)$$

In order to assess the influence of edge constraints on the stresses, let us put the temperature distribution for long times (Equations 18) into the form

$$T(Z,t) = \frac{I_a h}{k}\left[\tau + \frac{1}{2}\left(Z^2/_{h^2} - 1/3\right)\right] \quad (29)$$

where

$$\tau = \frac{\kappa t}{h^2}$$

is the dimensionless time previously introduced
Then the stresses are found to be, in each case:

I. For no edge constraints:

$$\sigma_{xx} = \sigma_{yy} = \frac{E\alpha}{1-\nu}\left(\frac{I_a h}{k}\right)\left\{\frac{Z}{2h} - \frac{Z^2}{2h^2} - 1/12\right\} \quad (31)$$

II. For edges constrained to prohibit rotation only (expansion permitted)

$$\sigma_{xx} = \sigma_{yy} = \frac{E\alpha}{1-\nu}\left(\frac{I_a h}{k}\right)\left\{\frac{1}{6} - \frac{Z^2}{2h^2}\right\} \quad (32)$$

III. For edges constrained to prohibit expansion only (rotation permitted)

$$\sigma_{xx} = \sigma_{yy} = \frac{E\alpha}{1-\nu}\left(\frac{I_a h}{k}\right)\left\{-\tau - \frac{Z^2}{2h^2} + 1/2\ Z/h - 1/12\right\} \quad (33)$$

IV. For edges constrained to prohibit both rotation and displacement

$$\sigma_{xx} = \sigma_{yy} = \frac{E\alpha}{1-\nu}\left(\frac{I_a h}{k}\right)\left\{-\tau + \frac{1}{6} - \frac{Z^2}{2h^2}\right\} \quad (34)$$

In all cases the maximum stress is compressive, and occurs at the heated face and is independent of plate size. We note that it is the in-plane constraints rather than the bending constraint which generates the large stresses at long times. At shorter times however, $\tau \sim .25$ or less, we note that greater stresses are generated through the bending constraint. Although these simple expressions are not valid for values of τ much smaller than this value, the same generalization is valid for very small τ.

At very short times, $\tau << 1$, we may regard the plate as being of infinite thickness. In this case,

$$T(Z,t) = \frac{2I_a}{k}\sqrt{\kappa t}\ \text{ierfc}\left(\frac{Z}{2\sqrt{\kappa t}}\right) \tag{35}$$

where Z is now measured into the slab, with Z = 0 being the heated face. Recognizing that the unheated (and therefore unexpanded) mass of thick plate serves as a constraint on the heated surface layer, the stresses are (from case IV)

$$\sigma_{xx} = \sigma_{yy} = -\frac{E\alpha T}{1-\nu} \tag{36}$$

The maximum stress is again compressive, at the surface, and given by:

$$\sigma_{xx}(0,t) = \sigma_{yy}(0,t) = -\frac{E\alpha}{1-\nu}\frac{2I_a}{k}\sqrt{\frac{\kappa t}{\pi}} \tag{37}$$

The dashed line of Figure 6 shows the stress at the surface computed from Equation 37. These values, which are analogous to complete constraint, are slightly greater, at small times than the numerical results obtained for the free plate. The stresses in the thick slab decay rapidly with depth according to

$$\sigma_{xx} = \sigma_{yy} = -\frac{E\alpha}{1-\nu}\frac{2I_a}{k}\sqrt{\kappa t}\ \text{ierfc}\left(\frac{Z}{2\sqrt{\kappa t}}\right) \tag{38}$$

with values at times comparable to $\kappa t/h^2 = .0057$. Computed results have been added (in dashed lines) to Figure 7 for purposes

of comparison with the results obtained for the plate of finite thickness. The rapid decay from the surface is evident. From a table of values of the ierfc function, it may be deduced that the stresses fall to 10% of the surface value at a depth $Z \sim 2\sqrt{\kappa t}$, and to 1% of the surface value at a depth of $Z \sim 3\sqrt{\kappa t}$.

C. Thermal Shock

As a first example of a problem wherein the effects of thermal inertia, as well as mechanical inertia, are significant, we consider a thin elastic plate, circular in planform, and supported at the outer periphery (clamped, or simply supported). A uniform energy flux I_a is absorbed over the entire surface, commencing at t = 0. Thus we assume a through-the-thickness temperature variation only, which generates a thermal moment. The response of the plate to the uniform, but time varying moment is desired.

We let w(r,t) be the deflection of the mid plane of a plate bounded by $-h/2 < z < h$. Then, using elementary plate theory

$$u_r = - z \frac{\partial w}{\partial r} \quad ; \quad u_\theta = 0 \qquad \text{and} \tag{1}$$

$$\epsilon_{rr} = - z \frac{\partial^2 w}{\partial r^2} \quad ; \quad \epsilon_{\theta\theta} = - \frac{z}{r} \frac{\partial w}{\partial r} \tag{2}$$

Hence, for a linear elastic material at temperature T above the ambient (unstressed) temperature

$$\sigma_{rr} = \frac{-E}{1-\nu^2} \left[z \frac{\partial^2 w}{\partial r^2} + \frac{\nu z}{r} \frac{\partial w}{\partial r} \right] - \frac{E}{1-\nu} \alpha T \tag{3a}$$

$$\sigma_{\theta\theta} = - \frac{E}{1-\nu^2} \left[\frac{z}{r} \frac{\partial w}{\partial r} + \nu z \frac{\partial^2 w}{\partial r^2} \right] - \frac{E}{1-\nu} \alpha T \tag{3b}$$

We define total moments (per unit length) and a thermal moment, according to

$$M_r = + \int_{-h/2}^{h/2} z\sigma_{rr} dz \tag{4a}$$

$$M_\theta = \int_{-h/2}^{h/2} z\sigma_{\theta\theta} dz \tag{4b}$$

$$M_T = \int_{-h/2}^{h/2} zE\alpha T dz \tag{4c}$$

This produces

$$M_r = -D\left\{\frac{\partial^2 w}{\partial r^2} + \frac{\nu}{r}\frac{\partial w}{\partial r}\right\} - \frac{M_T}{1-\nu} \tag{5a}$$

$$M_\theta = -D\left\{\frac{1}{r}\frac{\partial w}{\partial r} + \nu\frac{\partial^2 w}{\partial r^2}\right\} - \frac{M_T}{1-\nu} \tag{5b}$$

where

$$D = \frac{Eh^3}{12(1-\nu^2)} \tag{6}$$

An obvious division of the total moments into mechanical and thermal components can be made. Since no elongation of fibers on the neutral plane of symmetry is allowed in elementary theory, in-plane stresses will also develop.

From the sign conventions and free body diagrams of Figure 8 we deduce that equilibrium of moments about the θ axis requires that:

$$(M_r + \frac{\partial M_r}{\partial r}dr)(r + dr)d\theta - M_r r d\theta - (M_\theta + \frac{\partial M_\theta}{\partial \theta}rd\theta)drd\theta - Qrdrd\theta = 0 \tag{7}$$

or

$$r\frac{\partial M_r}{\partial r} + (M_r - M_\theta) - Qr = 0 \tag{8}$$

Summing vertical forces gives (from Fig 1d)

$$\int_0^r \hat{\rho}h2\pi\ddot{w}(r,t)rdr = 2\pi rQ \tag{9}$$

Thus one form of the governing equation for the plate is:

$$\frac{\partial M_r}{\partial r} + \left(\frac{M_r - M_\theta}{r}\right) - \frac{1}{r}\int_0^r \rho hr\ddot{w}(r,t)dr = 0 \tag{10}$$

We note, from 5, that

$$M_r - M_\theta = -D(1-\nu)r\frac{d}{dr}\left(\frac{1}{r}\frac{\partial w}{\partial r}\right) \tag{11}$$

We note differentiation produces

$$\frac{\partial}{\partial r}\int_0^r \rho hr\ddot{w}(r,t)dr = \rho hr\ddot{w}(r,t) \tag{12}$$

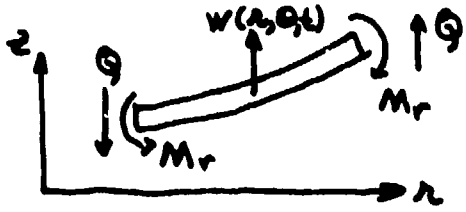

a. Sign Convention

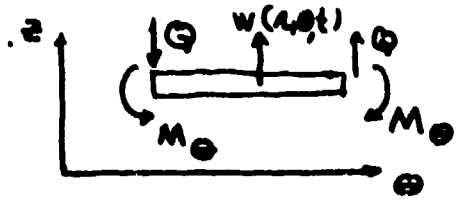

b. Sign Convention

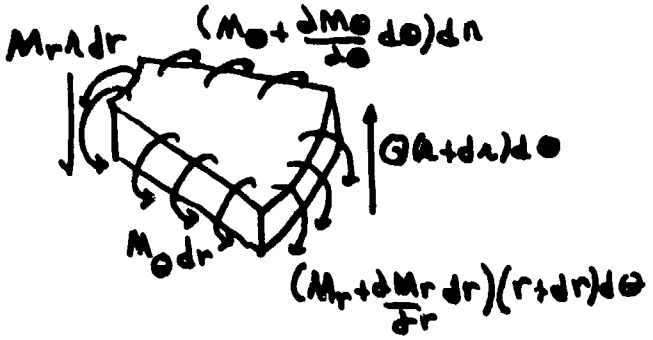

c. Free Body Diagram

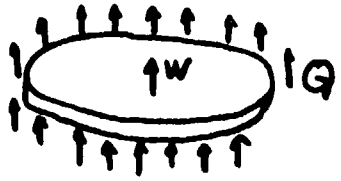

d. Vertical Force

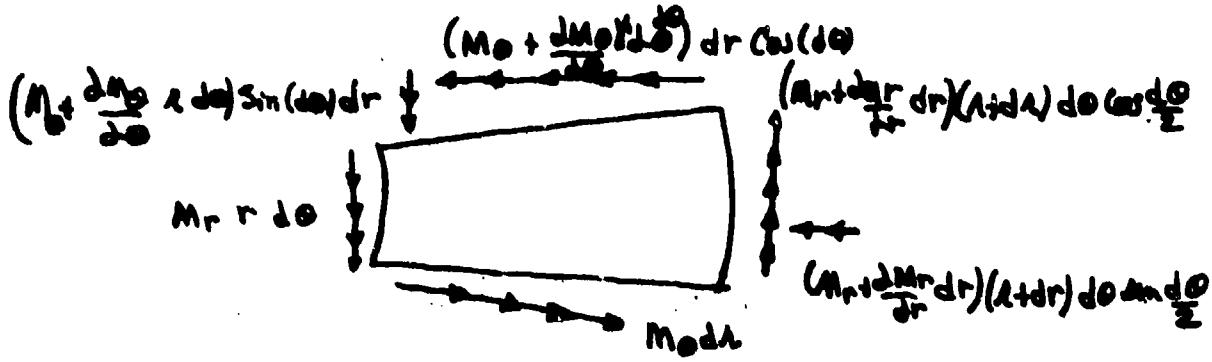

e. Resolution of Moments

Figure 8. Plate Elements.

and that

$$\nabla^2 w = \frac{1}{r}\frac{d}{dr}\left(r\frac{\partial w}{\partial r}\right) \tag{13}$$

for this axisymmetric problem. Differentiating Equation (5a) once gives

$$r\frac{\partial M_r}{\partial r} = -Dr\frac{\partial}{\partial r}\left(\partial^2 w/\partial r^2 + \nu/r\ \partial w/\partial r\right) - \frac{r}{1-\nu}\frac{\partial M_T}{\partial r} \tag{14}$$

Combining with 11, Equation (10) becomes:

$$Dr\left\{\frac{\partial}{\partial r}\nabla^2 w\right\} + \int_0^r \rho h r\ddot{w}(r,t)dr + r\frac{\partial}{\partial r}\left(\frac{M_T}{1-\nu}\right) = 0 \tag{15}$$

which, for static problems, is convenient to integrate. In dynamic problems, we differentiate all terms and divide by r to obtain the differential equation of the vibrating plate

$$D\nabla^4 w + \rho h\ddot{w} + \frac{1}{1-\nu}\nabla^2 M_T = 0 \tag{16}$$

which is to be solved, subject to initial conditions and boundary conditions. If the response to a simultaneous pressure and thermal loading is desired, a prescribed pressure may be added to the right hand side of 16. Such problems will be addressed in a later chapter.

We consider first the simply supported plate. The boundary conditions on r = a are

$$M_r(a,t) = 0 \tag{17a}$$

$$w(a,t) = 0 \tag{17b}$$

with initial conditions

$$w(r,o) = \dot{w}(r,o) = 0 \tag{18}$$

The associated homogeneous problem

$$D\nabla^4 w_H + \rho h\ddot{w}_H = 0 \tag{19}$$

$$M_r = \frac{\partial^2 w_H}{\partial r^2} + \frac{\nu}{r}\frac{\partial w_H}{\partial r} = 0 \quad \text{on} \quad r = a \tag{20a}$$

$$w_H = 0 \quad \text{on} \quad r = a \tag{20b}$$

$$w_H(r,o) = f(r) \tag{21a}$$

$$\dot{w}_H(r,o) = g(r) \tag{21b}$$

has the solution

$$w_H = \sum_{n=1}^{\infty} \{A_n \sin \omega_n t + B_n \cos \omega_n t\} R_n(r) \tag{22}$$

where the eigenfunctions $R_n(r)$ are

$$R_n(r) = J_o(p_n r) - \frac{J_o(p_n a)}{I_o(p_n a)} I_o(p_n r) \tag{23}$$

with

$$\frac{2p_n a}{1-\nu} = \frac{J_1(p_n a)}{J_o(p_n a)} + \frac{I_1(p_n a)}{I_o(p_n a)} \tag{24}$$

The coefficients A_n, B_n are given by

$$\begin{bmatrix} A_n\omega_n \\ B_n \end{bmatrix} = \frac{1}{N_n} \int_o^{\varepsilon} r \begin{bmatrix} g(r) \\ f(r) \end{bmatrix} R_n(r)dr \tag{25}$$

where

$$N_n = \int_o^a r\{R_n(r)\}^2 dr \tag{26}$$

Returning to Equation 16, we expand the left hand side in terms of the eigenfunctions:

Let

$$\frac{1}{1-\nu} \nabla^2 M_T = \sum_{n=1}^{\infty} F_n(t) R_n(p_n r) \tag{27}$$

and let

$$w(r,t) = w^*(r,t) + p(r)q(t) \tag{28}$$

where the functions $p(r)$ and $q(t)$ are to be chosen so as to leave homogeneous

boundary conditions on w^* at $r = a$. Such a choice is

$$p(r) = (a - r) \tag{29}$$

$$q(t) = \frac{a}{\nu D} \frac{M_T(a,t)}{1-\nu} \tag{30}$$

Let

$$\rho h(a-r)\ddot{q} = \sum_{n=1}^{\infty} G_n(t) R_n(p_n r) \tag{31}$$

and

$$w^*(r,t) = \sum W_n(t) R_n(p_n r) \tag{32}$$

Then substitution yields

$$\rho h \ddot{W}_n(t) + D p_n^4 W_n(t) = - (F_n + G_n) \tag{33}$$

where

$$F_n(t) = \frac{1}{N_n} \frac{1}{1-\nu} \int_0^a r \nabla^2 M_T(r,t) R_n(p_n r) dr \tag{34}$$

and

$$G_n(t) = \frac{1}{N_n} \frac{\rho h}{\nu D} \cdot \frac{a M_T(a,t)}{1-\nu} \int_0^a r(a-r) R_n(p_n r) dr \tag{35}$$

The new initial conditions become:

$$w(r,o) = 0 = w^*(r,o) + (a-r)q(o) \tag{36a}$$

$$\dot{w}(r,o) = 0 = \dot{w}^*(r,o) + (a-r)\dot{q}(o) \tag{36b}$$

Thus

$$\sum W_n(0) R_n(p_n r) = - (a-r) \frac{a}{\nu D} \frac{M_T(a,o)}{1-\nu} \tag{37a}$$

$$\sum \dot{W}_n(0) \cdot R_n(p_n r) = - (a-r) \frac{a}{\nu D} \frac{\dot{M}_T(a,o)}{1-\nu} \tag{37b}$$

or

$$W_n(0) = - \frac{a}{\nu D} \frac{M_T(a,o)}{1-\nu} \frac{1}{N_n} \int_0^a r(a-r) R_n(p_n r) dr \tag{38a}$$

$$\dot{W}_n(0) = - \frac{a}{\nu D} \frac{M_T(a,o)}{1-\nu} \frac{1}{N_n} \int_0^a r(a-r) R_n(p_n r) dr \tag{38b}$$

Given a time history of temperature, then, M_T may be computed from Equation 4c, and the time dependent amplitudes determined from equation 33, 34 and 35, with initial conditions given by 38.

The solution for the analogous problem of the beam and the rectangular plate have been given by Boley[1], and the observation made that the results for the thermal vibrations of beams differ but little from those of plates. That being the case, it would appear that the beam results should suffice for the circular plate as well, if the effective beam length is taken to be diameter. The results are expressible in terms of a ratio of dynamic to static deflection,

$$R = \frac{w_{max}}{w_{max\ static}} = \begin{cases} 1 + 2e^{-B_1} & \text{for } B_1 \geq \sim .69 \\ 2 & \text{for } B_1 < \sim .69 \end{cases} \tag{39}$$

where

$$B_1 = \frac{h}{2a\sqrt{\kappa}} \left(\frac{D}{h\rho}\right)^{1/4} \tag{40}$$

and a is the plate radius. Physically, B_1^2 corresponds to the ratio of thermal response time to mechanical response time. The static deflection of a simply supported plate under thermal load is obtained from Equation 16:

$$D\nabla^2\omega + \frac{M_T}{1-\nu} = \text{harmonic function of r only} \tag{41}$$

For a solid plate, with temperature independent of r, and having a simply supported edge,

$$w = \frac{M_T(a^2 - r^2)6}{Eh^3}$$

The stresses are

$$\sigma_{rr} = \frac{12M_T}{(1-\nu)h^3} z - \frac{E}{1-\nu} \alpha T \tag{42a}$$

---

[1] Boley and Weiner, pp 406-409.

$$\sigma_{\theta\theta} = \frac{12M_T z}{(1-\nu)h^3} - \frac{E\alpha T}{1-\nu} \qquad (42b)$$

These, it should be noted, are identical to the stresses obtained in Case III of section B2b, aside from changes in notation.

To account for the dynamic effect (approximately), we may compute the dimensionless ratio B_1, from equation 40, and the stresses from 42, and adjust by multiplying by the ratio R computed from equation 39.

In the case of clamped edges, we note that the boundary conditions are naturally homogeneous, even in the presence of the thermal loading, i.e.,

$$w(a,t) = \frac{\partial w}{\partial r}(a,t) = 0 \ .$$

Hence, for homogeneous initial conditions, we need only solve equation 16. We note immediately that in the special case where the temperature is independent of r, that

$$\nabla^2 M_T = 0$$

Hence, $w(r,t) = 0$ and the stresses for the dynamic problem (thermal shock) are the same as for the quasistatic problem, as no displacements develop. This is correct only to the limits of thin plate theory, which does not provide for "through the thickness displacements" in addition to those of the neutral axis.

III. STRESS GENERATION BY AIR ABSORPTION

A. The Generation of Front Surface Pressures

We consider a laser beam absorbed over a surface of a progressive front, leaving behind a pressure P, density ρ, particle velocity U, measured in an inertial frame. The front is taken to propagate at speed D. By conservation of mass

$$\rho_o D = \rho_f (D-U) \tag{1}$$

By conservation of momentum

$$P_f - P_o = \rho_o DU \tag{2}$$

By conservation of energy

$$E_f - E_o - \Delta E = \frac{P_o + P_f}{2}\left(\frac{1}{\rho_o} - \frac{1}{\rho_f}\right) \tag{3}$$

Aside from ΔE, the energy added per unit mass, these are the familiar Rankine Hugoniot Jump conditions across a shock front.

Here, the added energy per unit mass is computed by observing that, for any area, A, of the front, the laser flux f arriving over time Δt is assumed to be completely absorbed by the volume of material processed during the same interval, i.e.

$$\Delta E = fA\,\Delta t/\Delta m \tag{4}$$

The mass absorbing ΔE is

$$\Delta m = A\rho_o D\Delta t, \tag{5}$$

Hence

$$\Delta E = f/\rho_o D \tag{6}$$

For a perfect gas,

$$E = C_V T \tag{7}$$

$$P = \rho RT \tag{8}$$

$$R = C_P - C_V \tag{9}$$

$$\gamma = C_P/C_V \tag{10}$$

Hence we may put Equations (1), (2), and (3) into the form

$$\frac{1}{\rho_f} = \frac{1}{\rho_o}\left(1 - \frac{U}{D}\right) \tag{11}$$

$$P_f = P_o + \rho_o DU \tag{12}$$

$$\frac{P_f}{\rho_f(\gamma-1)} = \frac{P_o}{\rho_o(\gamma-1)} + \frac{f}{\rho_o D} + \frac{P_f + P_o}{2}\left(\frac{1}{\rho_o} - \frac{1}{\rho_f}\right) \tag{13}$$

The pressure density states achievable for a given f are those given by Equation (13) where D is to be eliminated through (11) and (12). Combining (11) and (12) to eliminate U yields (using $\eta = \rho_o/\rho_f$ as a compression factor)

$$U = D(1-\eta) \tag{14}$$

$$P_f = P_o + \rho_o D^2(1-\eta) \tag{15}$$

and finally

$$P_f = \frac{P_o}{\eta} + \frac{f(\eta-1)}{\eta\sqrt{\frac{P_f - P_o}{\rho_o(1-\eta)}}} + \frac{\gamma-1}{2}(P_f + P_o)\left(\frac{1}{\eta} - 1\right) \tag{16}$$

This is readily solved for P_f if we assume

$$P_o << P_f \tag{17}$$

whence

$$P_f^{3/2} = 2f\sqrt{\rho_o(1-\eta)}\left[\eta\left(\frac{\gamma+1}{\gamma-1}\right) - 1\right]^{-1} \tag{18}$$

This result has been given by Razier[1] who argues that the steady detonation wave occurs when the sonic speed behind the front given by

$$c^2 = \gamma \frac{P_f}{\rho_f} \tag{19}$$

is equal to the shock propagation speed, measured with respect to the wave. The sonic speed from (15) and the definition of η yields

$$c^2 = \gamma D^2(1-\eta)\eta \tag{20}$$

Thus, the condition

$$c = D - U \tag{21}$$

yields, after using (14), that

$$\eta = \frac{\gamma}{\gamma+1} \tag{22}$$

Taking this to Equation (18) yields

$$P_f = \left[2f(\gamma-1)\quad\frac{\rho_o}{\gamma+1}\right]^{2/3} \tag{23}$$

---

[1] Razier, Y. P. "Heating of a Gas by a Powerful Light Pulse," Soviet Physics JETP, Vol. 21, No. 5, 1965, pp. 1009-1017.

Substituting (22) into (15) gives the detonation speed in terms of pressure as

$$P_f = \frac{\rho_o}{\gamma+1} D^2 \tag{24}$$

from which we obtain Razier's result

$$D = \left[\frac{2f}{\rho_o} (\gamma^2-1) \right]^{1/3} \tag{25}$$

for the detonation speed as a function of energy absorbed.

Thus, we expect a cylinder of air to be shocked to this pressure P_f, the length of the cylinder increasing with time as the detonation front propagates up the beam at speed D.

However, the high pressure in the cylinder of air will relax as the cylinder expands radially as a cylindrical blast wave. Initially the cylinder is of beam radius a, and pressure P_f, given by (23). As the cylindrical blast wave expands, the same Rankine Hugoniot Jump relations must be satisfied across the shock, which we take to be strong, i.e.

$$\frac{\rho_f}{\rho_o} = \frac{1}{\eta} = \frac{\gamma+1}{\gamma} \tag{26}$$

Hence the radial particle velocity U_r is related to the shock speed by

$$U_r = \dot{R}(1 - \frac{\gamma}{\gamma+1}) = \frac{\dot{R}}{\gamma+1} \tag{27}$$

and

$$P_f = \frac{\rho_o \dot{R}^2}{\gamma+1} \tag{28}$$

From considerations of similarity, as in the Taylor Blast Wave solution, we note the energy per unit length in the z direction of the expanding cyclinder is

$$E = \int_0^R \{\frac{P(\xi)\rho_o \dot{R}^2}{\rho_f(\gamma-1)} + \frac{\dot{R}^2}{2} U^2(\xi)\} \, 2\pi r dr \tag{29}$$

where

$$\xi = r/R \tag{30}$$

$$P(r) = \rho_o \dot{R}^2 P(\xi) \tag{31}$$

$$U(r) = \dot{R} \, U(\xi) \tag{32}$$

Hence

$$E = \left[\int_0^1 \left\{ \frac{P(\xi)\rho_o}{\rho_f(\gamma-1)} + \frac{U^2(\xi)}{2} \right\} \xi d\xi \right] 2\pi R^2 \dot{R}^2 \tag{33}$$

must be constant, or

$$R\dot{R} = 2C^2 \tag{34}$$

from which we deduce that

$$R = 2C\sqrt{t} \; ; \; R = C(\sqrt{t})^{-1} \tag{35}$$

must describe the growth of the cylindrical blast wave.

For an initial radius, a, and initial pressure, P_f, we see

$$\dot{R}_o = \sqrt{\frac{(\gamma+1)P_f}{\rho_o}} \tag{36}$$

Hence

$$2c^2 = a\sqrt{\frac{(\gamma+1)P_f}{\rho_o}} = a(\gamma+1)c_f \tag{37}$$

where

$$c_f = \sqrt{\frac{\gamma P_f}{\rho_f}} \tag{38}$$

or

$$R^2\dot{R}^2 = a^2 P_f\left(\frac{\gamma+1}{\rho_o}\right) \tag{39}$$

Finally,

$$P(R) = a^2\,\frac{P_f}{R^2} \tag{40}$$

with

$$R = (2a(\gamma+1)c_f t)^{1/2} \tag{41}$$

This result differs slightly from that of Nielsen[2] who writes

$$R = \sqrt{2c_o a_t} \tag{42}$$

---

[2]Nielsen, P. E. "Hydrodynamic Calculations of Surface Response in the Presence of Laser-Supported Detonation Waves," Journal of Applied Physics, Vol. 46, No. 10, October 1975, pp. 4501-4505.

where

$$c_o = \sqrt{\frac{\gamma P_\theta}{\rho_o}} \tag{43}$$

From the foregoing, we may expect that a high intensity laser will produce a pressure pulse on a surface placed in the beam. The pressure will decay quickly as a blast wave spreads radially. For high intensity lasers operating in a pulsed mode, the result will be a pressure field, varying both spatially and temporally in a very complex manner.

The mechanism of pressure generation we have considered is that known as the LSD (laser-supported detonation) wave. At lower intensities, a different process, the LSC (laser-supported combustion) wave occurs[3]. In this case, the energy balance on the processed column of air (plasma) must include the radiation loss to the target material. Numerical studies have shown the pressure generated by this mechanism to be 50-60 atm, with up to 50% of the incident flux being re-radiated to the target. The absorption of this radiation produces the process known as thermal enhancement.

[3]Thomas, P. D. "Laser Absorption Wave Formation," AIAA Journal, Vol. 13, No. 10, October 1975, pp. 1279-1286.

B. The Response of Finite Plates

The response of an elastic plate to a spatially and time varying distribution of pressure arises in several contexts of the general problem of determining the response of structures to High Intensity Laser radiation. The differential equation of the elementary theory of plate bending

$$D\nabla^4 w + \rho h \frac{\partial^2 w}{\partial t^2} = P(x,y,t) \tag{1}$$

where w is the displacement normal to the plane was encountered earlier in determining the response to a thermally induced distributed moment. Here, we restrict our attention to the isothermal deformations of a simply supported circular plate under axisymmetric loading. Equation (1) is obtained by noting that Equation (9) (of Section II-C) must be replaced by

$$2\pi rQ = \int_o^r \rho h 2\pi r \ddot{w}(r,t) dr - \int_o^r P(r,t) 2\pi r dr$$

where P(r,t) is an axisymmetric, distributed pressure. Equations (5a) and (5b) go through with the only change being the deletion of the thermal moment. For the simply supported plate, the eigenfunctions are

$$R_n(r) = J_o(p_n r) - J_o(p_n a) I_o(p_n r)/I_o(p_n a) \tag{2}$$

with eigenvalues satisfying Equation (II-E-24). The first several are given (for $\nu = .3$) in Leissa's monograph[1] and others in more recent work[2]. The first

[1] Leissa, A. W., Vibration of Plates, NASA SP-160, 1969.

[2] Leissa, A. W. and Y. Narita, "Natural Frequencies of Simply Supported Circular Plates," accepted for publication, Journal of Sound and Vibration.

11 are tabulated in Table 1 for 2 values of Poissons' ratio. As each eigenfunction satisfies the condition of vanishing moment and displacement on r = a, any superposition does as well, and the general solution to Equation (1) may be written as

$$w(r,t) = \sum_{n=1}^{\infty} W_n(t)R_n(r) \tag{3}$$

We expand the prescribed pressure, P(r,t) as a series of these eigenfunctions

$$P(r,t) = \sum_{n=1}^{\infty} f_n(t)R_n(r) \tag{4}$$

Substitution into Equation (1) leaves, after multiplication by $R_n(r)$ and integration over the domain, a result analogous to II-C-33, or

$$Dp_n{}^4W_n + \rho h\ddot{W}_n = f_n(t) \tag{5}$$

where

$$f_n = \frac{1}{N_n}\int_o^a P(r,t)R_n(r)rdr \ .$$

Solutions to Equation (5) must satisfy desired initial conditions; typically, that the plate is at rest for negative time and is set in motion by a pressure distribution first achieving nonzero values for t = 0.

As a first example, consider a suddenly applied uniform pressure P_o, i.e.,

$$P(r,t) = P_o u(t)u(b-r) \tag{6}$$

Here u(s) is the unit step function

Table 1

Eigenvalues for Simply Supported Plates (Symmetric Modes)

ν	$P_0{}^a$	$P_1{}^a$	$P_2{}^a$	$P_3{}^a$	$P_4{}^a$	$P_5{}^a$	$P_6{}^a$	$P_7{}^a$	$P_8{}^a$	$P_9{}^a$	$P_{10}{}^a$
.2	2.18691	5.44093	8.60502	11.7563	14.9034	18.0484	21.1924	24.3358	27.4789	30.6214	33.7639
.3	2.22152	5.45161	8.61139	11.7609	14.9069	18.0513	21.1948	24.3379	27.4806	30.6230	33.7654

$$u(s) = 0 \quad \text{for} \quad s < 0 \tag{7a}$$

$$u(s) = 1 \quad \text{for} \quad s > 0 \tag{7b}$$

Then $f_n(t) = 0$ for $t < 0$, while for all $t > 0$

$$f_n(t) = f_n^{\,o} = \frac{P_o}{N_n} \int_o^b R_n(r) r dr = \frac{P_o}{N_n} \left[\frac{b}{p_n} J_1(p_n b) - \frac{J_o(p_n a)}{I_o(p_n a)} \frac{b}{p_n} I_1(p_n b) \right] \tag{8}$$

and

$$N_n = a^2 \left[\frac{J_1^{\,2}}{2} - J_o^{\,2} \left(\frac{1+\nu}{1-\nu} + \frac{1}{2} I_1^{\,2}/I_o^{\,2} \right) \right] \tag{9}$$

The modal amplitudes are

$$W_n = A_n \sin \omega_n t + B_n \cos \omega_n t + \frac{f_n^{\,o}}{D p_n^{\,4}} \tag{10}$$

and satisfaction of the homogeneous initial condition requires that

$$B_n = -f_n^{\,o}/D p_n^{\,4} \; ; \; A_n = 0 \tag{11}$$

Hence

$$w(r,t) = \frac{P_o b}{D} \sum_{n=1}^{\infty} \frac{\{J_1(p_n b) - \frac{J_o(p_n a)}{I_o(p_n a)} I_1(p_n b)\}}{N_n p_n} \{J_o(p_n r) - \frac{J_o(p_n a)}{I_o(p_n a)} I_o(p_n r)\}\{1 - \cos \omega_n t\} \tag{12}$$

where

$$\omega_n^{\,2} = \frac{D p_n^{\,4}}{\rho h} \tag{13}$$

and N_n are as given above. Now let

$$A_n = \frac{P_o b}{D}\left[\frac{\{J_1(p_n b) - \frac{J_o(p_n a)}{I_o(p_n a)} I_1(p_n b)\}}{N_n p_n^5}\right] \tag{14}$$

so that

$$w(r,t) = \sum A_n \{1 - \cos \omega_n t\}\{J_o(p_n r) - \frac{J_o(p_n a)}{I_o(p_n a)} I_o(p_n r)\} \tag{15}$$

The maximum moment occurs at r = 0 and is evaluated from

$$M_r = -D(\partial^2 w/\partial r^2 + \nu/r\ \partial w/\partial r) \tag{16}$$

We find

$$M_{r_{max}} = M_{\theta_{max}} = P_o(ba)\frac{(1+\nu)}{2}\sum \frac{J_1(p_n b) - \frac{J_o(p_n a)}{I_o(p_n a)} I_1(p_n b)}{(p_n a)^3} \cdot\left\{1 + \frac{J_o(p_n a)}{I_o(p_n a)}\right\}\left\{\frac{1 - \cos \omega_n t}{\frac{J_1^2}{2} - J_o^2\left[\frac{1+\nu}{1-\nu} + \frac{1}{2}\frac{I_1^2(p_n a)}{I_o^2(p_n a)}\right]}\right\} \tag{17}$$

Stresses are computed from the maximum moments from

$$\sigma_{rr_{max}} = \sigma_{\theta\theta_{max}} = \frac{6M_{max}}{h^2} \tag{18}$$

For computational convenience, let us define

$$F_n(b/a,n) = \frac{\{J_1(p_n b) - \frac{J_o(p_n a)}{I_o(p_n a)} I_1(p_n b)\}\{1 + \frac{J_o(p_n a)}{I_o(p_n a)}\}}{\left[\frac{J_1^2(p_n a)}{2} - J_o^2(p_n a)\ \{\frac{1+\nu}{1-\nu} + \frac{1}{2}\frac{I_1^2(p_n a)}{I_o^2(p_n a)}\}\right](p_n a)^3} \tag{19}$$

Then

$$M_{max} = P_o a^2 (b/a)(\frac{1+\nu}{2}) \sum_{n=1}^{\infty} F_n(b/a,n)(1 - \cos \omega_n t) \tag{20}$$

and the maximum stresses are

$$\sigma_{max} = 3(1+\nu)P_o(\frac{a}{h})^2(\frac{b}{a}) \sum_{n=1}^{\infty} F_n(b/a,n)(1 - \cos \omega_n t) \tag{21}$$

Table II presents values of F_n for several b/a and several modes for materials with $\nu = .3$, and may be used to determine which modes contribute most significantly to the stress history for any b/a. If b = a, the first mode predominates and we find (for $\nu = .3$)

$$F_1(1,1) = .344 \tag{22}$$

The stress history at the plate center is

$$\sigma_{max} = 1.34\ P_o(a/h)^2(1 - \cos \omega_1 t) \tag{23}$$

1. Response to a Single Pulse

We may deduce the response to a square pulse,

$$P = P_o \qquad 0 \leq t \leq \tau \tag{24a}$$

$$P = 0 \qquad t > \tau \tag{24b}$$

TABLE II $F_n(b/a,n)$ for $\nu = .3$

n	b/a=.1	b/a=.3	b/a=.5	b/a=1.0
1	.07601	.21608	.32204	.34395
2	.02802	.06120	.04644	-.03441
3	.01666	.02021	-.00739	.01113
4	.01120	.00286	-.00679	-.00515
5	.00788	-.00316	.00175	.00286
6	.00561	-.00333	.00234	-.00178
7	.00396	-.00135	-.00070	.00119
8	.00272	.00044	-.00111	-.00085
9	.00178	.00109	.00036	.00063
10	.00106	.00074	.00063	-.00048
11	.00052	.00003	-.00021	.00037

TABLE III $F_n(b/a,n)$ for $\nu = .2$*

n	b/a=.1	b/a=.3	b/a=.5	b/a=1.0
1	.07903	.22482	.33556	.35990
2	.02815	.06156	.04693	-.3431
3	.01669	.02028	-.00737	.01109
4	.01121	.00287	-.00681	-.00513
5	.00788	-.00316	.00174	.00285

*for $n \geq 6$, values same as for $\nu = .3$

by superposition. For $t < \tau$, Equation (21) applies. For $t > \tau$, we find

$$\sigma_{max} = 3(1+\nu)P_o(\frac{a}{h})^2(\frac{b}{a}) \sum F_n(b/a,n)[\cos \omega_n(t-\tau) - \cos \omega_n t] \tag{25}$$

The maximum contribution for any one mode occurs when $t = t_c$, where

$$\tan \omega_n t_c = -\cot(\omega_n \tau/2) \tag{26}$$

A useful approximation results for pulses of duration much less than the period of the dominant mode,

$$\omega_n t_c = \pi/2 \tag{27}$$

and

$$\sigma_{max} = 3(1+\nu)I_o(\frac{a}{h})^2(\frac{b}{a})F_N(b/a,N)\omega_N \tag{28}$$

where the impulse per unit area, $I_o = P_o\tau$, and N denotes the dominant mode. For a uniform pressure, the dominant mode is the first and

$$\sigma_{max} = 1.34\ I_o(a/h)^2\omega_1 \tag{29}$$

For a nonuniform pressure, the first mode response gives

$$\sigma_{max} = 3(1+\nu)\ \frac{\omega_1 I_{Total}}{h^2}\ (\frac{F_1}{b/a}) \tag{30}$$

Recall from Equation (13) that

$$\omega_n = \sqrt{\frac{D}{\rho h}}\ \frac{1}{a^2}\ (p_n a)^2 = \sqrt{\frac{E}{12(1-\nu^2)\rho}}\ (\frac{h}{a^2})(p_n a)^2 \tag{31}$$

Thus, the necessary modes for the modal analysis are governed by $(p_n a)^2 F_n(b/a,n)$.

This result may be used for comparison with computations performed by Holmes, Keough and Desmond[4] for pyrocerams ($E = 16.5 \times 10^6$ psi; $\rho = .0941$ lb/in^3) $\nu = .25$, $a = 4$ in., $h = 1/4$ in. subjected to a pulse

$$P(r,t) = P_o e^{-(r/s)^2} e^{-t/\tau} \tag{32}$$

$$\tau = 20 \text{ μsec}, \; s = 2.75 \text{ inches}, \; P_o = 1087 \text{ psi}$$

Such a pressure distribution history gives a total impulse of

$$I_{total} = \int_o^\infty 2\pi(P(r,t))rdr\, dt \tag{33a}$$

$$= \tau P_o 2\pi \int_o^a e^{-(r/s)^2} rdr \tag{33b}$$

$$= \tau P_o \pi s^2 (1 - e^{-(a/s)^2}) \tag{33c}$$

$$= (2.17 \times 10^{-2} \text{ psi sec}) \pi s^2 (.8795) \tag{33d}$$

which is equivalent to a uniform pressure P_o over $b = .938\, s$. For this disk,

$$\omega_1 = 6.127 \times 10^3 \text{ rad/sec} \tag{34}$$

and the period is

$$T = \frac{2\pi}{\omega_1} = 1.025 \times 10^{-3} \text{ sec} = 1025 \text{ μsec} \tag{35}$$

We obtain a maximum stress from Equation (30)

---

[4] Holmes, B. S., D. D. Keough and T. P. Desmond, Monthly Status Report #2, SRI International Project PYU-7259, Contract No. F29601-78-C-0041, August 1978.

$$\sigma_{max} = 3.9(2.17 \times 10^{-2} \text{ psi sec})(.8795)(6.127 \times 10^{3}/\text{sec}) \cdot \left(\frac{s^2}{h^2}\right) \frac{F_1(.645,1)}{.645} = 30.6 \text{ ksi} \quad (36)$$

occurring at the quarter period of the first mode, 256 μsec.

Values of the function $F_n(b/a,n)$ and the product $(p_n a)^2 F_n(b/a,n)$ are given in Tables III and IV for $\nu = .2$. Neither is very sensitive to the value of ν. The function F_n was seen from Equation (21) to be useful in determining the dominant mode in the response due to the step application of a uniform pressure, and the tabulated values show that the dominant mode is the first. The values tabulated as Table IV demonstrate that the response to a pulse loading which does not flood the entire plate will contain strong contributions from a number of modes. For example, in the case of $b/a = .1$, the contribution of the 11th mode is greater than the first.

2. Response to a Train of Pulses

Let us consider the response of a simply supported elastic plate of radius a to a train of pulses of a particular temporal variation:

$$P(r,t) = P_o\, U(b-r)[1 - \cos \Omega t] \quad \text{for } t > 0 \quad (37a)$$

$$P(r,t) = 0 \quad \text{for } t < 0 \quad (37b)$$

This may be considered to approximate a train of "square" pulses, of duration T/2 and amplitude $2P_o$, recurring with period $T = 2\pi/\Omega$, as shown in Figure 9.

Each pulse delivers an impulse

$$I_p = \int_o^a \int_o^T P(r,t) 2\pi r dr \quad (38a)$$

or

$$I_p = \pi P_o b^2 \int_o^{2\pi/\Omega} (1 - \cos \Omega t) dt = P_o \pi b^2 T \quad (38b)$$

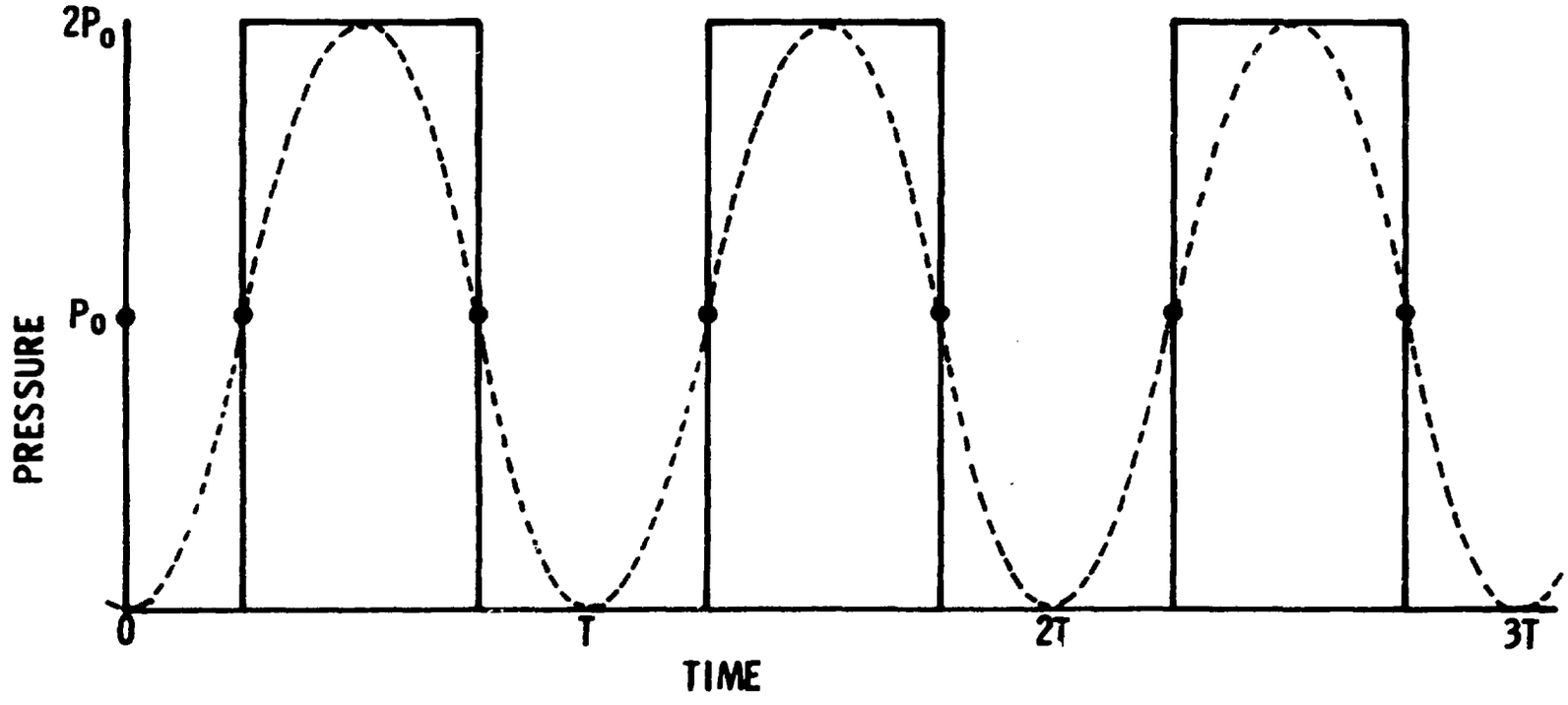

Figure 9. Approximation of Train of Square Pulses by Oscillating Pressure.

TABLE IV $(p_n a)^2 F_n(b/a)$ for $\nu = .2$

n	b/a=.1	b/a=.2	b/a=.3	b/a=.5	b/a=1.0
1	.37797	.74113	1.07522	1.60483	1.72125
2	.83325	1.48629	1.82233	1.38935	-1.01556
3	1.23567	1.82646	1.50143	- .54562	.82101
4	1.54893	1.66943	.39704	- .94082	- .70896
5	1.75084	1.08918	- .70196	.38713	.63343
6	1.82879	.28746	-1.08477	.76221	- .57789
7	1.77999	- .47691	- .60673	- .31562	.53485
8	1.61179	- .97354	.26017	- .65797	- .50023
9	1.34082	-1.07376	.82247	.27297	.47162
10	.99163	- .78715	.69000	.58750	- .44732
11	.59410	- .24977	.03482	- .24383	.42650

The modal amplitudes are given by

$$\rho h \ddot{W}_n + D p_n^4 W_n = f_n(t) \tag{39}$$

where

$$f_n(t) = \frac{1}{N_n} \int_o^a P(r,t) R_n(r) r dr \tag{40}$$

As before, we find N_n from Equation (9), and that

$$f_n(t) = \frac{P_o(1-\cos \Omega t)}{N_n} \left[\frac{b}{p_n} J_1(p_n b) - \frac{J_o(p_n a)}{I_o(p_n a)} \frac{b}{p_n} I_1(p_n b) \right] \tag{41}$$

or

$$\ddot{W}_n + \frac{D p_n^4}{\rho h} W_n = C_n(1 - \cos \Omega t) \tag{42}$$

where

$$C_n = \frac{I_p}{\rho h N_n} (b p_n)^{-1} \left[J_1(p_n b) - \frac{J_o(p_n a)}{I_o(p_n a)} I_1(p_n b) \right] \frac{1}{\pi T} \tag{43}$$

We first note the possibility of resonance if

$$\Omega^2_{crit} = \frac{D p_n^4}{\rho h} \tag{44}$$

or

$$T_{crit} = 4\pi \sqrt{3(1-\nu^2)} \sqrt{\frac{\rho}{E}} \frac{(a^2/h)}{(p_n a)^2} \tag{45}$$

It is to be noted here that in the pulse train modeled, T is the pulse spacing, rather than the pulse duration.

For a long train of pulses, with T near to T_{crit},

$$W_n = W_n^{(1)} + W_n^{(2)} + W_n^{(3)} \tag{46}$$

$$\omega_n = \sqrt{\frac{E}{12\rho}\frac{1}{(1-\nu^2)}}\,(p_n a)^2\,\left(\frac{h}{a^2}\right) \tag{47}$$

$$W_n^{(1)} = \frac{C_n}{\omega_n^2} \tag{48}$$

$$W_n^{(2)} = \frac{C_n}{\Omega^2-\omega_n^2}\cos \Omega t \tag{49}$$

$$W_n^{(3)} = -C_n\left[\frac{1}{\omega_n^2} + \frac{1}{\Omega^2-\omega_n^2}\right]\cos \omega_n t \tag{50}$$

For long times, $W_n^{(3)}$ will cease to be important, through energy dissipation not included in this analysis. We have, then, for such long times

$$w(r,t) = \sum_{n=1}^{\infty} \{\frac{I_p}{\rho h N_n(bp_n)}\frac{1}{\pi T}\}\{J_1(p_n b) - \frac{J_o(p_n a)}{I_o(p_n a)} I_1(p_n b)\}$$
$$\{\frac{1}{\omega_n^2} + \frac{\cos \Omega t}{\Omega^2-\omega_n^2}\} R_n(r) \tag{51}$$

where the eigenfunctions, $R_n(r)$, are as given previously, Equation (2). We may again compute moments, and stresses, finding the maximum stress at the plate center (for long times) to be

$$\sigma_{max} = 3(1+\nu)\,\left(\frac{a}{b}\right)\frac{I_p}{\pi T h^2}\sum_{n=1}^{\infty} F_n(b/a,n)(1 + \frac{\cos \Omega t}{\Omega^2/\omega_n^2-1}) \tag{52}$$

At short times, a greater stress may occur at $t = t_1$ such that

$$(\Omega^2/\omega_n^2 - 2) \sin \omega_n t_1 = \frac{\Omega}{\omega_n} \sin \Omega t_1 \tag{53}$$

of magnitude

$$\sigma_{max} = 3(1+\nu) \left(\frac{a}{b}\right) \frac{I_p}{\pi T h^2} \sum_{n=1}^{\infty} F_n(b/a,n)\{(1 - \cos \omega_n t) + \frac{(\cos \Omega t - \cos \omega_n t)}{(\Omega^2/\omega_n^2 - 1)}\} \tag{54}$$

If $\Omega \sim \omega_n$, the forced response [Equation (54)] may become very large. If, in fact, $\Omega = \omega_N$, we find

$$W_N = \frac{C_N}{\omega_N^2} (1 - \omega_N t \sin \omega_N t) \tag{55}$$

and

$$\sigma_{max} = 3(1+\nu) \left(\frac{a}{b}\right) \frac{I_p}{\pi T h^2} F_N(b/a,N)\{1 - \frac{\omega_N t}{2} \sin \omega_N t\} \tag{56}$$

It is not likely that a target can be driven precisely at one of its resonant frequencies; however, if this could be achieved, the stress level after M pulses would be (for a/b = 1 and resonating the first mode)

$$\sigma_{max} = 3(1+\nu) \frac{I_p}{\pi T h^2} F_1(1,1) \Omega \frac{MT}{2} \tag{57a}$$

$$= \frac{(1+\nu)}{2\pi} \frac{I_p}{h^2} M \sqrt{\frac{E}{12\rho} \frac{1}{(1-\nu^2)}} (p_1 a)^2 \left(\frac{h}{a^2}\right) \tag{57b}$$

$$= \frac{(1+\nu)}{2\pi} \frac{I_p}{a^2} \frac{M}{h} \sqrt{\frac{E}{12\rho} \frac{1}{(1-\nu^2)}} (2.231)^2 \tag{57c}$$

For the pyroceram disk previously cited, a stress of 18 ksi would be achieved in 100 pulses of $.7 \times 10^{-2}$ lb-sec per pulse, as opposed to the single pulse of about 60 times that magnitude. That the resonance effect is not more effective is somewhat surprising. The explanation probably lies in the fact that the long train of small pulses produces, even at resonance, what is essentially a static response, whereas the single pulse of short duration allows the dynamic amplification (typically a factor of two) that is characteristic of impulse response.

IV. A Fracture Criterion for Brittle Materials

A. Introduction

Experiments have shown that a ceramic material heated over some portion of its surface will fracture. These fractures appear to originate at the rear surface, under the heated zone. Consequently, we deduce that radial conduction, even in poor conductors such as ceramics, is sufficient to prevent large tensile stresses from forming outside of the heated region, as described in Section II.

Two other investigators have developed criteria for the fracture of ceramics. Mechlosky[1] assumes that stresses of magnitude

$$\sigma = \frac{\alpha}{1-\nu} E (\Delta T_z) \tag{1}$$

are developed and that fracture occurs when a critical value is reached. He takes the temperature rise to be that of Goodmans[2] premelting approximation

$$\Delta T_z = \frac{I_a h}{2k} (1 - \frac{x}{h})^2 + \frac{I_a \kappa}{kh} (t - t') \tag{2}$$

where

$$t' = \frac{h^2}{6\kappa} \tag{3}$$

Solving for the time t to reach a critical stress, σ_c, we find

$$\frac{\kappa t}{h^2} = \frac{1}{6} - \frac{1}{2} (1 - \frac{x}{h})^2 + \frac{2k}{I_a h} \frac{(1-\nu)\sigma}{\alpha E} \tag{4}$$

---

[1]Mecholsky, T. T., et al., "Effect of 3.8μ Laser Radiation on Ceramics", Proceedings of 2nd Conference on Laser Effects and Hardening, NASA Ames, July 1975.

[2]Goodman, T. R. and J. J. Shea, "The Melting of Finite Slabs", Journal of Applied Mechanics, Vol. 27, pp 16-24, March 1960.

A factor of two has been introduced into the last term to account for the radial expansion of the surrounding material, as in Section II, and is needed to produce Mechlosky's result.

Mechlosky assumes that the critical value of x is h/2, thus he finds a fracture time

$$\frac{\kappa t_f}{h^2} = \frac{1}{24} + \frac{2k}{I_a h} \frac{(1-\nu)\sigma}{\alpha E} \tag{5}$$

For sufficiently high flux (low strength) the right hand term becomes negligible leading to a dimensionless fracture time which is independent of intensity.

Several observations regarding this criterion must be made. First, the stress distribution assumed (Equation 1) is appropriate only for predicting the compressive stress arising under two-dimensional constraint, or, with the inclusion of the factor of 2, partial constraint. No out of plane deformation is allowed. Stresses, in this model, are compressive everywhere and, as such, the stresses at the midplane would appear to have no particular significance. Further, the model does not account for the observed origin of fracture at the rear surface. Finally, the result is extremely sensitive to the value of x employed. Nonetheless, it must be noted that quite good results have been obtained with it.

Laughlin[3] has developed a means of estimating fracture time based on the assumption that fracture will occur when tensile stresses on the rear face reach a critical value. He begins by using the exact solution for the

[3]Laughlin, W., 'Predicting the Laser Induced Thermal Fracture of Infrared and Radar Transmitting Materials', Proceedings of First Classified Conference on High Energy Laser Technology, San Diego CA, October 1974.

temperature rise in a uniformly heated slab to predict thermal stresses, under the assumption that the material surrounding the heated area constrains all bending deformation but allows radial expansion to freely occur. This corresponds to the mechanical boundary condition discussed as case II in Section II.B.2. To account for melting[4], he computes stresses in the same manner, with the temperature distribution taken to be that in a slab with front face temperature fixed at meeting. As the slab continues to heat, we note that the front face gradient decreases, and thus, the incident flux is treated as if it were reduced. Laughlin has also obtained generally satisfactory results with his method.

While Laughlin's model appears to have a firmer basis that that of Mechlosky, two questions remain open. First, the mechanical boundary condition at the edge of the heated zone, and secondly, the treatment of the influence of melting on the stresses in the solid portion.

B. The Influence of Mechanical Boundary Condition

Let us consider a section of a structural member to be subjected to a uniform absorbed intensity over a circle of radius a, the remainder of the structure remaining at the ambient temperature which, for convenience, will be taken as T = 0. If we neglect the consequences of radial heat flow out of the heated region*, then the temperatures for r < a are given by Equation (18) of Section II.B.2. or, in terms of a coordinate system in the midplane of the plate with the heated face being z = h/2, by

*Recall that it was shown in an earlier section that radial heat flow does not reduce the magnitude of stresses within the heated zone.

[4]Laughlin, W. T., "Predicting the Laser Induced Thermal Fracture of Partially Transparent Materials (U)", 2nd DOD Conference on Laser Effects and Hardening, NASA Ames, July 1975.

$$T(z,t) = \frac{I_a t}{\rho C_p h} + \frac{I_a h}{k}\left\{\frac{1}{2}\left(\frac{z}{h}\right)^2 + \frac{1}{2}\left(\frac{z}{h}\right) - \frac{1}{24}\right\}$$

$$- \frac{I_a h}{k}\frac{2}{\pi^2}\sum \frac{(-1)^n}{n^2} e^{-\kappa n^2\pi^2 t/h^2} \cos n\pi \left(\frac{z}{h} + \frac{1}{2}\right)\Big\} \qquad (1)$$

In what follows, a dimensionless time

$$\tau = \kappa t/h^2 \qquad (2)$$

will be used.

For $r < a$, the displacements and stresses are found to be

$$\sigma_{zz} = 0 \qquad (3a)$$

$$\sigma_{rr} = \sigma_{\theta\theta} = \frac{E}{1-\nu}\left[C_1 Z + C_2 - \alpha T\right] \qquad (3b)$$

$$U_r = C_1 Zr + C_2 r \qquad (4a)$$

$$U_\theta = 0 \qquad (4b)$$

where the constants C_1 and C_2 are to be determined from the boundary conditions on $r = a$. The four possible boundary conditions arising from the edge $r = a$ being free or constrained against in displacement and free or constrained against rotation were explored in a previous section.

We now assume the line $r = a$, circumscribing the heated zone, to be elastically restrained by the surrounding material, i.e., on $r = a$ the influence of the surrounding material may be represented by moments and forces per unit length

$$M_r = C_B \phi \qquad (5)$$

where

$$\phi = \frac{\partial \tilde{w}}{\partial r}\bigg|_{r=a} = -\frac{\partial \tilde{U}_n}{\partial r}\bigg|_{r=a^+} \tag{6}$$

$$M_r = \int_{-h/2}^{h/2} z\tilde{\sigma}_{rr}\,dz\,\bigg|_{r=a^+} \tag{7}$$

and

$$F_r = C_T\delta \tag{8}$$

where

$$F_r = \int_{-h/2}^{h/2} \tilde{\sigma}_{rr}\,dz\,\bigg|_{r=a^+} \tag{9}$$

$$\delta = \tilde{U}_r\,\bigg|_{r=a^+,\ z=0} \tag{10}$$

Further, the displacements and rotations of the heated region, on the line $r = a$, must match those of the exterior region. Here, $\tilde{U}_r$ and $\tilde{w}$ are the inplane and out of plane displacements, respectively in the exterior (unheated) region.

The constants of (3b) and (4a) result from matching displacement, slope, force and moment at $r = a$

$$\delta = U_r(a,o) = C_2 a \tag{11a}$$

$$\phi = -\frac{\partial U_r}{\partial z}(a,0) = -C_1 a \tag{11b}$$

$$M_r = \int_{-h/2}^{h/2} z\sigma_{rr}(a,z)dz = \frac{E}{1-\nu}\left[\frac{C_1 h^3}{12} - \alpha \int_{-h/2}^{h/2} zTdz\right] \tag{11c}$$

$$F_r = \int_{-h/2}^{h/2} \sigma_{rr}(a,z)dz = \frac{E}{1-\nu}\left[C_2 h - \alpha \int_{-h/2}^{h/2} Tdz\right] \tag{11d}$$

These four equations, together with the two stiffness constants, defined by Equations (5) and (8), permit the constants C_1 and C_2 to be determined. We find:

$$C_2 = \frac{\alpha \int_{-h/2}^{h/2} Tdz}{h - \frac{(1-\nu)}{E} aC_T} \tag{12}$$

$$C_1 = \frac{1}{\frac{h^3}{12} + \frac{(1-\nu)}{E} aC_B}\left[\alpha \int_{-h/2}^{h/2} zTdz\right] \tag{13}$$

The four cases considered in Section II.B.2. may, of course, be recovered by setting to zero, or infinity, the two stiffnesses, C_T and C_B, as appropriate.

We first consider the flat plate of thickness h surrounding the heated region. We provide that the elastic constants, $\tilde{E}$, $\tilde{\nu}$, may differ from those of the heated region so that a thermal softening effect may be included, if desired. The inplane displacements and stresses are those of the Lame solution, as used previously (Section II-B).

$$U_r = Ar + B/r \tag{14a}$$

$$U_\theta = 0 \tag{14b}$$

$$\sigma_{zz} = 0 \tag{15a}$$

$$\sigma_{rr} = \tilde{E}\left(\frac{A}{1-\tilde{\nu}} - \frac{B}{1+\nu}\,\frac{1}{r^2}\right) \tag{15b}$$

$$\sigma_{\theta\theta} = \tilde{E}\left(\frac{A}{1-\tilde{\nu}} + \frac{B}{1+\nu}\,\frac{1}{r^2}\right) \tag{15b}$$

For a finite circular plate, with $F_r = 0$ on the outer radius, $r = b$, we find

$$B = A\left(\frac{1+\tilde{\nu}}{1-\tilde{\nu}}\right)b \tag{16}$$

For an infinite sheet, $A = 0$.

These results may be combined to deduce the stiffness constant for the inplane motion, C_T. Using Equations (8), (9), and (10), we find

$$C_T = -\frac{h\tilde{E}}{a}\,\frac{\left(1 - \frac{a^2}{b^2}\right)}{(1+\tilde{\nu}) + (1-\tilde{\nu})\,\frac{a^2}{b^2}} \tag{17}$$

and

$$C_2 = \frac{\left[(1+\tilde{\nu}) + (1-\tilde{\nu})\frac{a^2}{b^2}\right]\frac{\alpha}{h}\int_{-h/2}^{h/2} T\,dz}{(1+\tilde{\nu}) + (1-\tilde{\nu})\,\frac{a^2}{b^2} + (1-\nu)\,\frac{\tilde{E}}{E}\left(1-\frac{a^2}{b^2}\right)} \tag{18}$$

In order to facilitate comparison with a fracture criterion developed by Laughlin, it is of interest to determine the stresses arising in a finite sheet of the same modulus, with the central region completely constrained against bending, $C_B = \infty$. In this case,

$$C_2 = \frac{\left[(1+\nu) + (1-\nu)\frac{a^2}{b^2}\right]\alpha\int_{-h/2}^{h/2} T\,dz}{2h} \tag{19}$$

From Equations (12) and (13), $C_1 = 0$ and

$$\sigma_{rr} = \frac{E\alpha}{1-\nu} \left\{ \frac{\left[(1+\nu) + (1-\nu)\frac{a^2}{b^2}\right]}{2h} \int_{-h/2}^{h/2} T dz - T \right\} \tag{20}$$

As $b \to a$, Case II of Section II-B-2 results. As $b \to \infty$, we find

$$\sigma_{rr} = \frac{E\alpha}{1-\nu} \left[\frac{(1+\nu)}{2h} \int_{-h/2}^{h/2} T dz - T \right] \tag{21}$$

In general, we should not assume that the surrounding, unheated material will suffice to completely constrain the edges of the heated disk from bending. Rather, the material in $a < r < b$ will deflect as an elastic plate, free on $r = b$ but with applied moment on $r = a$. The governing equation for the axisymmetric lateral deflection of a thin, unloaded elastic plate is

$$\nabla^4 w = 0 \tag{22}$$

has solution

$$w = C \ln r + Dr^2 \tag{23}$$

Strains, stresses and moments may be deduced as previously, Section II-C, Equations (1) to (4), to yield

$$U_r(r,z) = -z\left(\frac{C}{r} + 2Dr\right) \tag{24}$$

From which

$$\sigma_{rr} = -\frac{\tilde{E}z}{1-\tilde{\nu}^2} \left[-\frac{C}{r^2}(1-\tilde{\nu}) + 2D(1+\tilde{\nu}) \right] \tag{25}$$

The moment, M_r, is found to be

$$M_r = - \tilde{E} \frac{h^3}{12} \left[- \frac{C}{(1+\nu)} \frac{1}{r^2} + \frac{2D}{(1-\nu)} \right] \tag{26}$$

Since the moment at r = b must vanish, the moment at r = a is found to be

$$M_r = + \frac{\tilde{E}}{1+\nu} \frac{h^3}{12} \frac{C}{a^2} \left(1 - \frac{a^2}{b^2}\right) \tag{27}$$

The slope at r = a is seen to be

$$\frac{dw}{dr} = \frac{C}{a} \left(1 + \frac{1-\tilde{\nu}}{1+\nu} \frac{a^2}{b^2}\right) \tag{28}$$

from which Equation (7) may be used to deduce the stiffness as

$$C_B = \frac{\tilde{E}h^3}{12(1+\nu)a} \frac{\left(1 - \frac{a^2}{b^2}\right)}{\left(1 + \frac{1-\tilde{\nu}}{1+\nu} \frac{a^2}{b^2}\right)} \tag{29}$$

Hence

$$C_1 = \frac{12}{h^3} \frac{\alpha \int_{-h/2}^{h/2} zTdz}{\left[1 + \frac{\tilde{E}}{E} (1-\nu) \frac{\left(1 - \frac{a^2}{b^2}\right)}{\left(1+\tilde{\nu} + (1-\tilde{\nu}) \frac{a^2}{b^2}\right)}\right]} \tag{30}$$

In the case of an infinite sheet with elastic properties on r < a, these reduce to

$$C_1 = \frac{12}{h^3} \frac{(1+\ )}{2} \{\alpha \int_{-h/2}^{h/2} zTdz\} \tag{31}$$

with

$$C_2 = \frac{(1+\ )}{2h} \alpha \int_{-h/2}^{h/2} Tdz. \tag{32}$$

In order to evaluate the stresses from Equation (3b), we need compute certain integrals of the temperature distribution

$$\int_{-h/2}^{h/2} Tdz = \frac{I_a h}{2k} \{2\tau h\} \tag{33}$$

$$\int_{-h/2}^{h/2} zTdz = \frac{I_a h}{2k} \{\frac{h^2}{12} - \frac{8h^2}{\pi^4} \sum_{\text{odd}} e^{-n^2\pi^2\tau} \frac{1}{n^4}\} \tag{34}$$

Let us examine the following cases:

A: The edge r = a is completely constrained against rotation, but is only partially constrained against lateral expansion by the radial deformation of a finite, circular plate. The constant C_1, as noted previously, is zero and

$$C_2 = [\frac{(1+\nu) + (1-\nu)\frac{a^2}{b^2}}{2}] \frac{\alpha}{h} \int_{-h/2}^{h/2} Tdz \tag{35}$$

The stresses in r < a are

$$\sigma_{rr} = \sigma_{\theta\theta} = \frac{E\alpha}{1-\nu} \frac{I_a h}{2k} [\{(1+\nu) + (1-\nu)\frac{a^2}{b^2}\} 1 - 2\tau$$

$$- \{(\frac{z}{h})^2 + \frac{z}{h} - \frac{1}{12}\} + \frac{4}{\pi^2} \sum \frac{(-1)^n}{n^2} e^{-n^2\pi^2\tau} \cos n\pi(\frac{z}{h} + \frac{1}{2})] \tag{36}$$

For this boundary condition, the maximum stress occurs on the rear face (z = -h/2) and is

$$\sigma_{max} = \frac{2E\alpha}{1-\nu} \frac{I_a h}{k} \{\frac{1}{12} - \frac{(1-\nu)}{4} \tau(1 - \frac{a^2}{b^2}) + \frac{1}{\pi^2} \sum_{n} \frac{(-1)^n}{n^2} e^{-n^2\pi^2\tau}\} \tag{37}$$

Figure 1 displays graphically this equation for three cases: a/b = 1 (which

corresponds to Laughlins criterion); a/b = 0 (which corresponds to the infinite sheet with a heated spot and an intermediate case (a/b = 1/2), all with $\nu = .3$.

Qualitative differences between the two extreme cases are seen. For a/b = 1, the rear face stress increases monotonically reaching a maximum (as $t \to \infty$) of

$$\sigma_{max} = \frac{E\alpha}{1-\nu} \frac{I_a h}{k} \times \frac{1}{6}\left(\frac{E\alpha}{1-\nu} \frac{I_a h}{k}\right) \tag{38}$$

On the other hand, the elastic constraint caused by the infinite sheet leads to the eventual ($\tau \sim 1/2$) development of compressive stresses on the rear face, with the maximum tensile stress occurring at $\tau = .175$, of magnitude

$$\sigma_{max} = \frac{I_a h}{k} (0.07) \frac{E\alpha}{1-\nu} \frac{I_a h}{k} \tag{39}$$

From the results given in Figure 10, a failure time can be predicted. If the case a/b = 1 is used, Laughlins results will be recovered. It is interesting to note that for times in the region where most failures have been observed, that the case for a/b = 1 overestimates the stress by about 50% or equivalently provides an estimate of the fracture time which is about 60% of that which would be obtained if the $a/b = \infty$ results were to be used.

Let us now consider a second case: where the line r = a is only partially constrained against both expansion and rotation by the surrounding material. C_2 is as before, but C_1 is no longer zero, for the bending deformation will now take place. Using (33) and (34) in (35) and (30) (taking $E = \tilde{E}$ and $\nu = \tilde{\nu}$) we find the stress (Equation (3b) to be

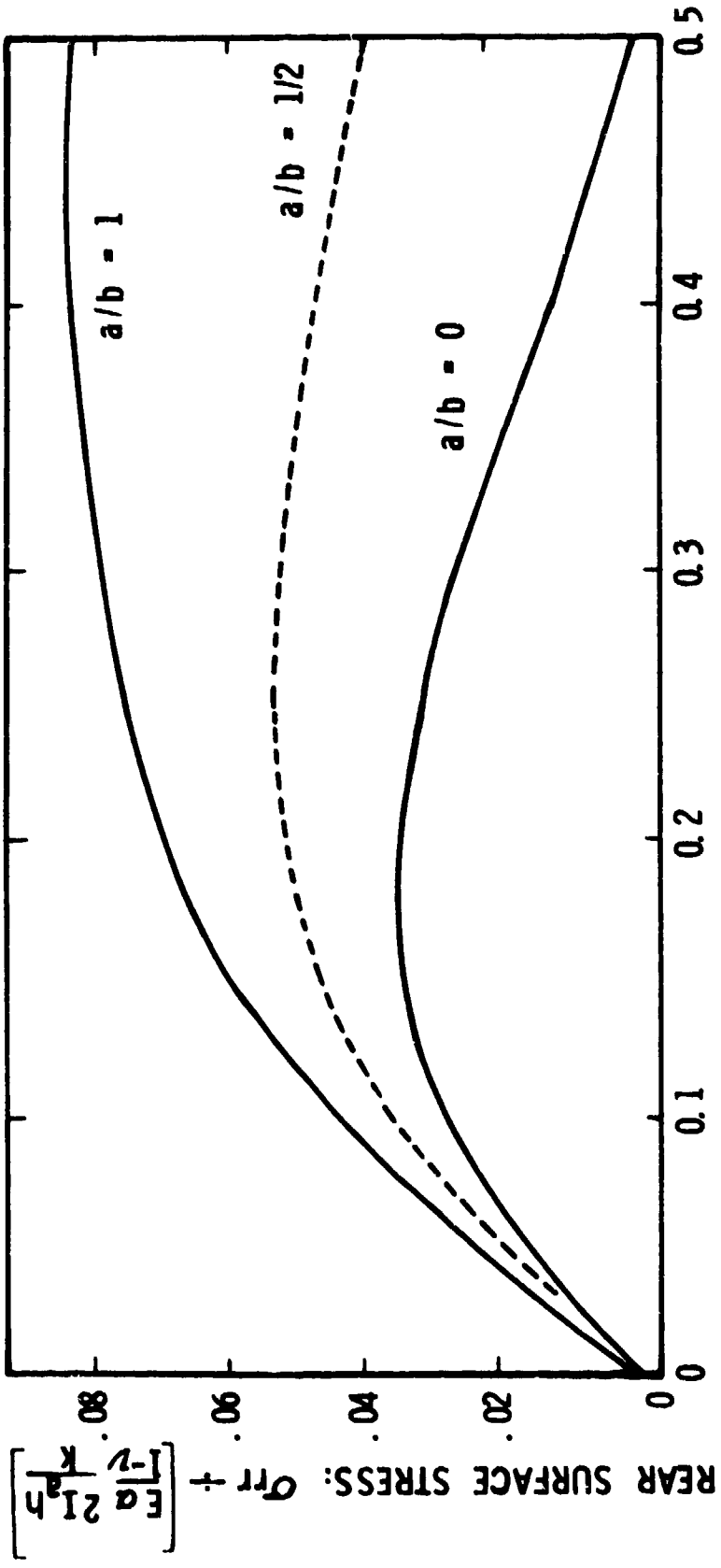

Figure 10. Rear Face Tensile Stress Under Healed Spot.

$$\sigma_{rr} = \sigma_{\theta\theta} = \frac{E\alpha}{(1-\nu)} \frac{I_a h}{2k} \{ \frac{6z}{h} R \left[\frac{1}{12} - \frac{8}{\pi^4} \sum_{\text{odd}} \frac{e^{-n^2\pi^2\tau}}{n^4}\right] + (R-2)\tau$$

$$- \left[(\frac{z}{h})^2 + \frac{z}{h} - \frac{1}{12}\right] + \frac{4}{\pi^2} \sum \frac{(-1)^n}{n^2} e^{-n^2\pi^2\tau} \cos n\pi(\frac{z}{h} + \frac{1}{2}) \} \quad (40)$$

where

$$R = (1+\nu) + (1-\nu) \frac{a^2}{b^2} \quad (41)$$

For a = b, R = 2, and we find, for long times,

$$\sigma_{rr} = \sigma_{\theta\theta} = \frac{E\alpha}{(1-\nu)} \frac{I_a h}{2k} \{\frac{1}{12} - (\frac{z}{h})^2\} \quad (42)$$

which is the result previously obtained for the free plate. For b = ∞, the long time stresses are

$$\sigma_{rr} = \sigma_{\theta\theta} = \frac{E\alpha}{(1-\nu)} \frac{I_a h}{2k} \{\frac{1}{12} - (\frac{z}{h})^2 - (\frac{1-\nu}{2})\frac{z}{h} - (1-\nu)\tau\} \quad (43)$$

Evaluating Equation (40) at the rear face (z = -h/2), we find that

$$\sigma_{rr_{rear}} = \sigma_{\theta\theta_{rear}} = \frac{2E\alpha}{(1-\nu)} \frac{I_a h}{k} \{- \frac{3}{4} \left[(1+\nu) + (1-\nu) \frac{a^2}{b^2}\right]$$

$$\left[\frac{1}{12} - \frac{8}{\pi^4} \sum_{\text{odd}} \frac{e^{-n^2\pi^2\tau}}{n^4}\right] - \frac{(1-\nu)}{4} \tau(1 - \frac{a^2}{b^2}) + \frac{1}{12}$$

$$+ \frac{1}{\pi^2} \sum \frac{(-1)^n}{n^2} e^{-n^2\pi^2\tau}\} \quad (44)$$

which is seen to differ from Equation (37) (the result when bending deforma-

tions are constrained) by the inclusion of the term

$$-\frac{3}{4}(1+\nu+(1-\nu)\frac{a^2}{b^2})(\frac{1}{12}-\frac{8}{\pi^4}\sum_{\text{odd}}\frac{e^{-n^2\pi^2\tau}}{n^4})$$

Stresses at the rear face, for short times, are given in Figure 11 and are seen to remain compressive. Long time values (Equation (42) and Equation (43)) are also seen to be compressive.

Thus, we see that properly accounting for the mechanical boundary condition at the edge of the heated region shows the stresses on the rear face to remain compressive.

Tensile stresses will develop in the interior. It is to be recalled from Chapter II (Figure 6) that a uniform flux over one face of an infinite sheet leads to compressive stresses on the outer surface and tensile stresses on the centerline. These results are reviewed as Figure 12a. If we now consider a heated radius a within a disk of outer radius b, the constraint of the unheated area superposes compressive stresses, leading to the time history shown in Figure 12b (for $a/b \to 0$). Small compressive stresses remain on the center only for short times.

Thus, if fracture due to tensile stresses on the rear surface is observed, the fracture must originate outside the heated area, according to the mechanism of Chapter IIB.

The stresses in a disk of radius b having an axisymmetric temperature distribution are given in Equations II-A-19 and 20. For a temperature distribution

$$T = T_o \quad \text{on} \quad r \leq a \tag{46a}$$

$$T = 0 \quad \text{on} \quad a < r < b \tag{46b}$$

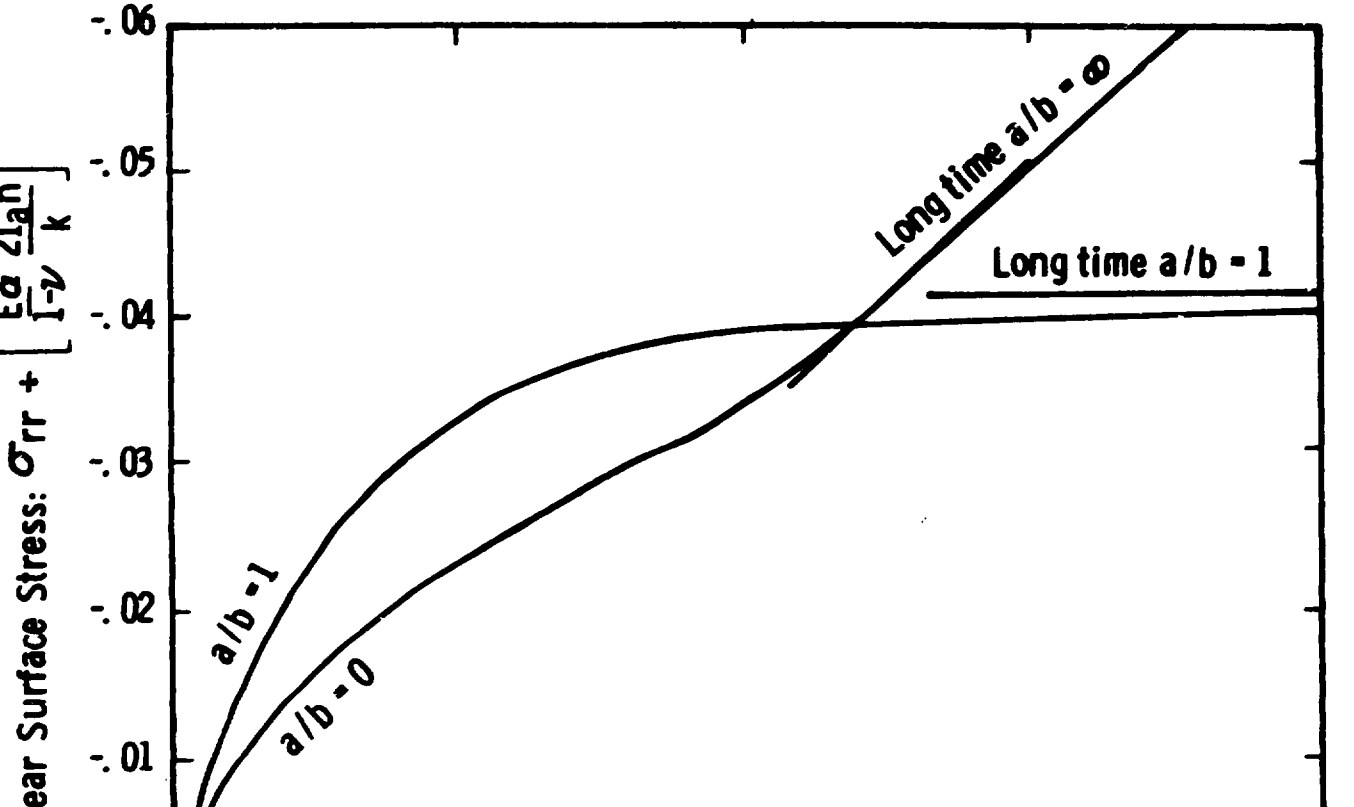

Figure 11. Rear Face Stresses, ν = .3.

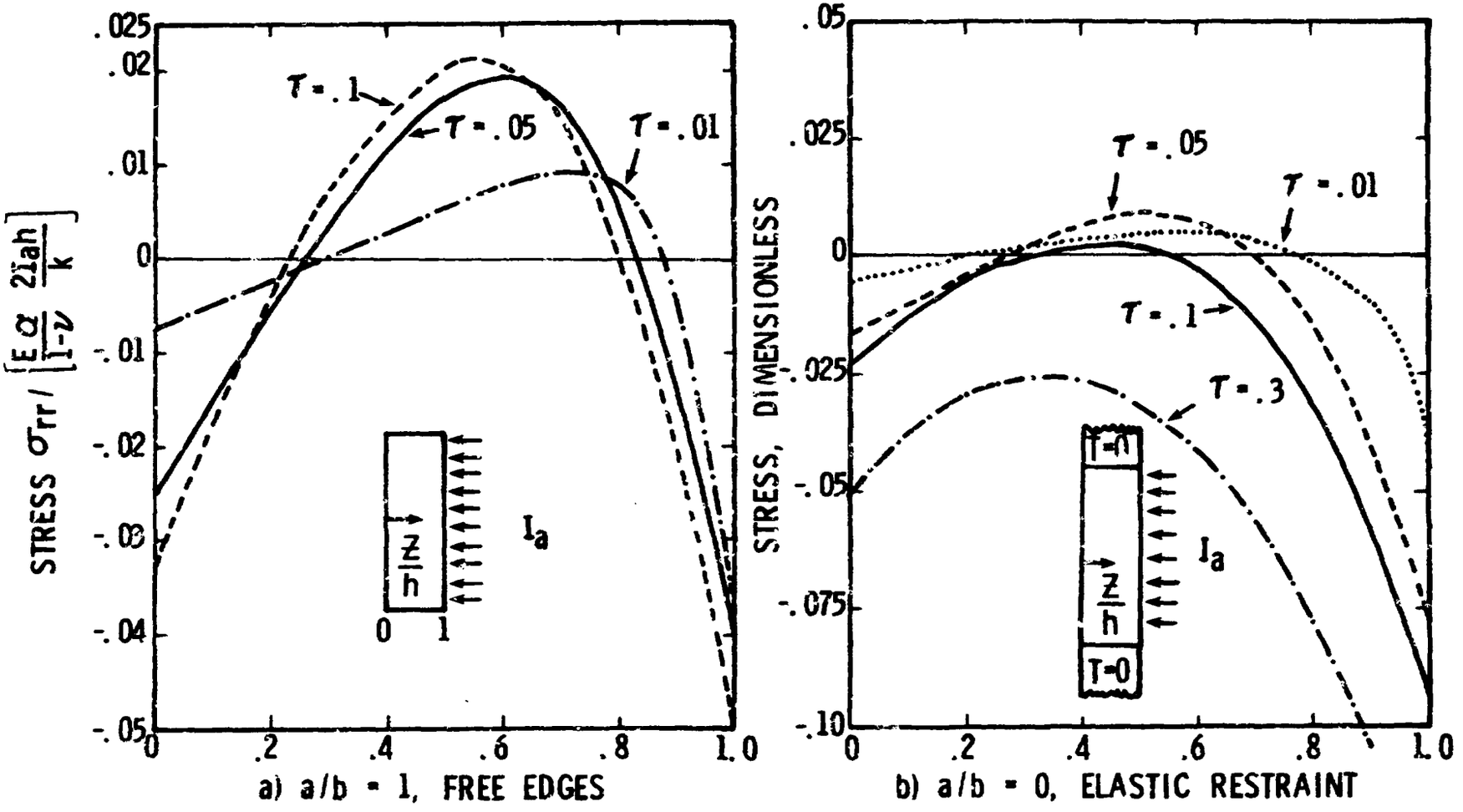

Figure 12. Stress Distribution at Several Times.

we find

$$\sigma_{\theta\theta} = \sigma_{rr} = E\alpha T_o(\frac{a^2}{b^2} - 1)/2 \quad \text{on} \quad 0 \leq r \leq a \tag{47a}$$

$$\sigma_{rr} = E\alpha T_o(\frac{a^2}{b^2} - \frac{a^2}{r^2})/2 \quad \text{on} \quad a \leq r \leq b \tag{47b}$$

and

$$\sigma_{\theta\theta} = E\alpha T_o(\frac{a^2}{b^2} + \frac{a^2}{r^2})/2 \quad \text{on} \quad a \leq r \leq b \tag{48}$$

Thus, the greatest tensile stress occurs at r = a, just outside the heated area.

For no losses, and no radial conduction, the average temperature on $r \leq a$ is

$$T_o = \frac{I_a}{\rho C_p h} t \tag{49}$$

and the corresponding average tensile stress for $r = a^+$ increases linearly with time as

$$\sigma_{max} = \frac{E\alpha I_a}{\rho C_p h} (\frac{a^2}{b^2} + 1) \frac{t}{2} \tag{50}$$

For the infinite disk, Equation II-B-1-12 is recovered. Radial conduction will lead to a reduction of these stresses, in the manner of Section II-A, where asymptotic values for long times have already been given. It should be noted that these are not the only stresses developed. Continuity of bending, as well as in-plane deformation, will give rise to a moment $M_{\theta\theta}$ and further stresses $\sigma_{\theta\theta}$. These will not be considered as they will quickly decay with distance into the unheated portion. Rather, the influence of radial conductivity on

tensile stresses for $r > a$ will be explored. The stress time history for $\kappa = 0$ is given by Equation (50). For non-zero κ, a numerical procedure was developed for the transient on dimensional radial temperature distribution in a finite disk. Once values of temperature were found, stresses were computed from Equations II-A-19 and 20. Typical results for the transient circumferential stress are given in Figure 13. Here the heated radius was taken to be 4 cm on a disk 1 cm thick of outer radius 9.73 cm. C_p was taken to be unity (1 Joule/gm^oK), $\rho = 3$ gm/cm^3 and two values of conductivity, leading to $K = .1$ cm^2/sec and $K = .01$ cm^2/sec, were considered. The radial conduction is seen to reduce, but not eliminate, the development of the tensile stress.

The influence of conductivity is more readily seen from the results presented as Figure 14. A family of hypothetical materials were considered, all with $\rho C_p = 3$ Joule/cm$^3{}^oK$. A disk 9.73 cm in radius and 1 cm thick was considered to be subjected to a constant absorbed flux over a central circle of 4 cm in radius. The time to generate tensile stresses of two values is presented. From the results it can be seen that tensile fracture outside the heated region may indeed occur, and that the time to produce a given stress is increased by thermal conduction. Thus, heating a uniform disk will produce significant tensile stresses outside the heated region, and these will provide the failure mechanism for a brittle material.

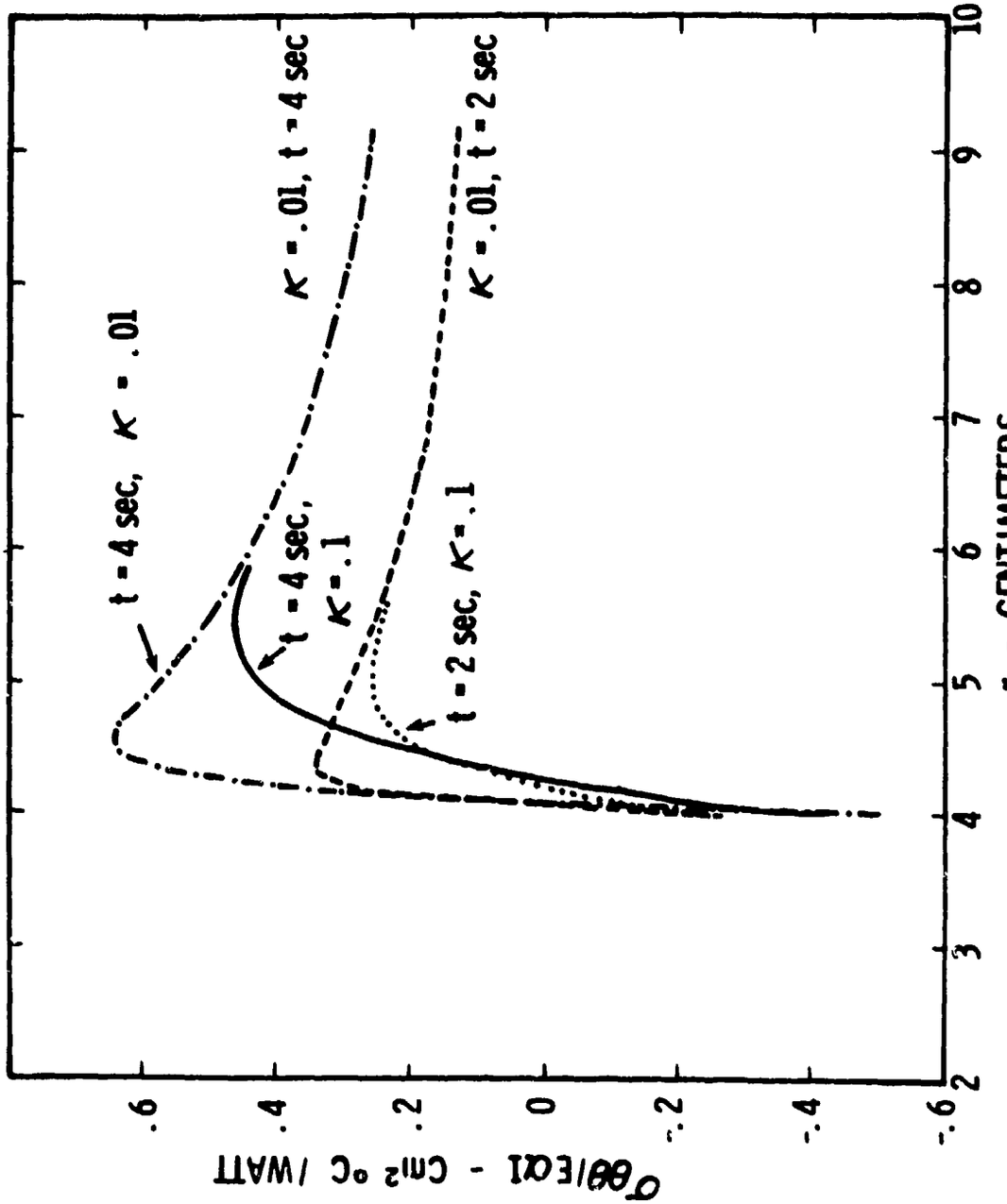

Figure 13. Tensile Stress Outside Heated Region.

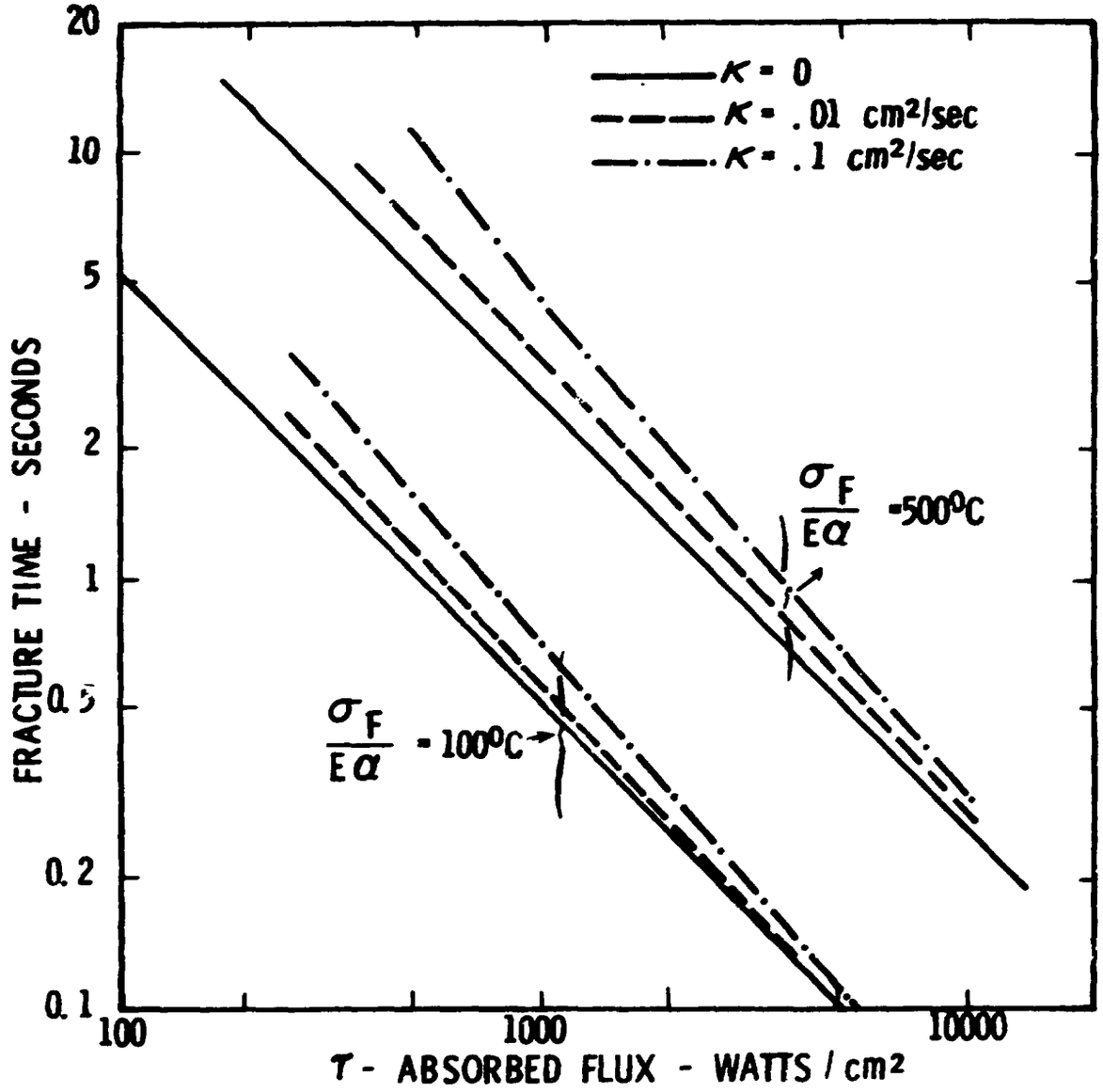

Figure 14. Fracture Times for Hypothetical Materials of Various Conductivity.

C. Influence of Melting

When the heated surface of the slab reaches the melting temperature, the temperature distribution is no longer that given by Equation (II.B.1.), and the stresses, as computed in the previous section, are no longer applicable. Since the problem of determining the temperature distribution is, in such cases, nonlinear, we must resort to approximate methods. The heat-balance integral method of Goodman and Shea is applicable in such cases and will be used to determine an approximate solution to the one-dimensional heat transfer problem with change in phase, and the thermal stress will then be determined from this approximate solution. It will prove useful to recognize two critical distinctions, first, whether the slab is thin or thick, and second, whether the melt is completely retained or completely removed. A slab will be regarded as thick if front face melting begins before the rear surface temperature changes and thin when the converse occurs.

1. Melting of Thin Slabs With Melt Retention

For temperatures below melting, we assume the temperature distribution in a slab of thickness ℓ absorbing a flux I_a on $x = 0$ to be

$$T = a(t) + b(t)x + c(t)x^2 \qquad \text{for } x < \delta \tag{1a}$$

$$T = 0 \qquad \text{for } x > \delta \tag{1b}$$

where $\delta(t)$ is a thermal penetration distance. On $x = 0$,

$$I_a = -k\frac{\partial T}{\partial x}\bigg|_0 = -kb(t) \tag{2}$$

on $x = \delta$

$$T = 0 \text{ and } \frac{\partial T}{\partial x} = 0 \tag{3}$$

hence

$$T = \frac{I\delta}{2k}\left(1 - \frac{x}{\delta}\right)^2 \tag{4}$$

This approximation cannot satisfy the differential equation exactly but only in an average manner. Thus, we require

$$\int_o^\delta k \frac{\partial^2 T}{\partial x^2} = \int_o^\delta \rho C_p \frac{\partial T}{\partial t} \tag{5}$$

$$k \frac{\partial T}{\partial x}\bigg|_\delta - k \frac{\partial T}{\partial x}\bigg|_o = I_a = \frac{I_a \rho C_p}{2k} \frac{2}{3} \delta\dot{\delta} \tag{6}$$

which may be integrated to give

$$\delta(t) = \sqrt{6\kappa t} \tag{7}$$

since $\delta = 0$ at $t = 0$. The time to front surface melting is then found from (4) to be

$$t_m = \frac{1}{6k}\left(\frac{2kT_m}{I}\right)^2 \tag{8}$$

and is valid if $\delta(t_m) = \frac{2kT_m}{I} < \mathcal{L}$. This notation suggests the introduction of a dimensionless measure of the applied flux. Let

$$i = \frac{I\mathcal{L}}{(2kT_m)} \tag{9}$$

then for $i > 1$, melting begins before the rear surface temperature changes, and the slab is thermally thick.

We first consider the case $i < 1$, the case considered by Goodman and

Shea[2], with results used by Mecholsky[1]. At some time t_ℓ less than t_m, given by (8), the penetration depth δ reaches $x = \ell$. The assumed temperature distribution, Equation (4), is no longer appropriate. The new boundary conditions become

$$I_a = -k\frac{\partial T}{\partial x} \qquad \text{on } x = 0 \tag{10a}$$

$$0 = -k\frac{\partial T}{\partial x} \qquad \text{on } x = \ell \tag{10b}$$

From (7),

$$t_\ell = \frac{\ell^2}{6k} \tag{11}$$

thus, the approximate solution for $t > t_\ell$ becomes

$$T = a(t) - \frac{I}{k}x + \frac{I}{2k\ell}x^2 \tag{12}$$

Again, we satisfy the averaged differential equation, this time obtained by integrating through the entire slab thickness

$$k\frac{\partial T}{\partial x}\bigg|_\ell - k\frac{\partial T}{\partial x}\bigg|_o = \frac{\partial}{\partial t}\int_o^\ell \rho C_p T dt = \rho C_p \dot{a}\ell \tag{13}$$

The resulting differential equation

$$\dot{a} = \frac{I_a}{\rho C_p \ell} \tag{14}$$

is easily solved and substituted into (12) to yield the approximate temperature distribution

$$T = \frac{I_a t}{\rho C_p \ell} + C - \frac{Ix}{k} + \frac{I}{2k\ell} x^2 \tag{15}$$

The constant of integration, C , is determined by requiring that the temperature distribution for $t \geq t_\ell$ (Equation (15)) matches that for $t \leq t_\delta$ (Equation (4)) when $\delta = \ell$. The result is

$$T = \frac{I_a}{\rho C_p \ell} (t - t_\ell) + \frac{I\ell}{2k} (1 - \frac{x}{\ell})^2 \tag{16}$$

This is Equation (2) of IV.A.

It is convenient to replace real time, t, by a dimensionless time,

$$\tau = \frac{kt}{\ell^2} \tag{17}$$

Then,

$$T = \frac{I_a \ell}{k} (\tau - \tau_\delta) + \frac{I\ell}{2k} (1 - \frac{x}{\ell})^2 \tag{18}$$

$$\tau_\delta = \frac{1}{6} \tag{19}$$

This solution is valid until the front surface reaches melting, or until

$$\tau = \tau_\ell + \frac{kT_m}{I_a \ell} - \frac{1}{2} + \frac{1}{2i} - \frac{1}{3} \tag{20}$$

where it is to be recalled that $i \leq 1$.

If the flux is continued at this same value for longer periods of time, a melting front will form and propagate into the solid, leaving behind molten material, with thermal properties we will denote by a subscript, m.

We again assume parabolic temperature distributions, measured above and

below melting, i.e., $T = T_m + U_m$ and $T = T_m + U$, respectively

$$U_m = d(t) + e(t)x + f(t)x^2 \qquad \text{on } 0 < x < s \tag{21a}$$

$$U = a(t) + b(t)x + c(t)x^2 \qquad \text{on } s < x < \ell \tag{21b}$$

with boundary conditions on the front and rear

$$- k_m \frac{\partial U_m}{\partial x}\bigg|_o = I_a \tag{22a}$$

$$- k \frac{\partial U}{\partial x}\bigg|_\ell = 0 \tag{22b}$$

On the melt line, $x = s$,

$$U_m = U = 0 \tag{23}$$

and

$$- k_m \frac{\partial U_m}{\partial x}\bigg|_s + k \frac{\partial U}{\partial x}\bigg|_s = \rho L \frac{ds}{dt} \tag{24}$$

The first four equations enable us to reduce each of (21) to two unknown functions, $f(t)$ and $C(t)$ in

$$U_m = \frac{I_a}{k_m}(s - x) + f(t)(x^2 - s^2) \tag{25}$$

$$U = C(t)\{2\ell(s - x) + (x^2 - s^2)\} \tag{26}$$

to be determined by the heat balance integral. The flux matching condition, Equation (24), then provides the means of determining the unknown time history

of the penetration depth, s.

Let

$$\theta_m = \int_o^s U_m dx = \frac{I}{k_m} \frac{s^2}{2} - f(t) \frac{2}{3} s^3 \tag{27}$$

$$\theta = \int_s^{\ell} U dx = C(t) \{-\frac{2}{3}\ell^3 + 2s\ell^2 - 2s^2\ell + \frac{2}{3} s^3\} \tag{28}$$

Applying the heat balance integral on

$$\int_o^s k_m \frac{\partial^2 U_m}{\partial x^2} dx = \int_o^s \frac{\partial U_m}{\partial t} \rho_m C_{pm} dx \tag{29a}$$

and

$$\int_s^{\ell} k \frac{\partial^2 U}{\partial x^2} dx = \int_s^{\ell} \frac{\partial U}{\partial t} \rho_m C_{pm} dx \tag{29b}$$

produces

$$k_m \frac{\partial U_m}{\partial x}\bigg|_s + I_a = \rho_m C_{pm} \frac{d\theta_m}{dt} \tag{30a}$$

and

$$- k \frac{\partial U}{\partial x}\bigg|_s = \frac{d\theta}{dt} \rho C_p \tag{30b}$$

But

$$\frac{\partial U}{\partial x}\bigg|_s = C(t)2(s - \ell) = \frac{3\theta(t)}{(s - \ell)^2} \tag{31}$$

and

$$\left.\frac{\partial U_m}{\partial x}\right|_s = -\frac{I}{k_m} + f(t)2s = \frac{I_a}{2k_m} - \frac{3\theta_m}{s^2} \tag{32}$$

Substituting, we arrive at

$$\rho C_p \frac{d\theta}{dt} = -\frac{3k\theta(t)}{(s-\ell)^2} \tag{33}$$

$$\rho_m C_{pm} \frac{d\theta_m}{dt} = \frac{3I_a}{2} - \frac{3k_m\theta_m}{s^2} \tag{34}$$

$$\frac{I_a}{2} + \frac{3k_m\theta_m(t)}{s^2} + \frac{3k\theta(t)}{(s-\ell)^2} = \rho L \frac{ds}{dt} \tag{35}$$

At the onset of melting, $t = t_m$, $s = 0$ and $\theta_m = 0$. The temperature distribution in the solid,

$$U = C(t_m)\{x^2 - 2\ell x\} \tag{36}$$

must match that previously given by the premelting solution, Equation (16). Therefore

$$C(t_m) = \frac{I_a}{2k\ell} \tag{37}$$

and

$$\theta(t_m) = -\frac{I_a\ell^2}{3k} \tag{38}$$

Introducing the same new variables as Goodman,

$$\sigma = \frac{s}{\ell} \tag{39}$$

$$\omega = \frac{\rho_m C_{pm}}{\rho C_p} \frac{\theta_m}{T_m \mathcal{L}} \tag{40}$$

$$v = \frac{\theta}{T_m \mathcal{L}} \tag{41}$$

$$\tau = \frac{k}{\mathcal{L}^2} (t - t_m) \tag{42}$$

$$\mu = \frac{C_p T_m}{L} \tag{43}$$

$$\nu = \frac{\kappa_m}{\kappa} \tag{44}$$

and the dimensionless flux, i, as previously defined, we arrive at

$$\frac{dv}{d\tau} = - \frac{3v}{(1 - \sigma)^2} \tag{45}$$

$$\frac{d\omega}{d\tau} = 3(i - \frac{\nu\omega}{\sigma^2}) \tag{46}$$

$$\frac{1}{\mu} \frac{d\sigma}{d\tau} = -i + \frac{3\nu\omega}{\sigma^2} + \frac{3v}{(1 - \sigma)^2} \tag{47}$$

with $\sigma(0) = 0$, $\omega(0) = 0$, $v(0) = - \frac{2i}{3}$ these are the same equations given by Goodman, who has given approximate solutions obtained by a perturbation technique.

We are now in a position to develop expressions for the stresses developed by these approximate temperature distributions. Three time ranges must be considered. To simplify comparison with Laughlin's results, we will consider the same boundary condition, i.e., no inplane force and no bending displacement. Hence,

$$\sigma_{rr} = \sigma_{\theta\theta} = \frac{E}{1-\nu} (C_1 x - \alpha T) \tag{48}$$

in the solid region, and $\sigma_{rr} = \sigma_{\theta\theta} = 0$ in the molten region. Hence,

$$\sigma_{rr} = \sigma_{\theta\theta} = \frac{E\alpha}{1-\nu} \left[\frac{1}{\ell - s} \int_s^{\ell} T dx - T\right] \tag{49}$$

Prior to the time, t_ℓ, when the rear surface temperature changes, the temperature is

$$T = \frac{I_a \delta}{2k} (1 - \frac{x}{\delta})^2 \qquad \text{for } 0 < x < \delta \tag{50a}$$

$$T = 0 \qquad \text{for } \delta < x < \ell \tag{50b}$$

with

$$\delta(t) = \sqrt{6Kt} \qquad \text{for } t < t_\ell = \frac{\ell^2}{6\kappa} \tag{51}$$

$$\sigma_{rr} = \sigma_{\theta\theta} = \frac{E\alpha}{1-\nu} \frac{I_a \sqrt{6Kt}}{2k} \left[\frac{1}{3} \frac{\sqrt{6Kt}}{\ell} - (1 - \frac{x}{\sqrt{6Kt}})^2\right] \quad \text{on } 0 < x < \sqrt{6Kt} \tag{52}$$

$$\sigma_{rr} = \sigma_{\theta\theta} = \frac{E\alpha}{1-\nu} \frac{I_a t}{\rho \ell C_p} \quad \text{on } \sqrt{6Kt} < x < \ell \tag{53}$$

Thus, the maximum tensile stress is at the rear surface and rises linearly in time reaching a maximum value

$$\sigma_{max} = \frac{E\alpha}{1-\nu} \frac{I_a \ell}{6k} \qquad \text{at } \tau = \frac{1}{6} \tag{54}$$

For $\tau > \frac{1}{6}$, but before the front surface melts, the temperature distribution is

$$T = \frac{I_a}{\rho C_p \ell}(t - t_\ell) + \frac{I_a \ell}{2k}(1 - \frac{x}{\ell})^2 \qquad (55)$$

and the stress distribution is

$$\sigma_{rr} = \sigma_{\theta\theta} = \frac{E\alpha}{1-\nu}\frac{I_a \ell}{2k}\left[\frac{1}{3} - (1 - \frac{x}{\ell})^2\right] \qquad \text{for } 0 < x < \ell \qquad (56)$$

The maximum tensile stress is again found on the rear surface and has value

$$\sigma_{max} = \frac{E\alpha}{1-\nu}\frac{I_a \ell}{ók} \qquad \text{for } \frac{1}{6} < \tau < \frac{1}{2i} - \frac{1}{3} \qquad (57)$$

Where it is to be recalled that the criterion for a thin plate was $i \leq 1$. Thus, we see the maximum tensile stress is constant during this second phase. At $\tau = \frac{1}{2i} - \frac{1}{3}$, melting begins at the front face. Assuming the stress in the melt to be zero and using the approximate temperature distribution

$$T = T_m + \frac{3}{2}\left\{\frac{2\ell(s - x) + (x^2 - s^2)}{(s - \ell)^3}\right\}\theta(t) \qquad (58)$$

The stress is

$$\sigma_{rr} = \sigma_{\theta\theta} = \frac{E\alpha}{1-\nu}\frac{\theta}{\ell - s}\left[1 - \frac{\frac{3}{2}(x - s)(2\ell - x - s)}{(\ell - s)^2}\right], \qquad (59)$$

and on the rear surface,

$$\sigma_{rr} = \sigma_{\theta\theta} = -\frac{E\alpha}{2(1-\nu)}\left(\frac{\theta}{\ell - s}\right) = \frac{E\alpha T_m}{2(1-\nu)}\left(\frac{-\nu}{1-\sigma}\right) \qquad (60)$$

Using Goodmans first term to evaluate the change in ν and σ immediately after melting, we discover that the numerator is reduced as $1 - C_1\tau$ while the denominator decreases as $1 - C_2\tau^2$. Hence, when melting begins, the stress

is reduced to

$$\sigma_{max} = [1 - 3(\tau - \tau_m)]\{\frac{E\alpha I_a \ell}{6k(1-\nu)}\} \tag{61}$$

Since the rear surface stress depends only on v and σ, we note that its derivative is

$$\frac{d\sigma_{rear}}{d\tau} = \frac{E\alpha T_m}{2(1-\nu)} [\frac{-\dot{\nu}}{1-\sigma} - \frac{\nu\dot{\sigma}}{(1-\sigma)^2}] \tag{62}$$

Substituting the differential equation for $\dot{\nu}$, we find

$$\frac{d\sigma_{rear}}{d\tau} = \frac{E\alpha T_m}{2(1-\nu)} \frac{3\nu}{(1-\sigma)^3} [1 - \frac{(1-\sigma)\dot{\sigma}}{3}] \tag{63}$$

Since v begins (and remains) negative, and $\sigma < 1$, the derivative of the stress remains negative, as can be seen from Goodmans computations of $\sigma(\tau)$ and the <u>average</u> value of $\dot{\sigma}$, which may be bounded above by the average recession rate with complete removal, $\dot{\sigma}_{ave} < 4i/3$.

Thus, within the limits of the assumptions made, if fracture does not occur <u>before</u> front surface melting begins, it will never occur. To recap the results for thin slabs ($i < 1$) in terms of dimensionless time

$$\tau = \frac{kt}{\ell^2} \tag{64}$$

and intensity

$$i = \frac{I_a \ell}{2kT_m} , \tag{65}$$

The tensile stress on the rear surface is

$$\sigma_{max} = \frac{2E\alpha T_m}{1-\nu} i\tau \qquad \text{for } 0 < \tau < \frac{1}{6} \tag{66}$$

$$\sigma_{max} = \frac{2E\alpha T_m}{1-\nu} \frac{i}{6} \qquad \text{for } \frac{1}{6} < \tau < \frac{1}{2i} - \frac{1}{3} \tag{67}$$

$$\sigma_{max} = \frac{2E\alpha T_m}{1-\nu} \frac{i}{6} \left[\frac{3}{2i} - 3\tau\right] \qquad \text{for } \tau - \frac{1}{2i} + \frac{1}{3} << 1 \tag{68}$$

If we let the tensile stress required to produce fracture be σ_c, and define

$$\hat{\sigma}_c = \frac{\sigma_c(1-\nu)}{E\alpha T_m} \tag{69}$$

the fracture threshold is $i = 3\hat{\sigma}_c$, and fracture times for two hypothetical materials are as shown in Figure 15.

It should be noted that all of these results are for the boundary condition considered by Laughlin[3], i.e., no bending deformation allowed, and no inplane constraint forces allowed to develop. Other boundary conditions will produce different stresses, as will be considered in a later section.

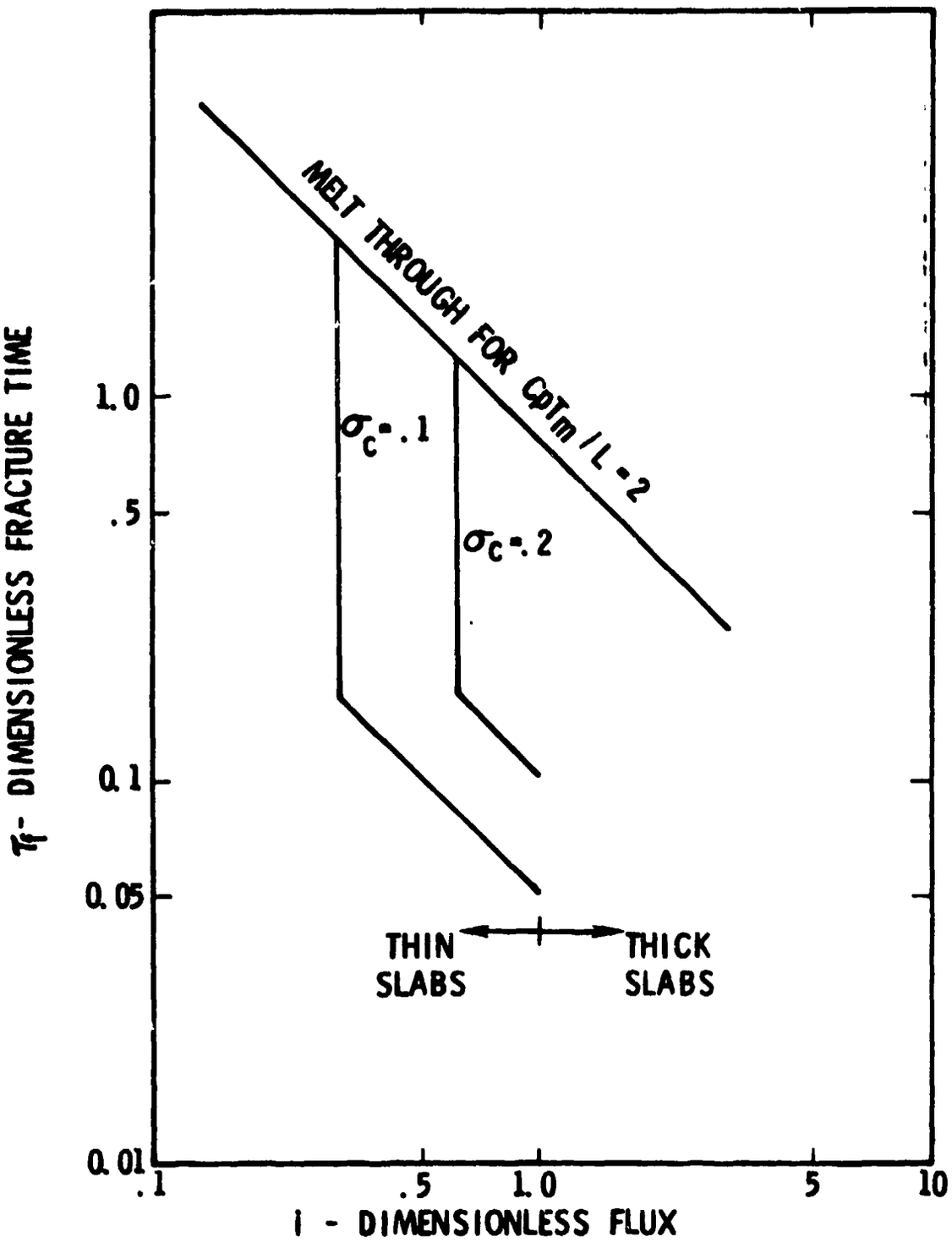

Figure 15. Failure Times for Thin Slabs With Melt Retention.

2. Thermal Stress in Thick Slabs, with Melt Retention.

In the previous section, the approximate temperature solution given by Goodman and Shea was used to predict times to fracture in thin slabs or good conductors where the rear face is reached by thermal penetration, and hence, the maximum stress develops, before front face melting begins. For poor conductors at high flux, however, the front force will melt before the rear surface heats. In such a case, the maximum stress, and hence, fractures, may occur after melting begins.

We therefore require a solution analogous to that of Goodman and Shea, applicable to the thick slab geometry. Let us assume the one dimensional heating, by absorbed intensity I_a, of a slab of thickness h. We denote by the subscript m the thermal properties of the molten state, and the depth of melting by s.

On $0 < x < s$

$$\kappa_m \frac{\partial^2 U_m}{\partial x^2} = \frac{\partial U_m}{\partial t} \qquad 1$$

on $s < x < s + \delta$

$$\kappa \frac{\partial^2 U}{\partial x^2} = \frac{\partial U}{\partial t} \qquad 2$$

The boundary conditions are

$$- k_m \frac{\partial U_m}{\partial x} = I_a \text{ on } x = 0 \qquad 3a$$

$$- k_m \left.\frac{\partial U_m}{\partial x}\right|_{x=s} + k \left.\frac{\partial U}{\partial x}\right|_{x=s} = \rho L \frac{ds}{dt} \text{ on } x = s \qquad 3b$$

$$U_m = U = 0 \text{ on } x = s \qquad 4a$$

$$- k \left.\frac{\partial U}{\partial x}\right|_{x=s+\delta} = 0 \text{ on } x = s + \delta \qquad 4b$$

$$U = = T_m \text{ on } x = s + \delta \qquad 4c$$

where Tm is the temperature at which the phase transformation of specific heat L occurs, and temperatures are given by

$$T = T_m + U_m \text{ on } 0 < x < s \qquad 5a$$

$$T = T_m + U \text{ on } s < x < s + \delta \qquad 5b$$

The initial conditions are the instance of front face melting,

$$U = 0 \quad @ \quad x = 0 \quad \text{and} \quad t = t_m \tag{6}$$

$$s = 0 \quad @ \quad t = t_m \tag{7}$$

$$U = -T_m + \frac{I_a}{2k\delta_m}(\delta_m - x)^2 \quad @ \quad t = t_m \tag{8}$$

$$2k = \frac{I_a}{V}\frac{\delta}{\delta_m}$$

$$\delta = \frac{2kV}{I_a}$$

where

$$\delta = \delta_m = \sqrt{6\kappa\, t_m} = \frac{2k}{I_a}T_m \quad @t = t_m \tag{9}$$

and the initial distribution is taken as the approximate solution prior to meeting.

Following Goodman, we choose the temperatures distributions to be parabolic, i.e.,

$$U = d(t) + xe(t) + x^2 f(t). \tag{10}$$

Employing the boundary conditions; 4a-c, we find

$$U = \frac{T_m}{\delta^2}\left[s^2 + s^2\sigma - 2x\,(s+\sigma) + x^2\right] \tag{11}$$

$$\text{or} \qquad T = T_m\left[\left(\frac{s+\delta-x}{\delta}\right)^2 - 1\right] + T_m \tag{12}$$

which more clearly displays the physical significance of the temperatures ahead of the melting front in terms of the two parameters, the melt thickness s, and the penetration depth, δ. The integral

$$\theta = \int_s^{\delta+s} U dx = T_m\left[\frac{2}{3}\delta\right] = -\frac{2}{3}T_m\,\delta \tag{13}$$

will prove useful. Physically, it is a representation of the additional energy required to bring the material within the penetration depth to melting.

We also choose a parabolic temperature in the molten layer,

$$U_m = a(t) + xb(t) + x^2 c(t) \tag{14}$$

From boundary conditions 3a and 4a,

$$U_m = c(t)\,(x^2 - s^2) - \frac{I_a}{k_m}(x-s) \tag{15}$$

The integral

$$\theta_m = \int_o^s U_m dx = \frac{I_a s^2}{2k_m} - \frac{2}{3} s^3 c(t) \qquad 16$$

represents the energy in the melt, above that required by the phase transformation. At $t = 0$, $\theta_m = 0$.

We now require the satisfaction, in the average, of the heat conduction equations, (equations 1 and 2) through averaging over each domain

$$\int_o^s \kappa_m \frac{\partial U_m}{\partial x} dx = \int_o^s \frac{\partial U_m}{\partial t} dx \qquad 17a$$

and

$$\int_s^{s+\delta} \kappa \frac{\partial U}{\partial x} dx = \int_s^{s+\delta} \frac{\partial U}{\partial t} dx \qquad 17b$$

Differentiating 13 and 16, we note:

$$\frac{d\theta}{dt} = (\dot{\delta} + \dot{s})U\Big|_{\delta+s} - \dot{s}\, U\Big|_s + \int_s^{s+\delta} \frac{\partial U}{\partial t} dx \qquad 18a$$

and

$$\frac{d\theta_m}{dt} = s\, U_m\Big|_s + \int_o^s \frac{\partial U_m}{\partial t} dx \qquad 18b$$

Hence

$$\kappa_m \frac{\partial U_m}{\partial x}\Big|_s + \frac{\kappa_m I_a}{\kappa_m} \quad \frac{d\theta_m}{dt} \qquad 19a$$

and

$$-\kappa \frac{\partial U}{\partial x}\Big|_s = \frac{d\theta}{dt} + (\dot{\delta} + \dot{\delta})\, T_m \qquad 19b$$

where equation 4b and 3a have been applied. Substituting 11 into 19b leaves, as a final form of the averaged energy equation in the solid, that

$$+2\kappa \frac{T_m}{\delta} = \frac{d\theta}{dt} + (\dot{\delta} + \dot{s})\, T_m \qquad 20a$$

θ and δ are related through 13, thus

$$\dot{\theta} = -\, 2/3\, T_m\, \dot{\delta} \qquad 21$$

Combining 15 with 19a

$$2\,\kappa_m\, a\, c(t) = \frac{d\theta_m}{dt} \qquad 22$$

which may be combined with 16 to give the a final averaged energy equation for the melt

$$\frac{I_a s^2}{2\kappa_m} = \theta_m + \frac{1}{3}\, s^2\, \frac{1}{\kappa_m}\, \frac{d\theta_m}{dt} \qquad 23a$$

We may also eliminate the gradients in 3b to obtain the equation for the energy balance on the melt line as

$$I_a - \frac{k_m}{\kappa_m}\, \frac{d\theta_m}{dt} - \frac{2k\ T_m}{\beta} = \rho L \dot{s} \qquad 24a$$

Equations 20, 23 and 24 form a system of three first order, non-linear, coupled equations which must be solved in order to find the temperature. Through the following substitutions

$$\tau = \kappa\ (t - t_m)/\ell^2 \qquad 25$$

$$\mu = C_p T_m / L \qquad 26a$$

$$\nu = \kappa_m / \kappa \qquad 26b$$

$$i = I_a \ell / (2k\ T_m) \qquad 26c$$

we arrive at the same dimensionless variables used by Goodman

$$\sigma = s / \ell \qquad 27$$

$$\gamma = \theta / (T_m\ \ell) \qquad 28$$

$$w = (\kappa\ k_m\ \theta_m) / (k\ \kappa_m\ T_m\ \ell) \qquad 29$$

The differential equations become:

$$\dot{\gamma} = \frac{8}{3\nu}\,(1+\mu) - 2\mu\ i + \frac{6\mu\nu w}{\sigma^2} \qquad 20b$$

$$\dot{\omega} = 3\,(i - \nu w/\sigma^2) \qquad 23b$$

$$\dot{\sigma} = \mu\,\{\frac{3\nu w}{\sigma^2} + \frac{4}{3}\,\frac{1}{\nu} - i\} \qquad 24d$$

The initial conditions ($\tau = 0$) are

$$\sigma = 0 \qquad 30a$$

$$w = 0 \qquad 30b$$

$$\nu = -\frac{2}{3i} \qquad 30c$$

It may be demonstrated that if τ is small, that

$$\sigma \approx 6\mu i(i\tau)^2 \qquad 31a$$

$$w \approx \frac{i}{\nu}(6\mu i)^2(i\tau)^4 \qquad 31b$$

$$v \approx -\frac{2}{3i} - 4i\tau + 12\mu i(i\tau)^2 \qquad 31c$$

The actual temperature distribution in the solid is obtained from 12 as

$$T = T_m\left(\frac{s+\delta-x}{\delta}\right)^2 \qquad 32$$

where s and δ are obtained from 27, 13 and 28. Stresses in the solid region depend on the mechanical boundary conditions at the edge of the heated region. If we again assume that bending displacements are completely constrained, then

$$\sigma = \frac{E}{1-\nu}\{C_1 - \alpha T\} \qquad 33$$

The requirement of no net axial force leads to

$$\sigma = \frac{E\alpha}{1-\nu}\left\{\frac{1}{\ell-s}\int_s^{s+\delta} T\,dx - T\right\} \qquad 34$$

This is found to be

$$\sigma = \frac{E\alpha T_m}{1-\nu}\left\{\frac{\delta}{3(\ell-s)} - \left(\frac{s+\delta-x}{\delta}\right)^2\right\} \quad \text{for } x < s+\delta \qquad 35$$

$$\sigma = \frac{E\alpha T_m}{1-\nu}\left(\frac{\delta}{\ell-s}\right)\frac{1}{3} \quad \text{for } s+\delta < x < \ell \qquad 36$$

The maximum tensile stress occurs on the rear face ($x = \ell$) and is

$$\sigma_{rear} = -\frac{E\alpha T_m}{2(1-\nu)}\frac{v}{1-\sigma} \qquad 37$$

valid until $-\frac{3}{2}v < 1-\sigma$. The greatest possible stress is

$$\sigma_{max} = \frac{E\alpha T_m}{3(1-\nu)}$$

For small time

$$\sigma_{rear} = \frac{E\alpha T_m}{(1-\nu)}\left\{\frac{1}{3i} + 2i\tau - 6\mu i(i\tau)^2 + 2\mu(i\tau)^2\right\} \qquad 38$$

The dimensionless time at which melting begins is (from 9, 25 and 26c)

$$\tau_m = \frac{1}{6i^2}$$

and the stress at that time is

$$\sigma_{rear} = \frac{E\alpha T_m}{1-\nu} \frac{1}{3i} \qquad 39$$

We note that for i = 1, the threshold of applicability of these results for the thick slab, that the maximum stress predicted is the same as for the thin slab. However, we also note an important difference. In the case of the thin slab, we found that the stress reduced after the onset of melting. In the thick slab, the stress will continue to increase as we may note from Equation 38. Hence, a numerical solution of the governing system of equations is necessary.

3. Thermal Stress in Melting Thick Slabs With Instantaneous Melt Removal

Let us now consider the case when the melt is removed as it forms. Again, two cases must be considered, depending on whether the melting begins before the rear surface changes temperature (the thick slabs) or after (thin slabs). For the thick slab, we assume a temperature profile

$$T = T_m \left[(1 - (\frac{x-s}{\delta})^2\right] \qquad \text{for } s < x < s+\delta \tag{1}$$

$$T = 0 \qquad \text{for } s+\delta < x \tag{2}$$

Here s is the instantaneous location of the front surface measured from its original location. This temperature profile is appropriate only after front surface melting begins, i.e., for

$$t > t_m = \frac{1}{6k} (\frac{2kT_m}{I})^2 \tag{3}$$

Again, we let

$$\theta = \int_s^{\delta+s} U dx = - \frac{2T_m \delta}{3} \tag{4}$$

where $U = T - T_m$. Requiring the satisfaction of the differential equation averaged over the instantaneous thickness leads to

$$- k \frac{\partial T}{\partial x}\Big|_s = \rho C_p \int_s^{s+\delta} \frac{\partial T}{\partial t} dx = \dot{\theta} + T_m(\dot{\delta} + \dot{s}) \tag{5}$$

The melting line coincides with the front surface and an energy balance leads to

$$I_a + k \left.\frac{\partial T}{\partial x}\right|_s = \rho L \dot{s} \tag{6}$$

The thermal gradient on x = s may be evaluated from

$$k \left.\frac{\partial T}{\partial x}\right|_s = - \frac{2kT_m}{\delta} \tag{7}$$

Application of Equation (4) and the elimination of the gradients leads to two equations

$$\rho L \dot{s} = I_a + \frac{4k}{3} \frac{T_m^2}{\theta} \tag{8}$$

$$\rho C_p \frac{\dot{\theta}}{2} - \rho(L + C_p T_m)\dot{s} = -I_a \tag{9}$$

In terms of the same dimensionless parameters introduced previously, we find

$$\frac{dv}{d\tau} = 4\mu i + \frac{8}{3}(1 + \mu)\frac{1}{v} \tag{10}$$

$$\frac{d\sigma}{d\tau} = 2\mu i + \frac{4\mu}{3v} \tag{11}$$

Again, the initial conditions ($t - t_m = 0$) are

$$\sigma = 0 \tag{12a}$$

$$v = - \frac{2}{3i} \tag{12b}$$

In this case, we note the first equation to be uncoupled. The substitution

$$\frac{1}{v} = C[1 + g(t)] \tag{13}$$

is found to be convenient. With

$$C = -\frac{3}{2}\frac{\mu i}{(1+\mu)} \tag{14}$$

and the change of independent variable

$$y = \frac{8}{3}(1+\mu)\, c^2\tau = \frac{6}{1+\mu}\mu^2 i^2 \tau^1 \tag{15}$$

where

$$\tau^1 = \tau - \tau_m \tag{16}$$

then

$$\frac{dg}{dy} = -g(1+g)^2 \tag{17}$$

with initial condition

$$g(0) = \frac{1}{\mu} \tag{18}$$

This equation may be integrated to yield

$$y = \frac{\mu}{1+\mu} - \frac{1}{1+g} + \ln\left(\frac{1+y}{g(1+\mu)}\right) \tag{19}$$

Substitution into Equation (11) then yields

$$3\mu i\sigma = \mu - \left(\frac{1+\mu}{1+g}\right) + \ln\left(\frac{1+g}{g(1+\mu)}\right) \tag{20}$$

This, together with

$$vi = \frac{-2(1+\mu)}{3\mu(1+g)} \tag{21}$$

enables the solution to be computed in terms of the parameter g, which is in turn related to y, and hence τ through (19) and (15). Pertinent values of solution parameters are presented as Table I.

For the same boundary condition as was considered in the previous section, i.e., no bending displacement or inplane force, we find

$$\sigma_{\theta\theta} = \sigma_{rr} = \frac{E\alpha}{1-\nu}\left[\frac{1}{\ell-s}\int_{s}^{\delta+s} Tdx - T\right] \tag{22}$$

Of particular interest is the maximum tensile stress, which again develops on the rear face, $x = \ell$, where $T = 0$ for times over which this thick slab solution applies. Hence,

$$\sigma_{max} = \frac{E\alpha T_m}{2(1-\nu)}\left(\frac{-\nu}{1-\sigma}\right) \tag{23}$$

In this case, a power series solution, valid for small time, shows the stress at the rear face to increase after front face melting begins, since both ν and σ increase in magnitude.

Values of a dimensionless stress

$$\hat{\sigma}_{max} = \frac{\sigma_{max}(1-\nu)}{E\alpha T_m} = -\frac{1}{2}\left(\frac{\nu}{1-\sigma}\right) \tag{24}$$

may be computed for any $i > 1$.

It is to be recalled that the temperature distribution becomes invalid when the thermal penetration front reaches the rear face, or

$$\sigma + \frac{\delta}{\ell} = 1 \tag{25}$$

This condition occurs, for any i, at a time y when $i = i_c$, as determined from

TABLE I. SOLUTION PARAMETERS COMPUTED FOR $\mu=2$.

g	y	$-\nu i$	$i\sigma$	$i_c=i\sigma-\frac{3}{2}i\nu$	σ_c
.5	0	.66667	0	1.0	
.45	.04847	.68965	.000415	1.0349	.000401
.4	.10653	.71430	.0018817	1.0733	.00175
.35	.17724	.74074	.004848	1.1160	.00434
.3	.26516	.76923	.010005	1.1639	.00860
.25	.37749	.8000	.018472	1.2185	.01516
.2	.52648	.83333	.032192	1.2822	.0251
.15	.73537	.86955	.05493	1.3593	.0404
.10	1.0569	.90909	.095335	1.4590	.065
.07	1.3604	.93460	.137427	1.5394	.0893
.05	1.6602	.95238	.18146	1.6100	.113
.03	2.1333	.97087	.25415	1.7105	.149
.02	2.5195	.98039	.31534	1.7859	.177
.01	3.1931	.9901	.42437	1.9095	.222
.001	5.4768	.999	.802182	2.302	.348
.0001	7.7786	.9999	1.18535	2.685	.441
.00001	10.081	.99999	1.56906	3.0690	.511
1.02×10^{-7}	15.667	1.0	2.5	4.0	.625
4.9×10^{-10}	20	1.0	3.2222	4.7222	.682
2.53×10^{-10}	21.6667	1.0	3.5	5.0	.70
2.24×10^{-14}	30	1.0	4.8889	6.3889	.765
3.85×10^{-18}	39.6667	1.0	6.5	8	.8125
1.014×10^{-18}	40	1.0	6.5556	8.0556	.813
2.7×10^{-23}	51.667	1.0	8.5	10	.85

the appropriate column in Table I. At that instant, the stress is a maximum and has value

$$\hat{\sigma}_{max} = \frac{1}{3} \tag{26}$$

independent of i. Thus, the maximum stress obtainable is independent of the dimensionless intensity, and μ as well, but the time required to generate the stress will be seen to depend on the intensity. The column labled σ_c in Table I denotes the fraction of the slab which has melted at the instant when the stress achieves the maximum value.

Figure 16 presents the time history of the evolution of the rear face tensile stress, for various values of the dimensionless flux. In Figure 17. the failure time as a function of intensity is given for materials of various ultimate strength, $\hat{\sigma}_u$, where

$$\hat{\sigma}_u = \frac{\sigma_u \ell_T (1-\nu)}{E\alpha T_m} \tag{27}$$

One notes what at first would appear to be an anomolous increase in fracture time with intensity. This arises because higher intensities confine the penetration depth, thus less thermal force develops. Further increases in intensity cause more rapid melt thru, thus reducing the load bearing area.

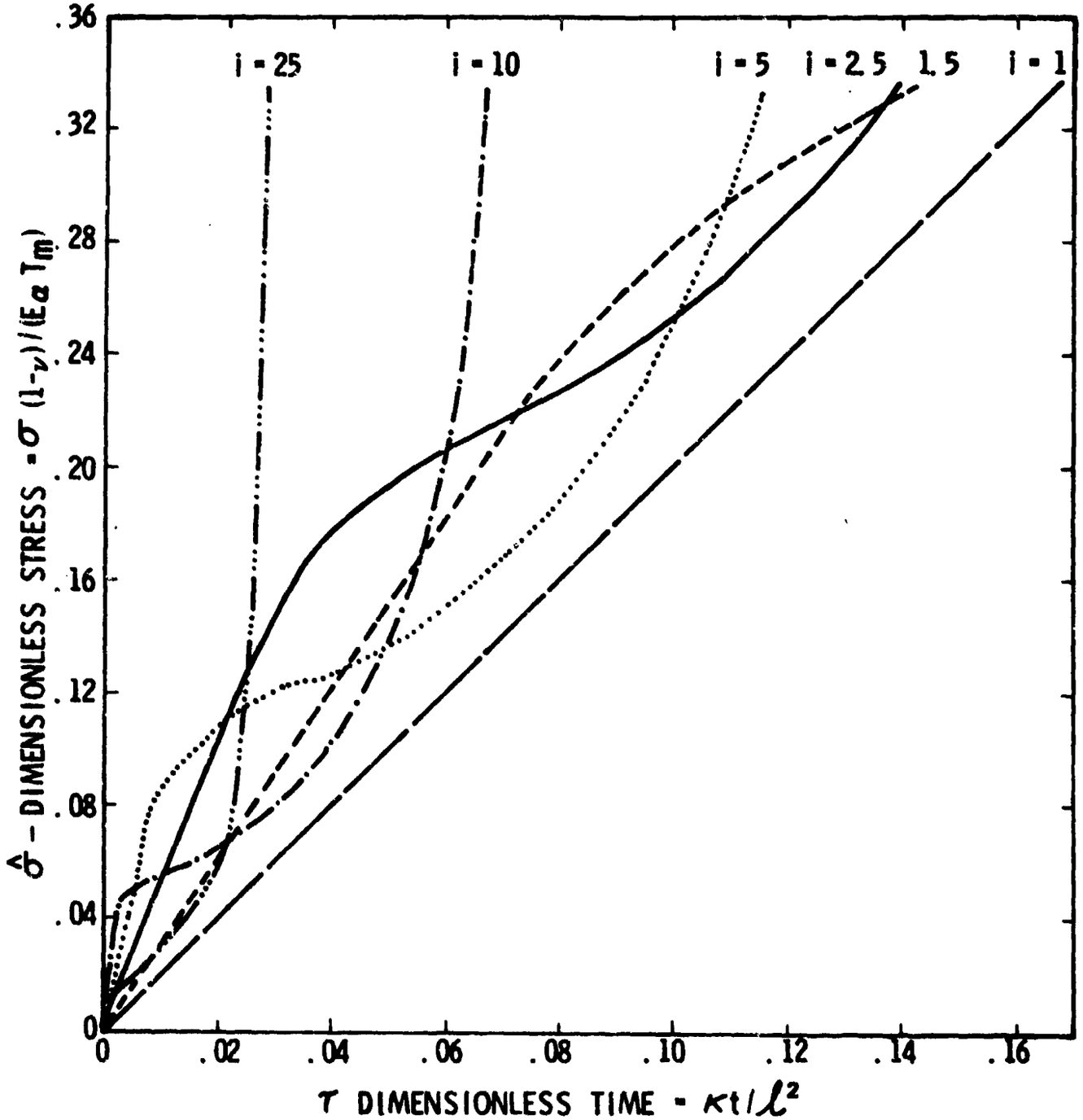

Figure 16. Stress Time History on Rear Surface of Thick Slab With Melt Removal.

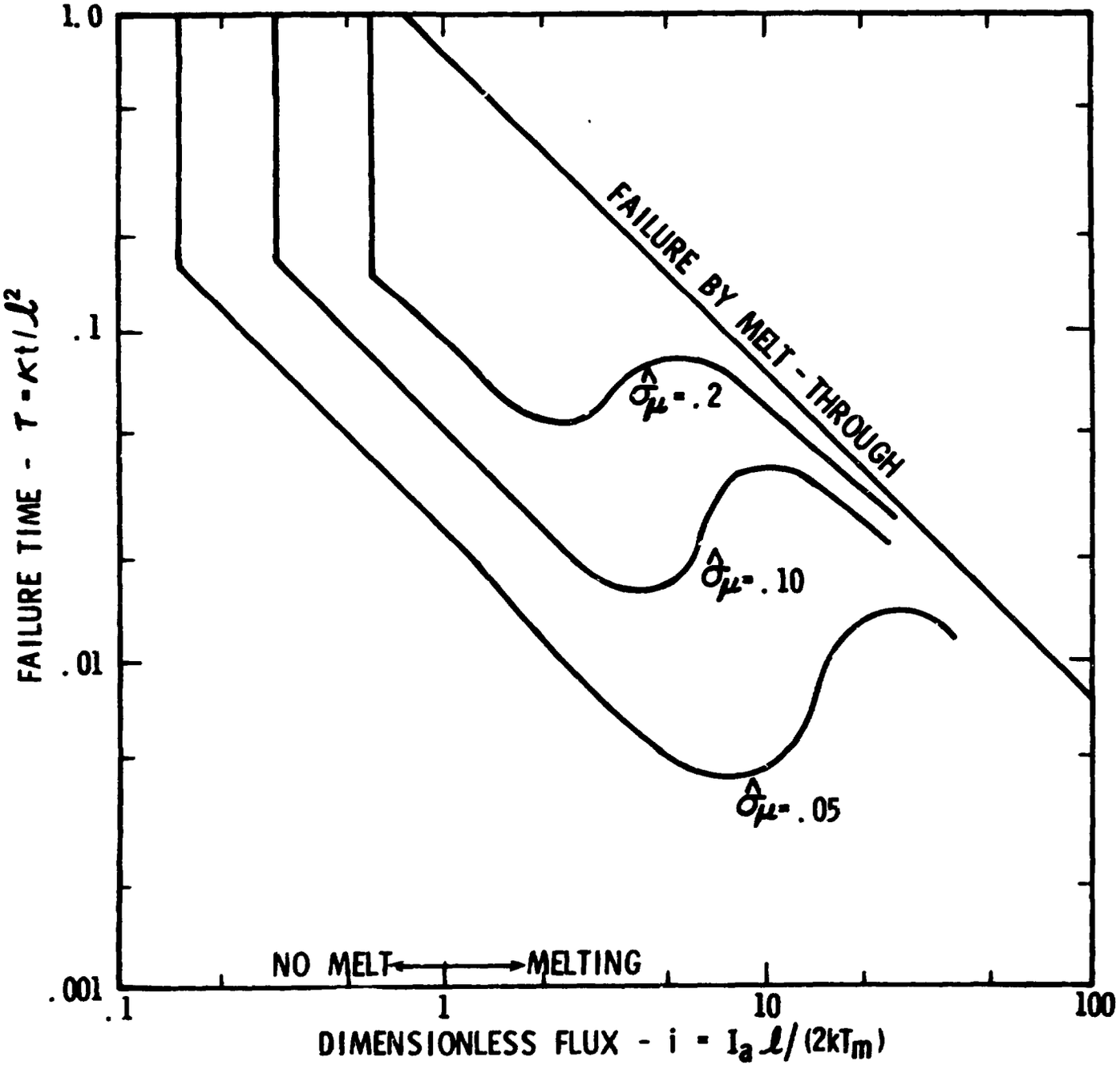

Figure 17. Failure Times for Thick Slabs With Melt Removal.

V. Summary and Discussion

Two mechanisms have been identified as significant in the generation of stress in solid elastic materials subjected to high intensity laser radiation. The absorption of some fraction of the incident energy was found to produce thermal stresses of significant magnitude, but these stresses are characteristically compressive in the region heated by the beam. In a ductile material, such stresses may produce failure in a shear mode, but this is less likely to occur in a brittle material. Rather, it is the significant tensile stresses found outside of the heated region which are believed to be the more significant in the generation of failure. Radial conduction of heat was found to diminish, but not remove, these tensile stresses.

Such thermal stresses are generated by both CW and pulsed lasers. In the latter case, the duration of the pulse and the time between pulses is usually small compared to the thermal diffusion times; thus a repeated pulse may be treated as an energy source of the same time averaged intensity. This approximation is especially appropriate in the case of poor conductors, such as glasses and ceramics.

In addition to the stresses developed by the absorption of energy by the solid, the absorption of energy in the medium adjacent to the solid produces an intense pressure field through the mechanism of LSD or LSC waves. The mechanical response of an elastic plate to such loadings was also considered. This mechanism is inherently of much greater significance in the case of pulsed lasers because of the higher peak intensities. Consideration of the response to a pulse showed that the response of a short pulse, acting over a small portion of the plate, can be accurately determined only if a large number of the plate modes are considered in the response. While the peak stresses occur

at the center of the spot, the stresses elsewhere in the plate remain significant.

The stresses produced by these two mechanisms are such that superposition occurs in the case of a repeated pulse laser of high intensity. The thermal stresses due to the time-averaged intensity increase with time. At later times, the peak values are to be found at greater distances from the heated area. The oscillating stresses resulting from the front surface pressures will diminish in magnitude with distance from the spot center. While oscillating at the "rep" frequency of the laser, the amplitude of succeeding peaks will be relatively constant. Thus, the superposition of the two stress generating mechanisms may well produce failure after a number of pulses have occurred. Failures occurring in the first few pulses may be expected to be due primarily to the oscillating pressure field and therefore at or near the spot center (barring stress raisers at the supports). Failures which occur after a number of pulses, on the other hand, may be expected to be due to the development of the tensile thermal stress outside of the heated region. Thus, the failure may originate outside of the heated region.

Other failure mechanisms were given some consideration. Tensile stresses were found to be present in the interior at early times, but the reported significance of surface flaws as failure origins is not accounted for by these stresses. Partial melting under the spot may be of significance. A preliminary investigation of this possibility was conducted, with the scope limited by the mechanical boundary condition considered at the edge of the melting region. Briefly, the failure mechanism deserving some further exploration is the following. As melting occurs, the central portion of the plate becomes thinner. The compressive forces generated by the surrounding unmelted portion of the plate will then have a resultant nearer to the melted surface than to the rear,

thus generating the proper moment to produce rear surface tension. While such a mechanism is conceivable, it is not likely to be of significance in a ceramic because of the long times required to produce the necessary melting (or thermal softening) necessary for the process to occur.

While the possibility of crack (flaw) growth under the oscillating stress produced by the fluctuating front surface pressure cannot be precluded as a producer of the observed failures after a number of pulses, thermal stresses of increasing amplitudes, upon which the fluctuating stresses are superposed, would seem to be a more probable cause. A carefully designed and properly instrumented series of experiments would establish the appropriateness of this conjecture.